



Graduate School of
Systemic Neurosciences

LMU Munich

Functional Mapping of Central Amygdala Feeding and Reward Circuits

*Dissertation der Graduate School of Systemic Neurosciences der
Ludwig-Maximilians-Universität München*

Hakan Kucukdereli

Submitted on June 13, 2017





Thesis Supervisor: Prof. Rüdiger Klein

Second Reviewer: Prof. Valentin Stein

Third Reviewer: Dr. Sabine Krabbe

Date of Defense: November 6, 2017



”The end justifies the means. But
what if there never is an end? All
we have is means.”

*Ursula K. le Guin,
The Lathe of Heaven*



Abstract

Survival of an animal depends upon its ability to attend and respond to salient environmental stimuli. The amygdala is a key brain region implicated in emotional behaviors including fear and anxiety, with much attention focused on the central nucleus of the amygdala (CeA). CeA neurons expressing protein kinase C δ (PKC δ) have been shown to suppress food intake, however, whether neurons in the CeA can promote appetitive behaviors and the identity of the neurons that do so remains unclear. In this thesis, I have characterized a relatively little described CeA neuronal population that expresses serotonin receptor 2a (Htr2a). First, I showed that CeA^{Htr2a} neurons constitute a subpopulation of CeA^{PKC δ -negative} neurons and are electrophysiologically homogeneous. Second, I demonstrated that CeA^{Htr2a} neurons inhibit CeA^{PKC δ} neurons, suggesting an antagonistic role for CeA^{Htr2a} neurons in food intake. Furthermore, *in vivo* Ca²⁺ imaging experiments showed that these neurons increase their activity proximal to food consumption but not food cues or instrumental responses. Together with behavioral experiments from our lab, the activity dynamics of these neurons suggests that they modulate the consummatory phase of eating behavior. Finally, I demonstrated a circuit mechanism that explains how CeA^{Htr2a} can positively modulate eating and reward seeking through long-range projections to the parabrachial nucleus (PBN). These results together highlight the complexity and intricacy of CeA circuits and demonstrate how molecularly-defined cell types in the same brain region can exert opposing effects on behavior.



Contents

| | |
|--|------------|
| List of Figures | xi |
| Abbreviations | xiv |
| 1 Introduction | 1 |
| 1.1 Neural circuits controlling emotional behaviors | 1 |
| 1.1.1 The amygdaloid complex | 1 |
| 1.2 The central amygdala | 3 |
| 1.2.1 Molecular architecture of the central amygdala | 3 |
| 1.2.2 Physiological properties of central amygdala neurons | 4 |
| 1.3 Central amygdala circuitry | 5 |
| 1.3.1 Microcircuitry | 5 |
| 1.3.2 Inputs of the central amygdala | 7 |
| 1.3.3 Outputs of the central amygdala | 8 |
| 1.4 Central amygdala-brainstem interactions | 10 |
| 1.4.1 Control of food intake | 10 |
| 1.4.2 Pain processing | 12 |
| 1.5 Using optogenetics to probe neural circuits | 13 |
| 1.5.1 Tools and strategies for targeting neurons | 13 |
| 1.5.2 Brief history of optogenetics | 15 |
| 1.5.3 Optogenetic actuators | 16 |
| 1.5.4 Channelrhodopsin-assisted circuit mapping | 17 |
| 1.5.5 <i>in vivo</i> Optogenetics | 18 |

| | | |
|----------|--|-----------|
| 1.5.6 | Considerations when using optogenetics | 19 |
| 1.6 | Using Ca ²⁺ imaging to probe neural circuits | 20 |
| 2 | Thesis Objectives | 23 |
| 3 | Methods | 27 |
| 3.1 | Animal subjects | 27 |
| 3.2 | Viral constructs | 28 |
| 3.3 | General practice for stereotaxic surgeries | 28 |
| 3.4 | Stereotaxic surgeries | 28 |
| 3.5 | Acute brain-slice preparation | 29 |
| 3.6 | Slice electrophysiology | 29 |
| 3.7 | Optogenetic manipulations | 30 |
| 3.8 | Anatomical retrograde tracing | 31 |
| 3.9 | Stretaxic surgery for GRIN lens implantation | 31 |
| 3.10 | <i>in vivo</i> freely moving Ca ²⁺ imaging | 32 |
| 3.11 | Ca ²⁺ imaging data analysis | 34 |
| 3.12 | Histology | 35 |
| 3.13 | Immunohistochemistry | 36 |
| 3.14 | Microscopy | 37 |
| 3.15 | Statistics | 37 |
| 4 | Results | 39 |
| 4.1 | Molecular characterization of CeA ^{Htr2a} neurons | 39 |
| 4.2 | Electrophysiological characterization of CeA ^{Htr2a} neurons | 41 |
| 4.3 | CeA ^{Htr2a} in the CeA microcircuitry | 44 |
| 4.3.1 | Controlling CeA ^{Htr2a} neurons with ChR2 | 44 |
| 4.3.2 | Local circuit connectivity | 44 |
| 4.4 | <i>in vivo</i> activity dynamics of CeA ^{Htr2a} during appetitive behaviors | 47 |
| 4.5 | CeA ^{Htr2a} neuron efferent projections | 56 |

| | | |
|----------|---|-----------|
| 4.5.1 | Anatomical mapping of CeA ^{Htr2a} neuron innervation fields | 56 |
| 4.5.2 | Optogenetic investigation of CeA ^{Htr2a} efferent projections to the PBN | 60 |
| 4.5.3 | Identification of PBN CeA ^{Htr2a} target neurons | 61 |
| 4.5.4 | CeA ^{PKCδ} neurons inhibit PBN-projecting neurons of the CeA | 61 |
| 4.6 | CeA ^{Htr2a} innervation of the PBN modulates feeding and reward behaviors . | 63 |
| 5 | Thesis Summary | 68 |
| 6 | Discussion | 70 |
| 6.1 | Identification of central amygdala neural subpopulations | 70 |
| 6.2 | Local connectivity of central amygdala neuronal subtypes | 73 |
| 6.3 | CeA ^{Htr2a} neurons increase their activity during food consumption | 74 |
| 6.4 | Inhibition of PBN neurons by CeA descending projections is rewarding and modulates consummatory behavior | 77 |
| 7 | Conclusions & Outlook | 80 |
| | Bibliography | 84 |
| I | Appendix | |

List of Figures

| | | |
|------|--|----|
| 1.1 | Anatomical organization of the amygdaloid complex | 3 |
| 1.2 | Molecular organization of the CeA | 4 |
| 1.3 | Electrophysiological properties of CeL neurons | 6 |
| 1.4 | Central amygdala microcircuitry underlying learnt fear expression | 7 |
| 1.5 | Long-range inputs to the CeA | 9 |
| 1.6 | Long-range outputs of the CeA | 10 |
| 1.7 | CeA-PBN interactions in the control of food consumption | 12 |
| 1.8 | Scheme of Cre-dependent adenoassociated virus | 14 |
| | | |
| 4.1 | Htr2a+ and PKC δ + neurons are mutually exclusive CeA neural populations | 40 |
| 4.2 | CeA ^{Htr2a} neurons are partially overlapping with CeA ^{SOM} neurons | 41 |
| 4.3 | CeA ^{Htr2a} neurons are electrophysiologically homogeneous | 42 |
| 4.4 | Membrane properties of CeA ^{Htr2a+} and CeA ^{Htr2a-negative} neurons do not display any significant difference | 43 |
| 4.5 | <i>ex vivo</i> validation of ChR2 to induce firing in CeA ^{Htr2a} neurons | 45 |
| 4.6 | CeA ^{Htr2a} neurons inhibit other neurons within the CeA local circuit | 46 |
| 4.7 | CeA ^{Htr2a+} neurons locally inhibit CeA ^{PKCδ+} neurons | 47 |
| 4.8 | <i>in vivo</i> Ca ²⁺ imaging of CeA ^{Htr2a} neurons | 49 |
| 4.9 | Ca ²⁺ imaging in freely behaving mice | 49 |
| 4.10 | CeA ^{Htr2a} neurons increase activity during eating | 51 |
| 4.11 | A subpopulation of CeA ^{Htr2a} neurons increase activity during eating | 52 |
| 4.12 | <i>in vivo</i> Ca ²⁺ imaging of CeA ^{Htr2a} neurons during a food-seeking task | 53 |
| 4.13 | CeA ^{Htr2a} neurons increase activity during eating but not during food-seeking | 54 |

Abbreviations

| | | |
|------|--|----|
| 4.14 | CeA ^{Htr2a} neurons increase activity during eating but not during food-seeking | 55 |
| 4.15 | Activity of CeA ^{Htr2a} neurons remains constant over FR1 trials | 55 |
| 4.16 | Innervation fields of axon terminals from CeA ^{Htr2a} neurons | 57 |
| 4.17 | PBN-projecting CeA neurons are predominantly Htr2a+ | 58 |
| 4.18 | CeA ^{Htr2a} neurons do not directly project to LH and VTA | 59 |
| 4.19 | CeA ^{Htr2a} neurons do not directly project to LH and VTA | 60 |
| 4.20 | CeA ^{Htr2a} neurons by not CeA ^{PKCδ} neurons strongly inhibit the PBN | 62 |
| 4.21 | CeA ^{Htr2a} neurons predominantly inhibit PBN ^{CGRP-negative} neurons | 63 |
| 4.22 | CeA ^{PKCδ} inhibit local CeA→PBN projecting neurons | 64 |
| 4.23 | Activation of CeA ^{Htr2a} →PBN projection modestly evokes food consumption | 65 |
| 4.24 | Activation of CeA ^{Htr2a} →PBN projection induces place preference | 66 |
| 4.25 | The CeA ^{Htr2a} →PBN projection supports self-stimulation behaviour | 67 |
| I | Location of retrobeads injection targeting PBN | |
| II | Location of optic fibers for <i>in vivo</i> optogenetics experiments | |

Abbreviations

| | |
|------------------|---|
| AAVs | Adenoassociated viruses |
| aCSF | Artificial cerebrospinal fluid |
| AHP | After-hyperpolarization potentials |
| Arch | Archaeorhodopsin |
| BAC | Bacterial artificial chromosome |
| BLA | Basolateral amygdala |
| BNST | Bed nucleus of the stria terminalis |
| Ca ²⁺ | Calcium |
| CeA | Central amygdala |
| CeL | Central lateral amygdala |
| CeM | Central medial amygdala |
| CGRP | Calcitonin gene-related peptide |
| CGRP-R | Calcitonin gene-related peptide receptor |
| ChR2 | Channelrhodopsin-2 |
| CMOS | Complementary metal-oxide-semiconductor |
| CNS | Central nervous system |
| CRH | Corticotrophin-releasing hormone |
| CS | Conditioned stimulus |
| DIO | Double floxed inverted open reading frame |
| DR | Dorsal Raphe |
| Drd1 | Dopamine receptor 1 |
| Drd2 | Dopamine receptor 2 |
| DVC | Dorsal vagal complex |
| Dyn | Dynorphin |
| Enk | Enkephalin |

Abbreviations

| | |
|-------------------|--|
| eYFP | Enhanced yellow fluorescent protein |
| FR1 | Fixed ratio 1 |
| GABA | gamma-Aminobutyric acid |
| GABA _A | gamma-Aminobutyric acid receptor A |
| GCaMP | Genetically-encoded Ca ²⁺ indicator |
| GRIN | Gradient refractive index |
| hGH-polyA | Human growth hormone poly A |
| Hip | Hippocampus |
| Htr2a | Serotonin receptor 2a |
| ICA | Independent component analysis |
| ICSS | Intracranial self-stimulation |
| InsCtx | Insular cortex |
| IPSC | Inhibitory post-synaptic current |
| IR-DIC | Infrared differential interference contrast |
| ITR | Inverted terminal repeat |
| LED | Light emitting diode |
| LH | Lateral hypothalamus |
| LiCl | Lithium chloride |
| IPBN | Lateral parabrachial nucleus |
| LPS | Lipopolysaccharide |
| mPBN | Medial parabrachial nucleus |
| MRN | Median raphe nucleus |
| NAc | Nucleus accumbens |
| NpHR | Halorhodopsin |
| NTS | Nucleus of the solitary tract |
| Nts | Neurotensin |
| pA | Pico ampere |
| PAG | Periaqueductal gray |
| PBN | parabrachial nucleus |
| PBS | Phosphate buffered saline |
| PCA | Principal component analysis |
| PFA | Paraformaldehyde |

Abbreviations

| | |
|--------------|---|
| PFctx | Prefrontal cortex |
| PKC δ | protein kinase C δ |
| PVH | Paraventricular hypothalamus |
| PVT | Paraventricular thalamus |
| RT-PCR | Real-time polymerase chain reaction |
| RTPP | Real-time place preference |
| SN | Substantia nigra |
| SOM | Somatostatin |
| Tac2 | Tachykinin 2 |
| US | Unconditioned stimulus |
| vIPAG | Ventrolateral periaqueductual gray |
| VPMpc | Parvicellular portion of the ventroposteromedial nucleus |
| VTA | Ventral tegmental area |
| WPRE | Woodchuck hepatitis post-transcriptional regulatory element |

Chapter 1

Introduction

1.1 Neural circuits controlling emotional behaviors

1.1.1 The amygdaloid complex

Behavioral reactions to salient stimuli including food, a predator, or a mate, are conserved across evolution and are critical for an animal's survival. In order to evoke the appropriate response to a specific stimulus, the animal must learn the significance of the stimulus and execute the correct action. The amygdala is a conserved brain region critical for the processing of emotionally salient stimuli and for the implementation of the appropriate behavioral responses [46]. The role of the amygdala was first described in seminal studies showing that monkeys and humans with amygdala damage were not able to identify and respond appropriately to salient events and cues in the environment [1, 4, 13, 54]. Therefore, these studies demonstrate the importance of amygdala in processing emotionally salient stimuli.

The amygdaloid complex is a collection of associated nuclei. These subregions can be distinguished based on their unique connectivity, neuronal physiology, and expression of

molecular markers. Throughout the history of amygdala research, two subnuclei have received the most attention: the basolateral amygdala (BLA) and the central nucleus (CeA) (Figure 1.1). For many years, the BLA and CeA were thought to function together, with the BLA receiving sensory information from the cortex and thalamus, with this information subsequently relayed onto the CeA which sends projections to motor autonomic control areas to elicit a behavioral response [27, 46, 34]. However, there is substantial evidence suggesting that the BLA and CeA do function independently, with the CeA also directly receiving sensory input [93, 102]. Thus, the amygdala does not appear to function as a single unit but rather as different nuclei serving different aspects of behavioral modulation. This view is supported by the marked difference in evolutionary origin of different amygdalar subregions, with the BLA being cortical and the CeA being striatal in origin. This suggests that the definition of the term "amygdala" is an arbitrary combination of cell groups rather than structural and functional units. It was suggested by Larry W. Swanson that "The amygdala is neither a structural nor a functional unit." [102]. However, despite major differences in their evolutionary origins and anatomical structures, recent studies brought a fresh perspective to the definition and function of brain regions including the amygdalar nuclei by identifying unique neuronal subtypes based on their genetic and molecular markers [3, 29, 39, 59]. These more recent approaches to defining neuronal populations based on genetic markers and how these tools improved our understanding of their functions will be further discussed in the following sections.

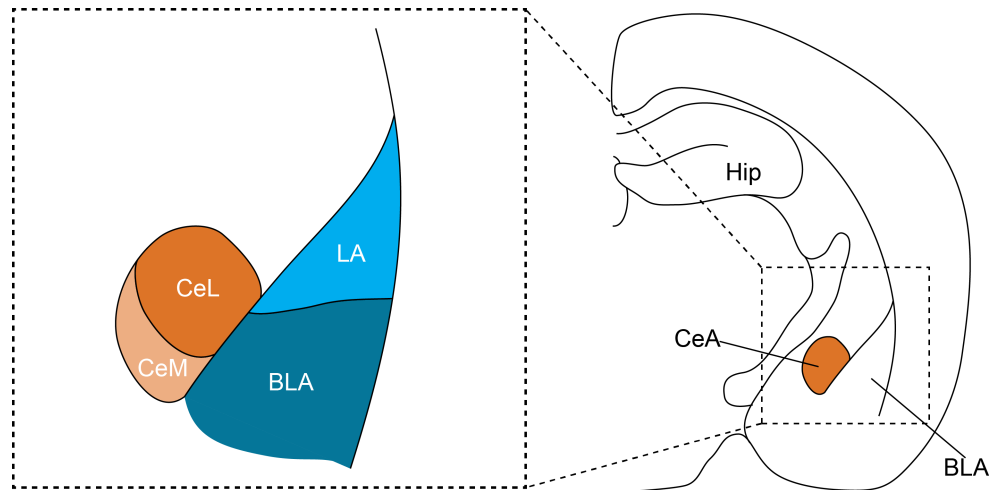


Figure 1.1: Anatomical organization of the amygdaloid complex. BLA: Basolateral amygdala, CeL: Central lateral amygdala, CeM: Central medial amygdala. Adapted from Sah et al. (2003) [93]

1.2 The central amygdala

1.2.1 Molecular architecture of the central amygdala

The CeA is morphologically divided into lateral (CeL) and medial nuclei (CeM) (Figure 1.1). Although neurons of the CeA are primarily GABAergic inhibitory neurons, many different neurotransmitters, neuropeptides, and receptors are expressed by CeA neurons (for examples see Figure 1.2). In order to classify CeA neurons into subpopulations and probe their function in behavior, previous studies have used molecular markers as a means to identify populations of neurons and target them *in vivo*. Some of these genes label non-overlapping neuron populations which have been shown to function in learnt fear behavior and feeding [3, 14, 39, 59]. However, it should be noted that within the CeA there is an overlapping expression of many markers in the same neuron, suggesting that this region is very heterogeneous and that classification using a single gene marker may have limitations. Further, it is not necessarily the case that expression of a given marker within a cell population reflects functional homogeneity. However, the use of modern neuroscience techniques to target molecularly defined cell types does have advantages, which will be

discussed further in the section 'Using optogenetics to probe neural circuits'.

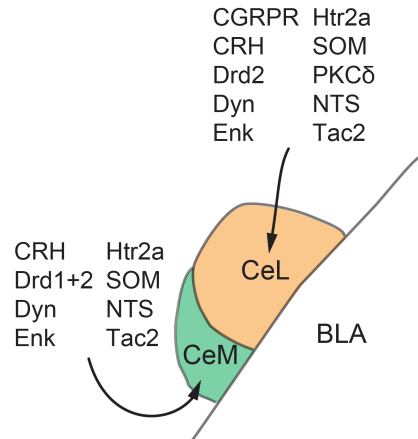


Figure 1.2: Molecular organization of the CeA. Example molecular markers used to identify subpopulations of CeA neurons and their location in CeL or CeM. BLA: Basolateral amygdala, CeL: Central lateral amygdala, CeM: Central medial amygdala, CGRP-R: Calcitonin gene-related peptide receptor, CRH: Corticotrophin-releasing hormone, Drd1+2: Dopamine receptor 1+2, Dyn: Dynorphin, Enk: Enkephalin, Htr2a: Serotonin receptor 2a, SOM: Somatostatin, PKC δ : protein kinase C- δ , NTS: Neurotensin, Tac2: Tachykinin 2. Adapted from: [18, 39, 53]

1.2.2 Physiological properties of central amygdala neurons

In addition to molecular classification of CeA cell types, previous studies attempted to classify CeA neurons based on their electrophysiological membrane properties. However, there was no consensus among these studies as to the properties that define different classes or what the distinct physiologies of CeA neurons mean in terms of functionality [93]. It is worth mentioning that lack of consensus on the electrophysiological characterization of CeA neurons could be due to the fact that studies used different recording methods in different animal species.

Schiess et al. (1993) described 2 main classes of neurons, so-called type A and type B, in the CeA using sharp electrode recording in rats. The majority of CeA neurons (74%) fell into Type A group. These neurons were those with no spike accommodation and displayed medium after-hyperpolarization potentials (medium-AHP). On the other hand, Type B neurons (26%) were accommodating and had both long duration slow-AHPs and

medium-AHPs [95, 96]. Furthermore, adding confusion to the classes defined by Schiess et al, in a mouse study by Tsetsenis and colleagues (2008) CeA neurons were reclassified as Type I and II by the presence or lack of depolarizing after-potentials (DAP) in a similar manner to the previous Schiess et al. (1993) study.

In another characterization effort, three distinct electrophysiological classes were identified in guinea pig, rat and mouse brain slices. The first class of neurons was named 'late firing' and displayed delayed firing upon current injection in whole-cell recordings (Figure 1.3). Most of the CeM (95%) neurons fell into this category. In contrast, only half of the CeL neurons showed late firing properties. The second class of neurons were termed regular spiking and fired their first action potential immediately after the current injection and kept a constant rate of firing afterward (Figure 1.3). 40% of CeL neurons were regular spiking. The third type, low-threshold bursting, was encountered rarely throughout the CeA (5%). This last class of neurons fired a short burst of action potentials right after depolarizing current injection. All three group of cells showed various degrees of AHPs [39, 63, 69].

1.3 Central amygdala circuitry

1.3.1 Microcircuitry

Despite the molecular and physiological heterogeneity of the CeA, major advances have been made in understanding the contributions of specific cell types in this region to behavior. Most knowledge about the circuitry within the CeA and with other brain regions has come from studies that used fear conditioning as a paradigm to investigate emotional learning and memory. This work involves the pairing of a neutral stimulus (the conditioned stimulus (CS)) with an aversive stimulus (unconditioned stimulus (US)). Over time, the

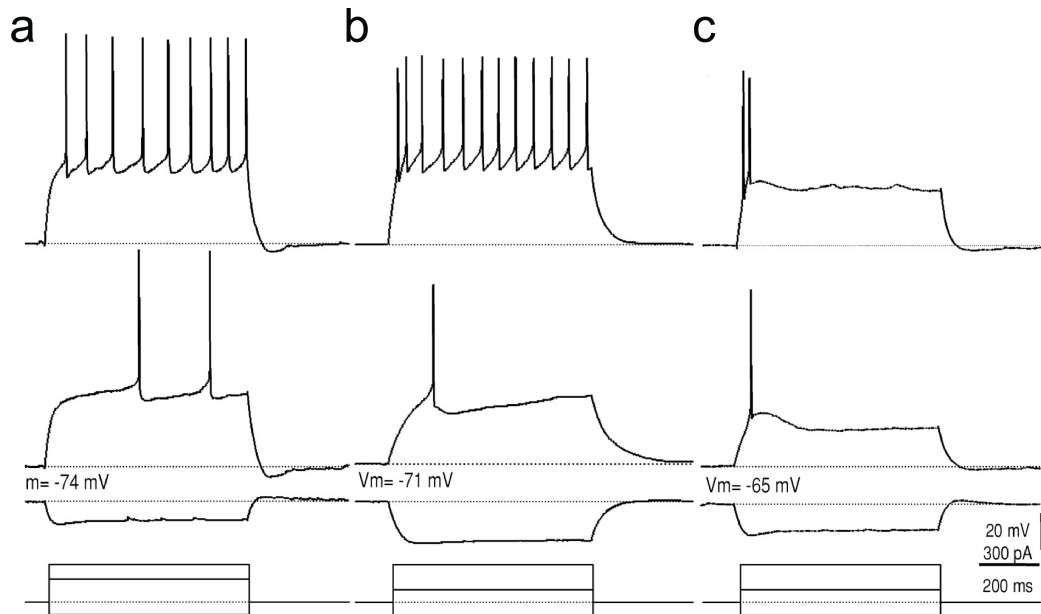


Figure 1.3: Electrophysiological properties of CeL neurons. Current clamp responses of three different types of CeL neurons to 600ms current injections of (-100, 200 and 300 pA (**A**)) or (-100, 100, 300 pA (**B, C**)). **A**) late firing neuron. **B**) regular spiking neuron. **C**) low-threshold bursting neuron. Modified from de Armentia *et al.* (2007) [63]

animal learns that these stimuli are associated, such that the CS alone will evoke fear behavior, most commonly defensive freezing responses in laboratory rodents. Classically, the BLA is considered the site where the CS and US association is made as synapses from sensory cortex and thalamus are potentiated in this region [82]. Upon CS presentation, projections from BLA to CeA then evoke the expression of the conditioned fear response through engagement of long-range CeA projections to the hindbrain and brainstem [58] (Figure 1.4). Even though the CeA has been viewed as the major output nucleus that relays information from BLA, a growing body of evidence has shown synaptic plasticity from the thalamus, parabrachial nucleus and lateral amygdala onto the CeA [50, 59, 64], suggesting this region can function independently of BLA input.

Within the CeA, reciprocal inhibitory connections between CeA neurons appear to be important for the processing of fear-related stimuli. The importance of intra-CeA connections was first shown by *in vivo* unit recordings, where two populations of CeA neurons with opposite responses to the CS were identified. Units excited by the CS were termed

CeL^{ON} units, while those inhibited by the CS were called CeL^{OFF} units. CeL^{ON} and CeL^{OFF} neurons were shown to inhibit each other which functions to gate the activity of output neurons in the CeM that control the behavioral expression of conditioned fear [22] (Figure 1.4). The likely molecular identity of CeL^{ON} and CeL^{OFF} neurons was subsequently resolved. CeL neurons that expressed protein kinase C δ (PKC δ) were equivalent to CeL^{OFF} neurons as their silencing during behavior boosted fear responses as predicted by the CeA microcircuit model [22, 39]. Conversely, CeL neurons expressing somatostatin (SOM) were shown to likely correspond to CeL^{ON} cells, as fear learning facilitated their activation by BLA neurons and CeA^{SOM} neuron activity was necessary for fear expression [59]. Both CeA^{PKC δ} and CeA^{SOM} neurons were shown to inhibit other neurons in the CeA, suggesting that local interactions were important for the function of the CeA in learnt fear [39, 59, 29, 28].

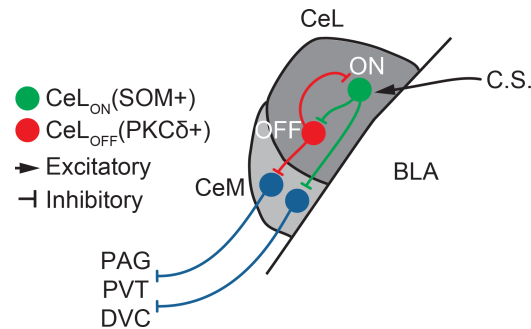


Figure 1.4: Central amygdala microcircuitry underlying learnt fear expression. Presentation of the CS excites CeL^{ON} (SOM+) neurons, which receive excitatory inputs from the LA. CeL^{ON} and CeL^{OFF} (PKC δ +) neurons, through reciprocal inhibitory inputs, gate the activity of CeM neurons that drive conditioned freezing through projections to the PVT, PAG, and DVC. CS: Conditioned stimulus, BLA: Basolateral amygdala, CeL: Central lateral amygdala, CeM: Central medial amygdala, PAG: Periaqueductal gray, PVT: Paraventricular thalamus, DVC: Dorsal vagal complex, SOM: Somatostatin, PKC: protein kinase C δ . Adapted from: [39, 34]

1.3.2 Inputs of the central amygdala

The amygdaloid complex as a whole receives input of multiple modalities including somatosensory, auditory, visceral and gustatory, olfactory and visual. The traditional

view of information flow in the amygdala denotes the BLA as the primary receiver of sensory input with the CeA coordinating the behavioral output. However, contrary to this view, the CeA itself receives many sensory inputs, demonstrating that this region is a key convergence point for sensory information. The CeA receives prominent inputs from the insular cortex, gustatory thalamus (parvocellular portion of the ventroposteromedial nucleus), the nucleus of the solitary tract (NTS) and parabrachial nucleus (PBN) which relay gustatory and visceral inputs [49, 31]. Somatosensory inputs also arise from the insular cortex and the PBN as well as directly from the BLA [38, 46, 31] (Figure 1.5). The CeA also receives multimodal inputs from the hippocampus and cortical areas including the prefrontal cortex as well as the paraventricular thalamus (PVT) [26, 93]. Inputs arising from hypothalamic regions including the arcuate nucleus also converge on the CeA and may be involved in the regulation of homeostasis [8] (Figure 1.5). The CeA also receives input from multiple neuromodulatory systems including the ventral midbrain dopaminergic system and the dorsal raphe [30, 86, 105] (Figure 1.5). Thus, the CeA receives a wide range of inputs from numerous different brain regions. This suggests that the CeA likely plays an important role in many different behavioral and autonomic processes.

1.3.3 **Outputs of the central amygdala**

Although the simplified model of information processing in the CeA suggests that efferent projections that execute conditioned fear responses arise from the CeM, there are also studies that document direct long-range projections from the CeL bypassing the CeM [93], suggesting that the influence over behavior by the CeA is more complicated than previously thought. Seminal anatomical studies have shown that the CeA sends long range projections to tegmental nuclei, mesencephalon, hypothalamus and pons as

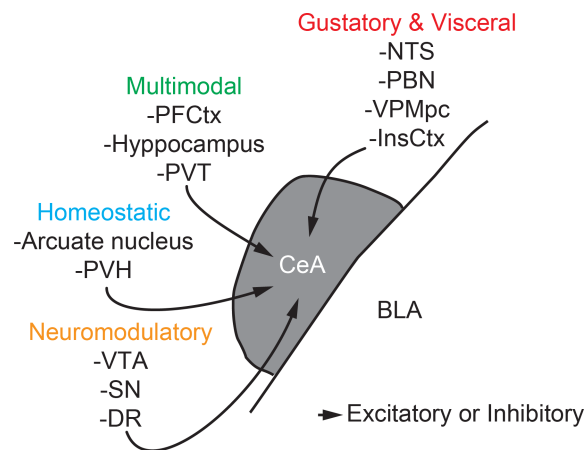


Figure 1.5: Long-range inputs to the CeA. BLA: Basolateral amygdala, CeA: Central amygdala, NTS: Nucleus of the solitary tract, PBN: Parabrachial nucleus, VPMpc: parvicellular portion of the ventroposteromedial nucleus, InsCtx: Insular cortex, PFCtx: Prefrontal cortex, PVT: Paraventricular thalamus, PVH: Paraventricular hypothalamus, VTA: Ventral tegmental area, SN: Substantia nigra, DR: Dorsal Raphe.

well as brainstem, with strong areas of innervation including the posterior hypothalamus, substantia nigra, ventral tegmental area (VTA), periaqueductal grey (PAG), PBN, PVT, bed nucleus of the stria terminalis (BNST), locus coeruleus as well as the NTS and dorsal motor nucleus of the vagus nerve in brainstem [33, 41, 58, 93] (Figure 1.6). The projection targets of the CeA are implicated in a suite of different behaviors including fear, anxiety, feeding, reward, and gustatory processing. Therefore, the neural circuits in which the CeA is embedded suggest a role for this region in the integration and execution of somatic and autonomic responses. Additionally, the functional diversity of regions innervated by CeA neurons implies a role for this region in diverse behaviors, many of which have not been thoroughly explored.

The projection targets of CeA neurons differ from those of the BLA, which sends a minor projection to the brainstem but more densely innervates cortical regions [41] which may reflect their different functions in fear learning and expression. There also appears to be a dissociation between CeL and CeM subregions in terms of projection targets, as only the CeM projects to tegmental nuclei [41], while both the CeL and CeM project to the PAG [91]. Further work is needed to determine the nature of the projections arising

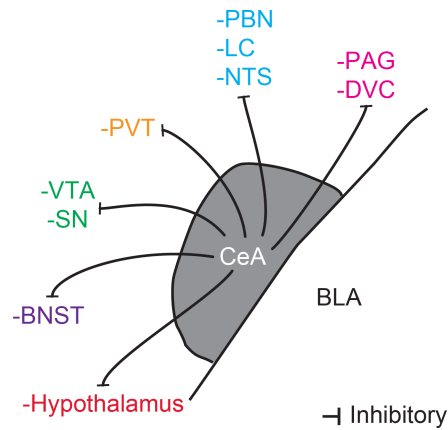


Figure 1.6: Long-range outputs of the CeA. BLA: Basolateral amygdala, CeA: Central amygdala, PAG: Periaqueductal gray, DVC: Dorsal vagal complex, PBN: Parabrachial nucleus, LC: Locus coeruleus, PVT: Paraventricular thalamus, VTA: Ventral tegmental area, SN: Substantia nigra, BNST: Bed nucleus of stria terminalis.

from the CeL versus the CeM and how this is important for orchestrating a behavioral response.

1.4 Central amygdala-brainstem interactions

1.4.1 Control of food intake

The position of the CeA as a circuit node that receives sensory input of various modalities and strongly innervates a diverse array of brain regions suggests that this region may function in other behaviors aside from the expression of learnt fear. Indeed, the CeA plays an important function in a neural circuit that governs eating behavior in response to malaise signals. The malaise pathway is critical for animal survival as activation of this circuit after ingestion of toxic compounds or during sickness functions to suspend eating behavior until conditions are favorable again. Malaise signals relayed from the gastrointestinal tract by the vagus nerve reach the nucleus of the solitary tract (NTS) in the brainstem which then conveys this information onto the PBN. The PBN is a heterogeneous region involved in the processing of gustatory signals and in appetite, pain, and thermosensation. The PBN sends dense projections to the CeA which appears to

be a critical component of the malaise circuit. Calcitonin gene-related peptide (CGRP)-expressing PBN neurons are activated by the malaise-inducing compounds lithium chloride (LiCl) and lipopolysaccharide (LPS) which strongly suppress appetite when administered to mice by intraperitoneal injection [17]. This effect is mediated through an efferent projection from the PBN to neurons in the CeA that express PKC δ (Figure 1.7). Activation of these neurons strongly inhibits feeding [14]. The mechanism by which CeA^{PKC δ} neurons mediate appetite suppression is not yet clear since activation of their main efferent projections to the BNST and PBN did not suppress feeding [14]. Blocking of intra-CeA inhibition using the GABA_A antagonist bicuculline abated the effect of CeA^{PKC δ} neuron activation. This suggested that CeA^{PKC δ} neurons mediated their effects locally by inhibiting other CeA neurons and that CeA^{PKC δ -negative} neurons may act to promote food consumption (Figure 1.7). Indeed, use of a 'Cre-out' strategy in which expression of the neural activity silencer halorhodopsin is restricted to Cre-negative (ie. CeA^{PKC δ -negative}) cells, to manipulate CeA^{PKC δ -negative} neurons suggested that this may be the case. However, activation using channelrhodopsin of two specific CeA populations considered to be predominantly PKC δ -negative: corticotrophin-releasing factor (CRF)-expressing and Tachykinin 2 (Tac2)-expressing neurons did not promote food consumption [14]. It is important to note that approximately 40% of both the CRF and Tac2 population also express PKC δ , demonstrating that efforts to identify and investigate the function of neurons that are mutually exclusive from CeA^{PKC δ} cells are required to fully understand the role of the CeA in food intake.

The dense innervation of the CeA by the PBN suggests a key role for this region in processing gustatory signals. However, this interaction is bidirectional with a large reciprocal connection extending from the CeA to PBN, originating from both CeL and CeM divisions [67]. The existence of this projection suggests that the CeA may send feedback or modulatory signals to the same region from which it receives sensory signals

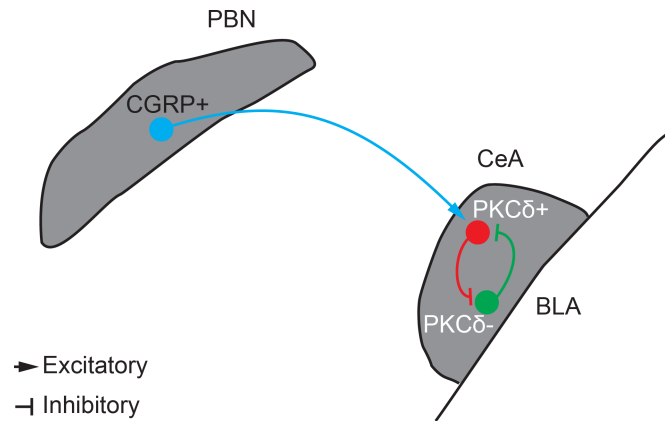


Figure 1.7: CeA-PBN interactions in the control of food consumption. PBN CGRP+ neurons suppress appetite under anorexigenic conditions through excitatory projections to PKC δ + neurons in the CeA. PKC δ + neurons were proposed to inhibit feeding through inhibition of PKC- CeA neurons. BLA: Basolateral amygdala, CeA: Central amygdala, PBN: Parabrachial nucleus, PKC δ : Protein Kinase C, CGRP: Calcitonin gene-related peptide. Adapted from: [14, 17]

to control its own activity. This projection is proposed to exert a modulatory effect on gustatory processing in the PBN as electrical stimulation of the CeA has been reported to modify the activity and tuning properties of PBN neurons to specific tastes [65]. However, the behavioral significance of these effects and whether processing of other modalities such as pain and appetite can be modulated by the CeA is unclear.

1.4.2 Pain processing

Interactions between the CeA and PBN are also important for the processing of painful stimuli. Pain information is relayed from the periphery to the forebrain by two parallel pathways. Neurons in lamina 1 of the spinal cord send input to the sensory thalamus, relaying sensory pain signals [44]. This pathway has been studied in the context of fear conditioning as sensory input about the US (usually a pain-inducing footshock) is conveyed onto the BLA from the thalamus [98]. There is also a parallel pathway, that transmits the affective-motivational features of pain from the spinal cord to the PBN and onto the CeA. Interestingly, the same PBN^{CGRP} neurons that inhibit feeding through the CeA also transmit pain signals and are responsible for conveying the US signal to the CeA

during fear conditioning when a painful stimulus is used [38]. It was additionally shown that neurons in the CeA that express the CGRP receptor receive the US signal and are responsible for the memory of the painful stimulus [38]. Interestingly, approximately 20% of the CeA^{CGRP-R} neurons express PKC δ , suggesting that anorexigenic and affective pain signals may be processed by different subpopulations of PBN and/or CeA neurons.

1.5 Using optogenetics to probe neural circuits

1.5.1 Tools and strategies for targeting neurons

A challenge for investigating the function of any brain region is that many areas are comprised of heterogeneous populations of neurons, many with opposing functions. Thus, the difficulty lies in targeting and manipulating selected populations of neurons in a specific manner. The central amygdala is no exception. Given that neurons of opposing function in learnt fear responses reside alongside one another, the possibility remains that other classes of functionally heterogeneous neurons also exist in this region. Since Ramón y Cajal discovered that the nervous system is composed of individual neurons that have broad diversity with respect to size, morphology, connectivity and projections, it has been a challenge to understand what mechanisms are responsible for this diversity and how to classify the neurons of the CNS. The characteristics used to classify neurons into subpopulations remains subjective and varies from study to study including projection target, morphology, and activity during behavior. One common feature used to define a neural subpopulation is expression of cellular markers including neuropeptides, receptors, and other genes. This has become a common approach due to the availability and relative ease of generation of mice that are genetically engineered to express a gene of interest under a specific promoter, generated via transgenic or knock-in approaches [42]. Using

these approaches, the bacteriophage enzyme Cre recombinase is targeted to neurons that express the gene of interest. Cre-expressing mice are used to express protein-based tools in a neuron population of interest that allow activity manipulation, circuit mapping or visualization of neural activity. These tools are stereotaxically delivered into the brain by engineered adenoassociated viruses (AAVs) that carry these tools flanked by inverted lox sites which are recognized by the Cre enzyme, allowing expression only in Cre-expressing neurons (Figure 1.8). Thus, the use of Cre-expressing mice in combination with AAVs is a powerful way to target specific populations of neurons *in vivo*. It should be noted that the approach of using a genetic marker to classify neurons is inherently biased as it assumes that genetic homogeneity is equivalent to functional homogeneity, which may not always be the case. However, this approach has provided significant insight into the function of specific neural circuits especially within brain regions containing heterogeneous neuron populations.

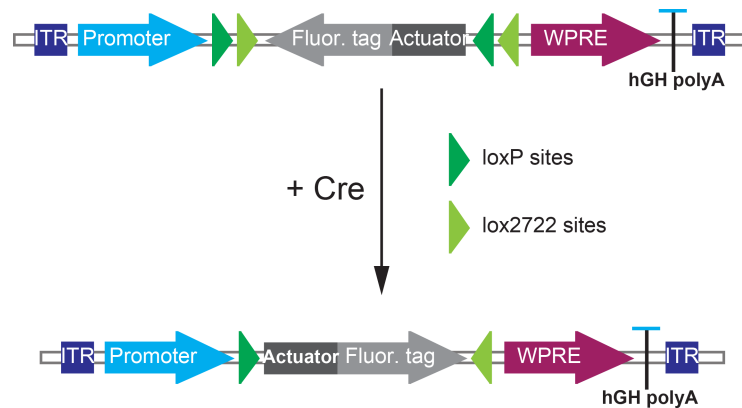


Figure 1.8: Scheme of Cre-dependent adenoassociated virus. Actuators for manipulation or imaging of neural activity, often with a fluorescent tag, are flanked by double inverted lox sites, allowing expression of the actuator in the presence of Cre. ITR: Inverted terminal repeat, WPRE: woodchuck hepatitis post-transcriptional regulatory element, hGH polyA: Human growth hormone poly A. Adapted from https://web.stanford.edu/group/dlab/optogenetics/sequence_info.html.

1.5.2 Brief history of optogenetics

Although throughout history, the brain has been functionally compartmentalized based on morphological landmarks, this has proved a challenge for neuroscientists as the brain, for the most part, inherently lacks organized structure. As a network of neurons entangled with one another, it has been most challenging for the electrophysiological study of brain circuits. For decades it was not possible to stimulate one single region of the brain without affecting nearby regions due to the high degree of interconnectivity and dense fibers of passage that traverse the brain. Fundamental changes to the neuroscience field came in 2005 when it was shown that the activity of a target population of neurons could be specifically controlled in behaving animals [60]. This study, and many others that followed employed light-activated microbial opsins that when expressed in the neurons of choice, allow their activity to be controlled by light. This technology termed optogenetics allowed neuroscience to enter the age of light. Optogenetic tools have fundamentally changed not only how neuroscience was done but also the kind of neuroscientific questions asked. Neurons can be selectively manipulated with temporal and spatial specificity with millisecond precision, allowing their function in specific aspects of behavior to be assessed. Additionally, the targeting of optogenetics tools to specific neurons allows cell type-specific circuit mapping and manipulation studies which were previously not possible with conventional electrical recording methods. With the advancement of the cell targeting strategies, such as the Cre/lox system, as well as viral delivery methods, using optogenetics became the method of choice for modern neuroscientists [42]. Today, the ever increasing number of Cre-expressing mouse lines to target specific cell populations and the large range of viral vectors to deliver any Cre-dependent opsins on the market has made this technology particularly powerful.

1.5.3 Optogenetic actuators

The optogenetic activation of neurons is most commonly achieved using channel-rhodopsin-2 (ChR2), a light-gated passive cation channel with rapid kinetics [12]. Since its first characterization [75], it has been developed further by codon optimization to achieve higher expression levels in mammalian cells [76]. The most commonly used version has an introduced H134R mutation that resulted in a ChR2 that has stronger photocurrents but slower kinetics [74]. It can drive low-frequency spike trains precisely in neurons. Upon light activation, ChR2 facilitates the flow of cations into the cell, thus, having a net depolarizing effect. Since it allows passage of cations unselectively as long as it is open, it does not require energy expenditure. It has an optimum excitation wavelength peaking at 470nm [76]. When expressed in neurons, light-induced depolarizing currents will lead to the generation of axon potentials [12]. The precise control with light enables temporal precision when stimulating neurons. In addition to its ability to activate neurons when light is introduced onto the cell bodies, independent studies have demonstrated that axonal terminals could independently generate action potentials even when separated from the cell body [5, 85].

Inhibition of neurons is achieved by use of halorhodopsin (NpHR), a chloride pump maximally activated at 590nm [110] and archaerhodopsin (Arch), which is activated by 560nm light and pumps protons out of the cell [21]. Both silencers have similar light sensitivities and kinetics and when expressed in neurons produce a hyperpolarizing current within the cell that decreases the overall firing rate of the cell [70]. However, Arch has been shown to generate larger photocurrents but is less efficient than NpHR for pre-synaptic terminal-specific silencing as sustained inhibition using Arch leads to an increase in spontaneous neurotransmitter release [68]. Conversely, prolonged activation of NpHR has also been shown to allow postsynaptic spiking [89]. However, despite these caveats,

both NpHR and Arch effectively silence neurons *in vivo* and produce behavioral consequences as a result.

1.5.4 Channelrhodopsin-assisted circuit mapping

For centuries neuroscientists have been using anatomical tracing techniques to map the connectivity between brain regions and known cell types, including methods for anterograde and retrograde tracing. Using these techniques it is possible to target neurons with Cre-dependent fluorophores, bulk filling them with membrane permeable dyes to trace their collateral axons to map their outputs [19, 34]. On the other hand, retrograde tracers such as cholera toxin subunit B [23] or retrogradely traveling beads [51, 52] have been extensively used to identify inputs to any given brain region. Furthermore, the addition of new viral tracing techniques to the toolbox has increased the scope and specificity of anatomical tracing experiments. Perhaps the most useful of these is the pseudo-rabies tracing strategy [15, 108] which allows mapping of the monosynaptically-connected input neurons to a genetically identified neuronal subpopulation. However, these anatomical mapping strategies come with their individual limitations. Even though they are useful for setting out an initial connectivity map, they fail to address the functionality of the proposed connections. Furthermore, it is not possible to investigate the synaptic strength or neurotransmitter profiles involved using these anatomical tracing methods.

A different approach, targeted patch clamp recordings in brain slices, has proven to be a very useful tool to map connections between neurons. Using this method, the type of synaptic transmission can be determined with single cell resolution. Additionally, it is possible to determine the identity of the recorded cells using post-hoc immunohistochemical staining [31, 94] or single cell RT-PCR [87]. Despite the advantages of electrophysiological recordings, using electrical stimulation to activate presynaptic terminals of potential

inputs is unspecific as axon bundles usually are not well organized in many brain regions. This approach of recording multiple potential pre- and post-synaptic neurons in brain slices has proven to be useful in cortical areas which have a layered, organized structure and where the connection rate is high. However, overall this approach is deemed to be an inefficient and slow method to map cell specific connections [85].

The caveats of anatomical and electrophysiological-based mapping have been overcome by the use of optogenetic technology in circuit mapping studies. One of the most prominent applications of optogenetics is to identify connections between neurons in the same or nearby regions as well as investigating the connectivity at a mesoscale level between distant regions of the central nervous system. Optogenetics permits neuronal circuit mapping at cellular precision, *in vitro*, in acute brain slices and, *in vivo*, in the freely behaving intact animal. Using this method, optogenetics is used to stimulate a specific population of presynaptic neurons and their connectivity to other neurons is assessed by electrical recordings in individual postsynaptic cells. Use of optogenetics to investigate neural circuit connectivity has been successfully applied in different brain regions including cortex [85], hypothalamus [5] and amygdala [39].

1.5.5 *in vivo* Optogenetics

Another challenge encountered by neuroscientists is understanding how a brain region of interest contributes to behavior. Conventional methods for addressing this question include electric stimulations, lesions, and drug infusions but these approaches fail to appreciate the intrinsic neuronal heterogeneity of any give brain structure and thus, fail to capture the underlying mechanisms. Additionally, the complex connectivity patterns within the brain mean that such manipulations not only affect cells within the target region but also fibers of passage that traverse between and through different areas.

Use of optogenetics *in vivo* to manipulate the activity of specific groups of neurons within a certain brain area in behaving animals has allowed a much more precise dissection of the neural circuits underlying behavior than was previously possible. Most commonly, Cre-expressing mice with the opsin of choice expressed in a particular neuron population are chronically implanted with optic fibers above the target structure to deliver light into the brain. Optic fibers can also be placed above an efferent projection field of the neurons of interest in order to determine the function of a specific output projection [47, 57, 80]. The light is delivered into the brain from lasers or LEDs through optic fiber cables that are connected to the implanted fibers or via remotely-powered wireless LED systems [72]. Use of optogenetics *in vivo* offers many advantages including the time-locked manipulation of neural activity to dissect neuron function in a specific aspect of behavior but importantly it allows a thorough investigation of brain regions that contain functionally heterogeneous cell populations.

1.5.6 Considerations when using optogenetics

The revolution in neuroscience research brought about by optogenetics has allowed detailed insight into neural circuits. However, as with all technological innovations, certain limitations must be considered. The way in which optogenetics is most commonly used, namely the simultaneous manipulation of a defined group of neurons, is unlikely to reflect the natural circuit dynamics. Bulk activation of neurons can alter the network properties and the physiology of neighboring neurons in the local circuit. Since these undesired effects are unpredictable, they may complicate the interpretation of the resulting circuit manipulation and its link to the observed behavior [81]. Further, such manipulations likely do not reflect the endogenous activity patterns of neurons during behavior, since optogenetic activation parameters rarely match the recorded *in vivo* firing patterns.

The delivery of high powered light may induce unnaturally large depolarizing photocurrents and high-frequency stimulation may drive action potential firing at unphysiological frequencies. Both of these factors may have adverse effects on the network and complicate the interpretation of behavioral experiments. High-powered light may also lead to local heating of the brain tissue which has been shown to affect the physiology of neurons [2]. Additionally, the penetration of light from an implanted optical fiber is not homogeneous, meaning that neurons will be differently affected depending on the distance from the source [88].

1.6 Using Ca^{2+} imaging to probe neural circuits

Neural activity manipulation strategies such as optogenetics as discussed above provide causal information. However, without an appreciation of the *in vivo* activity dynamics of neurons of interest, no context is provided in which to interpret neural activity manipulation and thus, it is difficult to interpret how these neurons control behavior. *in vivo* electrophysiology and calcium (Ca^{2+}) imaging approaches are thus commonly used to reveal the activity dynamics of specific neural populations. Ca^{2+} imaging takes advantage of the fact that Ca^{2+} levels inside a neuron fluctuate with neural activity. In the inactive state, Ca^{2+} levels are relatively stable. However, upon membrane depolarization, Ca^{2+} levels inside the cell rise [6, 103]. Intracellular Ca^{2+} levels can be read out by use of genetically-encoded proteins called GCaMPs which bind to Ca^{2+} and emit fluorescent signal [20, 77].

The benefits of using electrophysiology or Ca^{2+} imaging approaches depends on the application but the major differences are in terms of temporal and spatial resolution. While electrophysiology methods measure voltage changes across the membrane, GCaMP fluorescence does not correlate with voltage changes and is therefore only a proxy for

neuronal activity [37]. The parallels that can be drawn between neural spiking and Ca^{2+} changes largely depend on two factors: 1) The sensitivity and kinetics of the Ca^{2+} indicator. Of the currently available GCaMP variants, GCaMP6f (f = fast) has the fastest kinetics and so is the best tool to approximate neural spiking [20]. 2) The specific properties of the neurons with respect to Ca^{2+} buffering, signaling and spike rate influences the Ca^{2+} transient dynamics and thus the ease with which spike rates can be extrapolated from Ca^{2+} transients [37]. The spatial resolution afforded by Ca^{2+} imaging is an important advantage of this technique. The Ca^{2+} activity of large numbers of neurons can be recorded simultaneously and their relative locations are known. Furthermore, Ca^{2+} transients in subcellular structures can be resolved eg. soma, axons, dendrites and dendritic spines [35]. Electrophysiology approaches are essentially blind to the precise anatomical location of recorded neurons and very few neurons can be recorded simultaneously within the same animal. Thus, Ca^{2+} imaging and electrophysiology techniques for recording neural activity have distinct benefits and disadvantages that will be differentially important depending on the biological question.

The implementation of Ca^{2+} imaging in living, behaving animals is most commonly achieved by several methods. The first is two-photon microscopy which circumvents one of the major issues associated with Ca^{2+} imaging- the light scattering properties of brain tissue which is a major issue for conventional single-photon excitation. Two-photon imaging uses fast scanning near-infrared light to excite the Ca^{2+} sensor. This provides several advantages including 1) spatial focusing of excitation which reduces scattering and thus reduces background signal, 2) deeper tissue penetration, 3) increased resolution [25, 40]. Despite these advantages, several factors restrict the application of two-photon imaging. First, imaging is performed using a conventional microscope objective, which means that the animal must be head fixed under the objective. Although this has advantages, as the behavioral repertoire of the animal engages can be easily controlled, the limited range of

movements may only be ideal for specific applications. Secondly, this method has been used to successfully image Ca^{2+} activity up around 600 μm below the cortical surface [40] which means that deeper structures must be accessed using a prism or relay lens to focus the light and resolve images at some distance from the objective (see below).

Two recent methods have allowed access to deep brain structures permitting their interrogation with Ca^{2+} imaging. Fiber photometry allows measurement of population-scale changes in the fluorescent signal via an implanted optical fiber [36]. A caveat of this approach is that heterogeneity within a population is masked as the global signal is collected. Thus, this technique is well-suited to measuring Ca^{2+} changes from axon terminals and to gain an indication as to the activity dynamics of a neural population of interest. For cellular-resolution imaging of deep-brain structures in freely-moving animals, GRIN (gradient refractive index) lenses are implanted above the GCaMP-expressing population of interest. GRIN lenses relay GCaMP fluorescent signal from deep-brain structures as their refractive properties guide and focus light [7], with changes in the GCaMP signal recorded by a miniaturized microscope that is mounted on the animals head with an integrated LED for GCaMP excitation and a CMOS (complementary metal-oxide-semiconductor) sensor for image acquisition [32]. The image quality is poor compared to two-photon imaging due to the use of single-photon excitation, which produces extensive out-of-focus, scattered light, while the free movement of the animal permitted by this technique can lead to brain motion artifacts. Despite these shortcomings, isolation of single cells and reliable Ca^{2+} transients has been consistently achieved [34, 90, 19]. Thus, this technique has afforded new insights into the activity dynamics of neural populations with cellular resolution in deep-brain structures.

Chapter 2

Thesis Objectives

The central amygdala has a well-characterized role in modulating aversive behaviors such as fear and anxiety. However, the amygdala has also been shown to modulate reward-related behaviors, since the same manipulations and ablations affect both aversive and reward-related behaviors. This is true for the amygdala as a whole but also for the CeA specifically, since manipulations of this region elicit a range of different behavioral effects [11, 56, 83, 109]. In addition to behavioral studies, the fact that the CeA receives a wide variety of information from diverse brain regions is suggestive of a general role in the integration of input signals of different types. It can be appreciated, from the molecular and electrophysiological diversity of neurons, that the CeA is a heterogeneous brain region. The array of behaviors potentially modulated by this region suggests that specific neurons within this region and their associated circuits may underlie specific behaviors.

The use of the expression of molecular markers as a means of defining CeA neural subpopulations has allowed the functional description of a number of CeA subpopulations [10, 14, 39, 59, 71]. Since CeA^{PKC δ} neurons were one of the first described populations, it is accepted within the field that CeA neurons can be functionally divided into PKC δ + and

PKC δ -negative neurons. However, most neural populations that are considered PKC δ -negative, are actually not mutually exclusive, as between 15 and 40% of the neuron in each of the populations also express PKC δ [14, 59]. This suggests that other approaches must be taken to define CeA^{PKC δ -negative} neuron populations.

The first aim of my thesis was to identify and characterize a novel subpopulation of CeA^{PKC δ -negative} neurons that would be mutually exclusive from PKC δ . In doing so, I identified an as yet little described population of CeA neurons that expresses the Cre recombinase under control of regulatory elements of the gene encoding the serotonin receptor Htr2a. The pattern of Cre expression in this line did not overlap with PKC δ . I further characterized these neurons molecularly, by determining the overlap with other described populations of CeA^{PKC δ -negative} neurons. I also performed whole cell recordings of CeA^{Htr2a} neurons in acute brain slices to determine their electrophysiological properties. In order to understand the integration of CeA^{Htr2a} neurons in the local CeA circuit, I used ChR2-assisted circuit mapping to map their local connectivity within the CeA and specifically determined the connectivity between these and CeA^{PKC δ} neurons.

Given that, CeA^{PKC δ} neurons are implicated in reducing food consumption under anorexigenic conditions [14], I hypothesized that CeA^{Htr2a} neurons may functionally antagonize CeA^{PKC δ} neurons. I, thus, determined whether the endogenous activity dynamics of CeA^{Htr2a} neurons indicates an involvement of these neurons in positively regulating food intake. To do so, I used *in vivo* Ca²⁺ imaging using a GRIN lens to access the CeA in conjunction with a head-mounted miniaturized microscope to record Ca²⁺ dynamics in CeA^{Htr2a} neurons in freely behaving mice.

The Ca²⁺ imaging experiments suggested that CeA^{Htr2a} neurons may function in food consumption. Thus, to gain an insight into the neural circuits in which these neurons function, I used *ex vivo* ChR2-assisted circuit mapping to probe the prominent long-range

efferent projections of CeA^{Htr2a} neurons. I combined these experiments with retrograde tracing methods from the output regions, in order to validate the specificity of these projections. I was interested in understanding how projections from PKC δ + and PKC δ -negative neurons differ given that these two populations have been proposed to function antagonistically. To do this, I compared the projections of CeA^{PKC δ} and CeA^{Htr2a} neurons both anatomically and electrophysiologically. Based on the results of these experiments I focused on the projection from the CeA to the PBN. Interestingly, although this is one of the largest projections from the CeA, I found this projection to predominately arise from PKC δ -negative neurons. These and previously published data indicate the presence of a loop between with PBN and CeA with PBN neurons giving input largely to CeA^{PKC δ} while CeA^{Htr2a} neurons projecting back to the same output region. This suggests that CeA^{Htr2a} neurons may modulate the activity of the PBN and thus, the input coming into the CeA. To explore this further, I ascertained the molecular identity of PBN neurons inhibited by CeA^{Htr2a} neurons to determine if they are the same neurons that provide CeA input.

Finally, to assess the functionality of the CeA^{Htr2a} PBN projection I used *in vivo* optogenetics to specifically activate the terminals of CeA^{Htr2a} neurons in the PBN. I focused on the role of this projection in feeding-related behaviors considering that malaise and satiety signals are relayed to the forebrain from the PBN and that inhibition of this region by CeA^{Htr2a} neurons may modulate such behaviors. Further, since the PBN processes negative valence signals of different modalities including pain and sickness [38, 44, 97], I considered that inhibition of the PBN may have appetitive consequences and so focused on the modulation of feeding and reward behaviors by the CeA. Overall, this work has shed light on a population of CeA neurons that are exclusively PKC δ -negative and provided insight into the different anatomical circuits in which CeA^{PKC δ} and CeA^{Htr2a} neurons function. Furthermore, the *in vivo* optogenetic experiments have provided insight

into the functionality of PBN inhibition by the CeA and provide a circuit mechanism for how modulation of feeding and reward occurs by reciprocal interactions between the CeA and the brainstem.

Chapter 3

Methods

3.1 Animal subjects

Mice were housed on a 12 hour cycle (7am lights on) with *ad libitum* food access except experiments involving food restriction. All animals were in accordance with the regulations of the government of the Upper Bavaria. For behavior and imaging experiments 1-4 month old mice were used. Mice used in these experiments were single housed after implantation surgeries. Behavior assays were conducted during light cycle (8am-1pm). Mice used for behavior experiments were male whereas females were used for imaging experiments exclusively. For electrophysiology and tracing experiments 5-8 weeks old mice were used. A mixture of males and females were used for these experiments.

The Htr2a-Cre BAC transgenic line (STOCK Tg[Htr2a-Cre] KM208Gsat/Mmucd) was imported from the Mutant Mouse Regional Resource Center. *Td-Tomato* (B6.Cg-Gt(ROSA) 26Sortm9(CAG-tdTomato)Hze/J) [66, 73] and *Rosa26R* [99] mouse lines were described previously. *PKC-Cre* (Tg(Prkcd-glc-1/CFP,-Cre)EH124Gsat) BAC mice were purchased from The Jackson Laboratory.

3.2 Viral constructs

Cre-dependent AAV vectors expressing ChR2-eYFP and eYFP, AAV5-Ef1a-DIO-ChR2-eYFP and AAV5-Ef1a-DIO-eYFP, respectively, were obtained from the Gene Therapy Center Vector Core at the University of North Carolina Chapel Hill. The AAV2/9-Ef1a-DIO-GCaMP6s-eYFP viral construct was obtained from University of Pennsylvania Vector Core.

3.3 General practice for stereotaxic surgeries

Mice were anesthetized for surgery with isoflourane (1.5-2%) and Carprofen (5 mg / kg bodyweight) was administered. Animals were then placed in a stereotaxic frame (Kopf Instruments). During the surgery procedure body temperature was maintained at 37°C using a heating pad (Fine Science Tools).

3.4 Stereotaxic surgeries

For *ex vivo* and *in vivo* optogenetic experiments, mice were bilaterally injected with 250-500 nl of virus in the CeA using the following coordinates with respect to bregma: -1.22 mm anteroposterior, 2.8 mm lateral, -4.72 mm ventral. For *ex vivo* experiments, the incision was closed with sutures at the end of the surgery. These mice were sacrificed after 3-4 weeks after the surgery to allow enough time for viral construct to express ChR2 in Cre+ neurons. For *in vivo* optogenetic experiments, mice were bilaterally implanted with optic fibres (200 μ m core, 0.22 NA, 1.25 mm ferrule (Thor labs)) above the CeA (-4.2 mm ventral) or PBN (-5.1 mm anteroposterior, 1.7 mm lateral, -3.0 mm ventral) during the same surgery session where virus was delivered. Skull of the animal was scored to create

a rough surface using a scalpel. Fiber optic implants were secured onto the skull using cyanoacrylic glue. Once the glue was set, exposed skull was covered with dental cement (Paladur).

3.5 Acute brain-slice preparation

The mice were deeply anesthetized by intraperitoneal injection of Ketamine/Xylazine mixture (100 mg/kg and 10 mg/kg body weight, respectively) and transcardially perfused with ice-cold protective cutting solution containing: 92 mM N-methyl-D-glucamine (NMDG), 2.5 mM KCl, 1.25 mM NaH₂PO₄, 30 mM NaHCO₃, 20 mM HEPES, 25 mM glucose, 2 mM thiourea, 5 mM Na-ascorbate, 3 mM Na-pyruvate, 0.5 mM CaCl₂·4H₂O and 10 mM MgSO₄·7H₂O (305-310 mOsm). Coronal brain sections of 200-250 μ m thickness were cut with a vibratome (Leica, VT1000S) in ice-cold cutting solution. Slices were recovered for 15 minutes at 32°C in the cutting solution. After recovery slices were kept in regular aCSF containing 126 mM NaCl, 1.6 mM KCl, 1.2 mM NaH₂PO₄, 1.2 mM MgCl₂, 2.4 mM CaCl₂, 18 mM NaHCO₃, 11 mM glucose (305-310 mOsm), oxygenated with carbogen at room temperature until recording.

3.6 Slice electrophysiology

Slices were visualized using fluorescent microscope with IR-DIC optics (Olympus BX51). All electrophysiological recordings were performed in a chamber constantly superfused with carbogenated regular aCSF at 30-32 °C. Whole-cell voltage and current-clamp recordings were performed with a MultiClamp 700B amplifier. Data were digitized and acquired using Digidata 1550 (Molecular Devices), and sampled at 10 kHz, filtered at 2.0 kHz.

The patch pipette with a resistance of 4-6 M was filled with intracellular recording solution. The composition of the intracellular solution for current clamp recordings was following: 130 mM K-Gluconate, 10 mM KCl, 2 mM MgCl₂, 10 mM HEPES, 2 mM Na-ATP, 0.2 mM Na₂GTP, 0.2% neurobiotin, pH 7.35 and 290 mOsm. The composition of the intracellular solution for voltage clamp recordings was following: 125 mM CsCl, 5 mM NaCl, 10 mM HEPES, 0.6 mM EGTA, 4 mM Mg-ATP, 0.3 mM Na₂GTP, 10 mM lidocaineN-ethyl bromide (QX-314), pH 7.2 and 290 mOsm. The holding potential for voltage clamp recordings was -70 mV. 100 μ M Picrotoxin (PTX) and 10 μ M NBQX diluted in aCSF was used to inhibit inhibitory and excitatory synaptic transmission, respectively, during optogenetic assisted circuit mapping experiments.

For ChR2-assisted circuit mapping a multi-LED array system (CoolLED) connected to the epifluorescence port of the Olympus BX51 microscope was used. LED power was chosen to achieve illumination ranging from 1 to 10 mW \cdot mm² in the recording chamber. 1-2 ms light pulses at $\lambda = 470$ nm was delivered through the microscope objective onto the brain slice to trigger action potentials in presynaptic cell bodies or axon terminals.

Data was analyzed with pCLAMP10 (Molecular Devices) and Stimfit (stimfit.org).

3.7 Optogenetic manipulations

CeA^{Htr2a::ChR2}, CeA^{Htr2a::eYFP}, CeA^{Htr2a-Cre+::ChR2→PBN} and CeA^{Htr2a-Cre-negative::ChR2→PBN} mice were bilaterally tethered to optic fibre patch cords (Thorlabs) connected to a 473 nm or 561 nm laser (CNI lasers; Cobolt) via a rotary joint (Doric Lenses). For photoactivation experiments, 10 ms, 473 nm light pulses at 5,10 or 20 Hz and 10-15 mW were used. Constant 561 nm light at 1 mW was used for photoinhibition experiments during the 'laser on' phase. The lasers were triggered and pulses controlled by Bonsai data

streaming software [62] and Arduino microcontrollers (arduino.cc).

Both virus expression and the optic fiber placement were confirmed after the behavioral experiments. After the completion of behavioral experiments mice were sacrificed and their brains were processed for histology. Mice with the following exclusion criteria was excluded from the analysis: (1) absence of viral expression (lack of eYFP fluorescence), (2) viral expression outside of the CeA, (3) misplaced optical fibers, and (4) damaged CeA.

3.8 Anatomical retrograde tracing

For retrograde tracing experiments 0.15 μ l retrogradely traveling green or red retrobeads (Lumafuor Inc.) were injected into PBN following the same stereotaxic surgery protocol described in the methods. Following coordinates were used with respect to bregma: -4.8 mm anteroposterior, \pm 1.7 mm lateral, -3.72 mm ventral. After 5-7 days post-surgery mice were perfused and brains were processed for histology as described in the method section.

3.9 Stereotaxic surgery for GRIN lens implantation

For *in vivo* calcium imaging experiments, mice were injected in the left CeA using the following coordinates with respect to bregma: -1.22 mm anteroposterior, \pm 2.8 mm lateral, -4.72 mm ventral with 300 nl Cre-dependent AAV construct expressing GCaMP6s. 7-10 days after virus injection a GRIN lens was implanted above CeA and secured to the skull to ensure physical stability during imaging. During the implantation surgery a 0.8 mm hole was drilled in the skull above the CeA (coordinates with respect to bregma: -1.22 mm anteroposterior, -2.8 mm lateral). Debris was removed from the hole with the tip of a 27G needle. Then, a sterile 20G needle secured to the pipette holder was slowly lowered into the brain to a depth of -4.35 mm from the cortical surface to clear a path for the

lens. The GRIN lens (GLP-0673; diameter: 0.6 mm, length: \sim 7.3 mm Inscopix) secured to the pipette holder was slowly lowered into the brain to a depth of -4.25 mm from the cortical surface using a custom lens holder. The skull was scored with a scalpel to create a rough surface. The lens was secured in place by applying cyanoacrylic glue (Loctite 4305) around the lens rim. A head bar was fixed to the skull adjacent to the lens to assist with mounting of the miniaturized microscope. Afterwards, the skull was covered with dental cement (Paladur) around the lens leaving the tip of the lens exposed for optical access. The exposed lens tip was protected by covering it with a silicone elastomer (Kwik-cast).

2 weeks after the lens implantation mice were checked for observable GCaMP6 fluorescence. Mice were head fixed on a running wheel to allow them partial freedom of movement and reduce stress during the procedure. Debris from the silicon elastomer was cleaned with 70% ethanol. Miniscope (nVista, Inscopix) with a baseplate (BLP-2, Inscopix) attached to it was positioned above the lens to observe GCaMP6 fluorescence of the neurons. After confirming the right focal plane containing cells with GCaMP6 fluorescence, mice were lightly anesthetized with 0.5% isoflurane and the baseplate was mounted onto the implant with dental composite (Vertise Flow, Kerr Dental). The baseplate was covered with a baseplate cap (BCP-2, Inscopix) until imaging experiment to protect the lens implant.

3.10 *in vivo* freely moving Ca^{2+} imaging

CeA^{Htr2a}::GCaMP6s mice were head fixed over a running wheel and the miniscope was secured onto the mounted baseplate. Afterwards, mice were allowed to acclimate in their homecage for 10 minutes before proceeding to the experiment. Images of 1080 by 1080 pixels size were acquired at 20 Hz using nVista HD V2 acquisition software (Inscopix). LED power was set 40-60% of the maximum LED power (approximately 0.4-0.6 mW).

Fluorescent images were acquired at auto exposure setting and the gain was set to 1-2X.

For the free feeding assay, 4 mice from multiple litters were used. Mice were habituated to the weight of the microscope using a dummy microscope (DMS-2, Inscopix) and to the behavior arena for 3 daily 15 minute sessions before the day of the experiment. Mice were, then, food deprived overnight before the day of the imaging experiment. On the day of the experiment, mice were free to explore the behavior arena where they were presented with a regular food pellet. Throughout the session, they were allowed to consume to food pellet freely.

For the FR1 assay, 3 mice from multiple litters mice were habituated to the weight of the microscope for 3 days prior to training. Mice were food restricted to 85-90% of their free-feeding food intake and trained daily to nose-poke into the active port of a two port apparatus to receive food rewards carrying a dummy microscope (DMS-2, Inscopix). Mice were trained until they reach to at least 75% success rate of discriminating between the active and the inactive ports for 3 consecutive days. Training duration was 7-10 days and all 3 mice to reach to a stable performance. On the imaging, mice were habituated to the arena for 5 minutes before the FR1 assay was initiated. The assay was terminated once each mice reached to 12 total rewards in 15-25 minutes. On average each mice poked 12 ± 0 time into the active port and 1.70.3 times into the inactive port. The mean bout duration for reward consumption was 8.3 ± 2.5 s.

For both imaging experiments, mice were recorded using overhead and side-mounted camera for future offline observation of their behavior. Synchronization of the miniscope software and behavior cameras was achieved using Bonsai data streaming software [62] and a microcontroller (Arduino). Time of the nose-poke, cue and reward delivery was recorded using in house built sensors coupled to an Arduino microprocessor. Related data was transferred to a PC via the serial connection using custom written Python (Python

2.7, python.org) scripts using PySerial module. Food contact, eating start and stop events were manually scored offline from the recorded video.

3.11 Ca^{2+} imaging data analysis

To eliminate the effect of the global and slowly varying illumination in the imaging field of view, image frames were normalized by dividing them by a low-passed FFT filtered frame (length constant: 100px) using ImageJ (NIH, imagej.nih.gov/ij) [34, 19]. Motion correction was performed using Mosaic softwares in-built motion correction algorithms (v1.1.3; Inscopix) [73]. Mean projection of the first 20 frames (corresponding the first second of the imaging video) was used as the reference image during the motion correction. Following motion correction, individual cell filters were identified using PCA/ICA using Mosaic software (v1.1.3; Inscopix) based on previously described methods by Mukamel *et al* [73]. Each cell filter was identified by zeroing the values that are <60% of the maximum intensity. Then, the raw fluorescence traces were obtain from the 20Hz imaging video by applying the thresholded cell masks. To ensure that Ca^{2+} signals were obtained from individual neurons, the Ca^{2+} activity traces and cell masks from each individual unit were visually inspected. Duplicate or overlapping image filters were not included in the analysis.

For free feeding imaging experiment, $\Delta F/F_0$ was calculated as $(FF_0)/F_0$ from the raw fluorescence traces. Lowest 5% of the fluorescence of each Ca^{2+} activity trace was used as F_0 [9]. The mean Ca^{2+} activity during first 20 seconds of the first eating bout was compared to the mean activity during 20 seconds preceding the bout onset was analyzed. On the other hand, all of the eating bouts that are longer than 20 seconds were taken into account while classifying the neurons. Ca^{2+} activities were compared for each cell along all the eating bouts to the average activity of the preceding non-eating bout.

For FR1 imaging experiments, area under the curve was calculated during a defined event (eg. cue, eating bout, first or second half of the eating bout, etc.) and compared to a same length of baseline before the event offset.

For both imaging experiments, eating (F_{eating}) and non-eating bout or baseline (F_{baseline}) activities were compared using Wilcoxon rank-sum test. Neurons that have significantly different activity changes were considered as responsive neurons. Next, preference indices (P.I.) were calculated for each neuron using the following formula:

$$P.I. = \frac{(F_{\text{eating}} - F_{\text{baseline}})}{(F_{\text{eating}} + F_{\text{baseline}})}$$

Cells that increased their activity significantly from the baseline to the eating bout ($p < 0.05$, and P.I. > 0) were classified as activated during eating, and cells that decreased their activity significantly ($p < 0.05$, and P.I. < 0) were classified as inhibited during eating. Normalized $\Delta F/F_0$ was used to transform the range of $\Delta F/F_0$ to [0 1] by the equation:

$$\frac{\frac{\Delta F}{F_0} - \min(\frac{\Delta F}{F_0})}{\max(\frac{\Delta F}{F_0}) - \min(\frac{\Delta F}{F_0})}$$

All analysis for the imaging experiments was performed using custom written Matlab (2015a, Mathworks) and Python (Python 2.7, python.org) scripts.

3.12 Histology

Animals were deeply anesthetized with ketamine/xylazine (100 mg/kg, 16 mg/kg respectively). They are, then, transcardially perfused with phosphate-buffered saline (PBS) and 4% paraformaldehyde (PFA) (w/v) in PBS. Brains were dissected and post-fixed at

4°C in 4% PFA gently shaking overnight. Brains for immunostaining or verification for viral expression or fiber placement were cryopreserved sequentially until they equilibrate in 15% and 30% sucrose in PBS at 4°C before embedding. Afterwards, cryopreserved brains in O.C.T. (Fisher Scientific). Sections of 50 μm thickness were cut using a cryostat (Leica).

For verification of viral expression and fiber placement after behavioral experiments, sections were mounted on glass microscope slides (SuperFrost Plus, Thermo Scientific) using a fluorescence mounting medium (Dako). Sections were imaged immediately after mounting.

For immunohistochemistry, floating sections were stored in 1X PBS at 4°C until further processing.

3.13 Immunohistochemistry

For immunostaining, floating sections were washed in 1X PBS 0.5% with TritonX-100 and blocked at room temperature for two hours in blocking solution containing 1% bovine serum albumin (BSA) in 1X PBS 0.1% with TritonX-100. Following blocking, sections were incubated in primary antibody diluted in blocking solution at 4°C overnight. After primary antibody incubation, sections were washed 3 times for 15 minutes in 1X PBS 0.1% with TritonX-100. Then, sections were incubated in secondary antibody diluted in blocking solution at room temperature for 2 hours. After washing the sections 3 times for 15 minutes in 1X PBS 0.1% with TritonX-100. Afterwards, sections were incubated in DAPI (1 $\mu\text{g}/\text{ml}$) (ThermoFisher Scientific) and mounted using a fluorescence mounting medium (Dako) and coverslipped for imaging.

Following primary antibodies were used: mouse anti-PKC δ (1:100) (610398, BD Bio-

sciences), chicken anti-LacZ (1:200) (ab9361, Abcam), rabbit anti-SOM (1:1000) (T-4103, Peninsula Laboratories International), and goat anti-CGRP (1:500) (Abcam, ab36001). Following secondary antibodies were used depending on the species of the primary antibody that was used: Alexa Fluor donkey anti-rabbit/mouse/goat 488/Cy3/647, (1:500) (Jackson).

3.14 Microscopy

Fluorescent Z-stack images were acquired using a Leica SP8 confocal microscope and a 20X/0.75 IMM oil immersion objective (Leica). Images were minimally processed using ImageJ software (NIH) to enhance brightness and contrast. Median and mean filters were used to reduce noise. For colocalization analyses of Htr2a-Cre⁺ neurons with PKC δ , and retrobead tracing experiments, sections were quantified from anterior to posterior CeA (bregma -1.22 to -1.58 mm) (n=3 sections from 3 mice) using ImageJ (NIH).

3.15 Statistics

No statistical methods were used to predetermine sample size. The number of samples in each group were based on published studies. Blinding was not used. For behavior experiments, littermate animals were randomly assigned to the experimental group and were identified by unique identification number. Data presented as boxwhisker plots display median, interquartile range and 5th–95th percentiles of the distribution. Data presented as bar and line graphs indicate mean \pm SEM. Pairwise comparisons were calculated by unpaired or paired two-tailed t-tests and multiple group data comparisons were calculated by one-way or two-way ANOVA with Bonferroni post-hoc test. Normality was assessed using Shapiro-Wilk tests. In the case where normality tests failed, Mann-Whitney or Wilcoxon

rank-sum tests were used. Statistical analysis were performed using Graphpad Prism 6.0, Matlab or Python. Significance levels are indicated as follows: * $p < 0.05$, ** $p < 0.01$, *** $p < 0.001$, **** $p < 0.0001$.

Chapter 4

Results

4.1 Molecular characterization of CeA^{Htr2a} neurons

In order to identify novel populations of CeA^{PKC δ -negative} neurons, we consulted the GENSAT BAC transgenic mouse collection for suitable Cre-expressing mouse lines to target molecularly defined populations of CeA neurons. The top candidate was Htr2a (KM208Gsat/Mmucd line) which was strongly expressed in the CeA. After importing this line, we visualized expression of the Cre by breeding the *Htr2a-cre* line to a *ROSA:LacZ* reporter mouse. We found Htr2a-Cre expression confined to CeL and CeM along the entire anterior-posterior axis. We also confirmed that expression of Cre faithfully recapitulated endogenous expression of Htr2a by comparing the pattern of in situ hybridizations for the endogenous Htr2a gene and the LacZ reporter (data not shown).

I next assessed the expression of *Htr2a-cre;LacZ* with respect to PKC δ by performing immunohistochemistry analysis for PKC δ and β -galactosidase, I found very little overlap between the two populations (Figure 4.1a, b), thus demonstrating that CeA^{Htr2a} neurons comprise a PKC δ - neuron population. Interestingly, I observed a compartmentalization of PKC δ and Htr2a expression in the CeA, with PKC δ predominantly located in the lat-

eral/capsular region while Htr2a expression was localized in more medial parts of the CeL and in the CeM (Figure 4.1a). Both Htr2a and PKC δ were each expressed by 25% and 30% of the CeL neurons, respectively. There was another group of neurons with unknown molecular identity comprising 40% of CeL that expressed neither of the markers (Figure 4.1c).

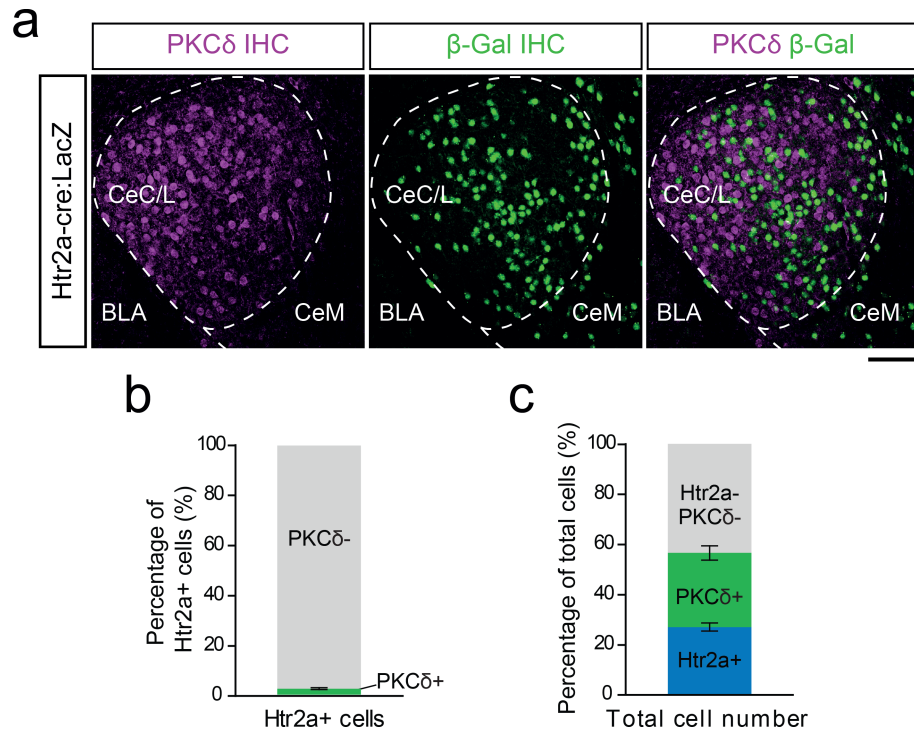


Figure 4.1: Htr2a⁺ and PKC δ ⁺ neurons are mutually exclusive CeA neural populations. **a)** Representative image of the CeA from a coronal brain section from a *Htr2a-Cre;floxed-lacZ* mouse showing the relative location of Htr2a-cre⁺ and PKC δ ⁺ neurons. Left: PKC δ immunostaining. Middle: β -Gal immunostaining marks the location of Htr2a-Cre⁺ neurons. Right: overlap between Htr2a-cre⁺ and PKC δ ⁺ neurons. **b)** Expression of Htr2a and PKC δ do not overlap in CeA. Quantification of the percentage of CeA^{Htr2a} neurons that express PKC δ . (n = 3 sections from 3 mice) **c)** The Htr2a⁺ and PKC δ ⁺ populations each comprised approximately 25% of the total CeA neuron population. Quantification of the percentage of CeA neurons that express either Htr2a or PKC δ . (n = 3 sections from 3 mice)

CeC/L; central capsular and lateral amygdala, CeM; central medial amygdala, BLA; basolateral amygdala. Scale bar is 100 μ m. Bar graphs indicate mean \pm SEM.

I also assessed the overlap between CeA^{Htr2a} and somatostatin (SOM)-expressing CeA neurons, the best-characterized CeA^{PKC δ -negative} population. I found by immunohistochemistry that CeA^{Htr2a} and CeA^{SOM} neurons show a partial overlap mostly in the CeL region (Figure 4.2). However, since the somatostatin peptide is predominately located in

neurites, it was difficult to accurately quantify the overlap. In summary, we identified a population of CeA neurons expressing Htr2a that constitute a PKC δ -negative population with a partial overlap with SOM expressing neurons.

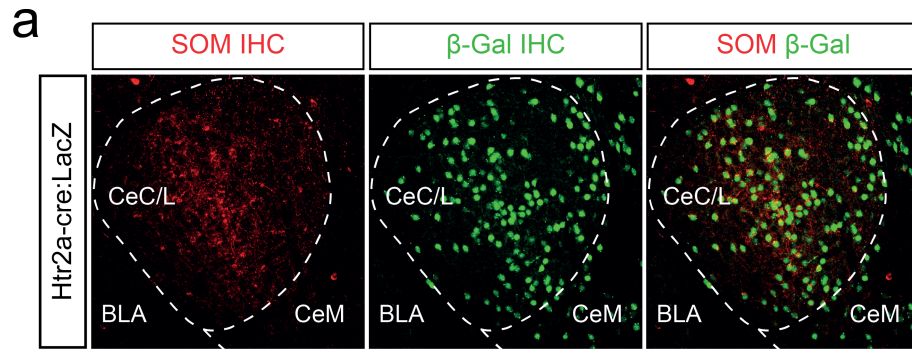


Figure 4.2: CeA^{Htr2a} neurons are partially overlapping with CeA^{SOM} neurons. a) CeA^{Htr2a} neurons partially overlap with the those that express SOM. Image of the CeA from a coronal brain section from a *Htr2a-Cre;floxed-lacZ* mouse showing the relative location of Htr2a-cre+ and SOM+ neurons. Left: SOM immunostaining. Middle: β -Gal immunostaining marks the location of Htr2a-cre+ neurons. Right: overlap between Htr2a-cre+ and SOM+ neurons. (n = 3 sections from 3 mice)

CeC/L; central capsular and lateral amygdala, CeM; central medial amygdala, BLA; baso-lateral amygdala. Scale bar is 100 μ m.

4.2 Electrophysiological characterization of CeA^{Htr2a} neurons

Next, I examined the electrophysiological properties of CeA^{Htr2a} neurons. Within the CeA, two major firing types of neurons have been reported. Late firing neurons are identified by their delayed action potentials compared to accommodating regular spiking neurons that fire earlier upon depolarizing current injection [39, 63, 69]. I, therefore, investigated which firing type category Htr2a neurons fall into. To do so, *Htr2a-cre* mice were crossed to a floxed tdTomato reporter mouse, allowing visualization of Htr2a+ neurons under an epifluorescent microscope. Acute brain slices were prepared from these mice and whole-cell recordings were performed from both Htr2a+ and Htr2a-negative neurons. In

order to identify the firing properties of individual neurons, depolarizing current steps were injected in a range from -150pA to 200pA (at 25pA steps and 5pA steps around the action potential threshold) (Figure 4.3a). I found that the majority of CeA^{Htr2a} neurons were late firing (85%) while half of $CeA^{Htr2a-negative}$ neurons were late firing and half regular spiking (Figure 4.3a, b). This is a similar picture to the reported properties of $CeA^{PKC\delta}$ neurons [39]. Thus, both $CeA^{PKC\delta}$ neurons and a select subpopulation of $CeA^{PKC\delta-negative}$ neurons, expressing $Htr2a$, are predominantly physiologically homogeneous.

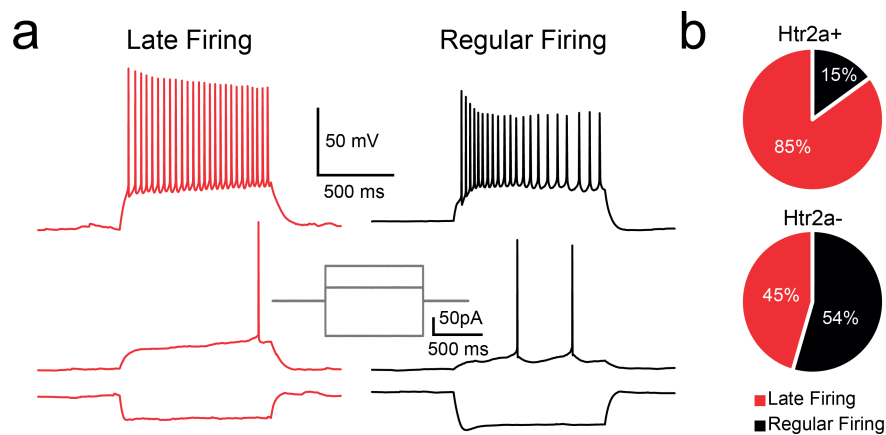


Figure 4.3: CeA^{Htr2a} neurons are electrophysiologically homogeneous. a) Whole-cell current clamp recordings from CeA^{Htr2a+} and CeA^{Htr2a-} neurons. Middle: current injection steps. Left: example voltage trace of late firing neuron. Right: example trace of regular firing neuron. The majority (16/20) of CeA^{Htr2a+} neurons are late firing while the $CeA^{Htr2a-negative}$ populations display heterogeneous firing pattern comprised of late (5/11) and regular firing neurons (6/11).

Vertical scale bars are 50mV and 50pA for voltage and current traces, respectively. Both horizontal scale bars are 500ms. Red traces: Late firing type, black traces: regular firing type.

Late firing type neurons were identified by the delay of firing their first action potential upon injection of a depolarizing current injection. In, both, CeA^{Htr2a+} and $CeA^{Htr2a-negative}$ neurons late firing neurons displayed a significant delay compared to regular spiking neurons (Figure 4.3a). Additionally, I quantified several membrane properties for CeA^{Htr2a+} and CeA^{Htr2a-} neurons among late and regular spiking types. Both late and regular firing neurons of either subpopulation showed similar passive membrane properties, such as resting membrane potential and input resistance (Figure 4.4b, c). Furthermore, all types of neurons displayed similar dynamics of action potentials. Among CeA^{Htr2a+} and

$CeA^{Htr2a\text{-negative}}$ neurons action potential generation threshold, peak and half-width are similar (Figure 4.4d-f).

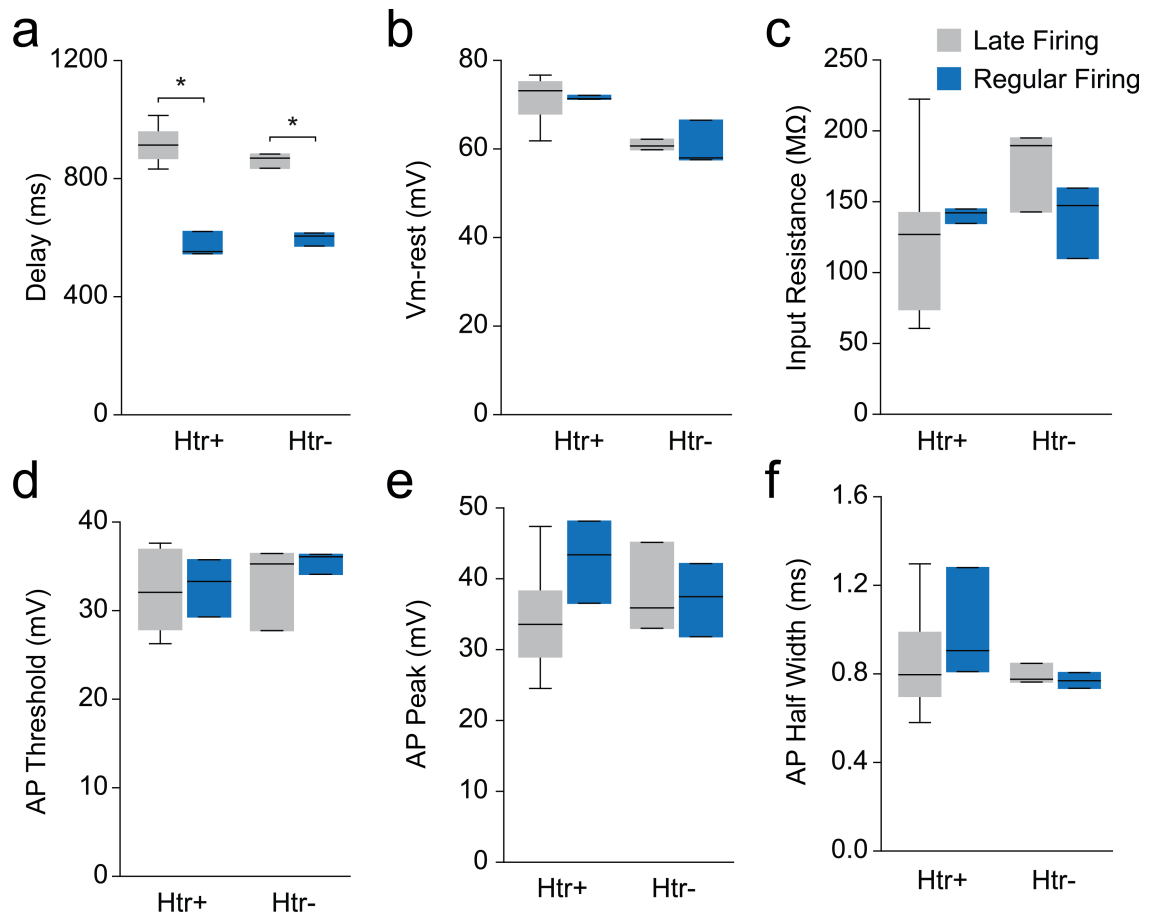


Figure 4.4: Membrane properties of CeA^{Htr2a+} and $CeA^{Htr2a\text{-negative}}$ neurons do not display any significant difference. a) Late firing neurons show delayed firing of their first action potential upon depolarizing current steps compared to regular firing neurons in both CeA^{Htr2a+} and $CeA^{Htr2a\text{-negative}}$ neurons. Both CeA^{Htr2a+} and $CeA^{Htr2a\text{-negative}}$ neurons had similar delays in first action potential among late and regular firing types. (n= 31 cells from 5 mice) b-c) Passive membrane properties of CeA^{Htr2a+} and $CeA^{Htr2a\text{-negative}}$ neurons regardless of their type. Resting membrane potential and input resistance of Htr2a+ and Htr2a-negative neurons have similar values. (n= 31 cells from 5 mice) d-f) Properties of action potentials generated by CeA^{Htr2a+} and $CeA^{Htr2a\text{-negative}}$ neurons regardless of their type. Action potential threshold, peak and half-width are similar in Htr2a+ and Htr2a-negative neurons. (n= 31 cells from 5 mice)

Boxwhisker plots display median, interquartile range and 5th/95th percentiles of the distribution. Two-tailed unpaired t-test. * $p < 0.05$

4.3 CeA^{Htr2a} in the CeA microcircuitry

4.3.1 Controlling CeA^{Htr2a} neurons with ChR2

In order to map the neural circuits in which CeA^{Htr2a} neurons function, I stereotaxically transduced CeA^{Htr2a} neurons in *Htr2a-cre;tdTomato* mice with an AAV carrying cre-dependent channelrhodopsin (ChR2) tagged with eYFP (ChR2-eYFP). ChR2-eYFP expression was observed in the CeL and CeM mainly in the neural processes rather than in the tdTomato cell bodies (Figure 4.5a and Figure 4.6a). I first determined if the firing properties of Htr2a+ neurons were unaltered after ChR2-eYFP was expressed. CeA^{Htr2a} neurons displayed late firing properties as expected, suggesting that AAV transduction of ChR2 did not change the physiology of Htr2a+ neurons (Figure 4.5b). Then, I validated that ChR2 can be used to evoke action potentials in Htr2a neurons while maintaining their electrophysiological properties. Whole-cell recordings from ChR2-eYFP transduced Htr2a+ neurons demonstrated light-evoked photocurrents (Figure 4.5c) that increased with increasing LED light intensity (Figure 4.5d).

4.3.2 Local circuit connectivity

Previous studies have shown that CeA^{PKC δ +} neurons inhibit any CeA^{PKC δ -negative} cell in their vicinity in CeL [14, 39]. Next, I investigated how CeA^{Htr2a+} neurons are integrated in the local circuitry of CeA. Since ChR2 could reliably be used to control the activity of CeA^{Htr2a} neurons, I first investigated using ChR2-assisted circuit mapping how CeA^{Htr2a} neurons are connected to other CeA neurons in the local circuit. Cre-dependent ChR2-eYFP was expressed in CeA^{Htr2a} neurons (as described above) and whole-cell recordings were obtained from CeA^{Htr2a-negative} neurons (Figure 4.6a, b). Then, I recorded light-evoked whole-cell currents from tdTomato-negative neurons of CeA in acute brain slices

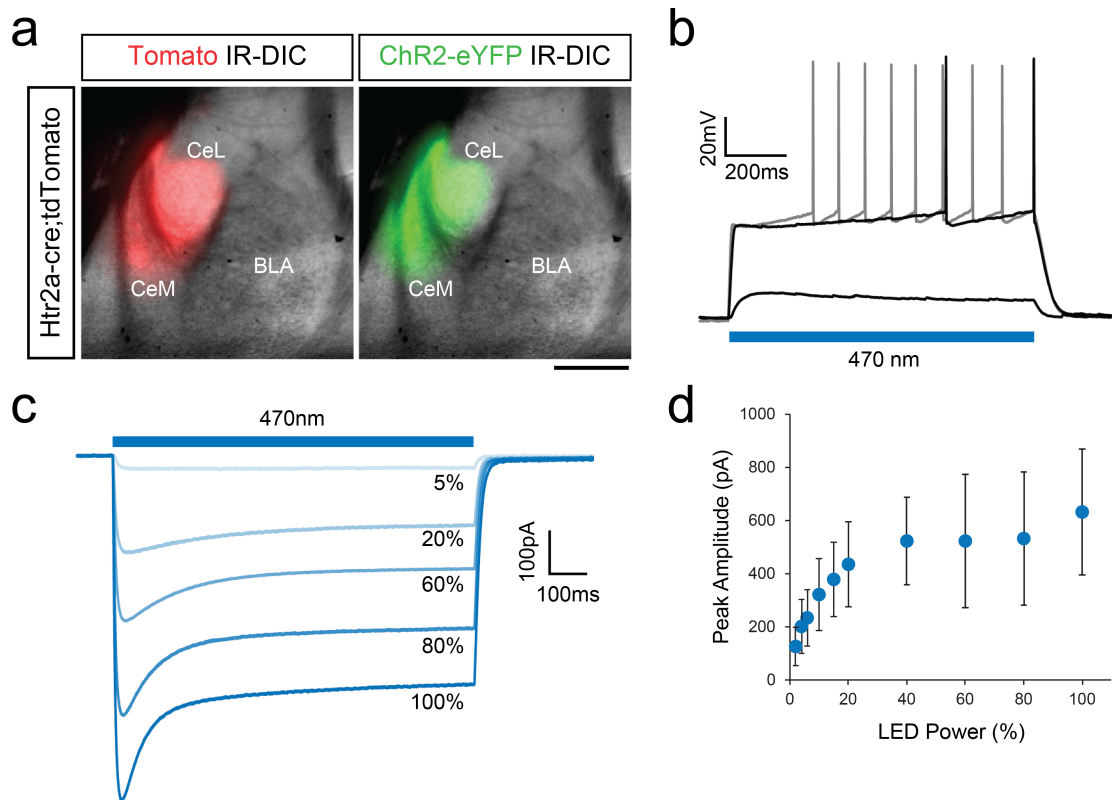


Figure 4.5: *ex vivo* validation of ChR2 to induce firing in CeA $Htr2a$ neurons. **a)** Representative image of cre-dependent ChR2-eYFP expression (Right) delivered via AAV by stereotaxic injection into the CeA of a $Htr2a$ -cre;tdTomato mouse (Left). **b)** Representative depolarizing photocurrents in tomato positive neurons generated upon delivery of 1sec light pulses at varying LED power. **c)** Average photocurrents generated at different LED powers (0-100%). ChR2 dependent photocurrents increase as the LED power increases. (n= 6 neurons from 1 mouse)

CeL; central lateral amygdala, CeM; central medial amygdala, BLA; basolateral amygdala. Scale bar is 500 μ m. Dot-plots indicate mean \pm SEM.

(Figure 4.6b). Using this method, light-evoked, short latency inhibitory postsynaptic currents (IPSCs) were detected in all postsynaptic recorded neurons (19 out of 19), demonstrating that CeA $Htr2a$ neurons inhibit other local CeA neurons (Figure 4.6c). Additionally, these currents were found to be sensitive to picrotoxin, suggesting this inhibition likely occurs via GABA_A receptors (Figure 4.6c, d).

In order to investigate the identity of the putative CeA $Htr2a$ -negative neurons, recorded neurons were filled with neurobiotin and post-hoc immunohistochemistry was performed for PKC δ on the brain slices. This revealed that 50% of the postsynaptic neurons were PKC δ + (Figure 4.7). In summary, these results indicate that CeA $Htr2a$ neurons inhibit

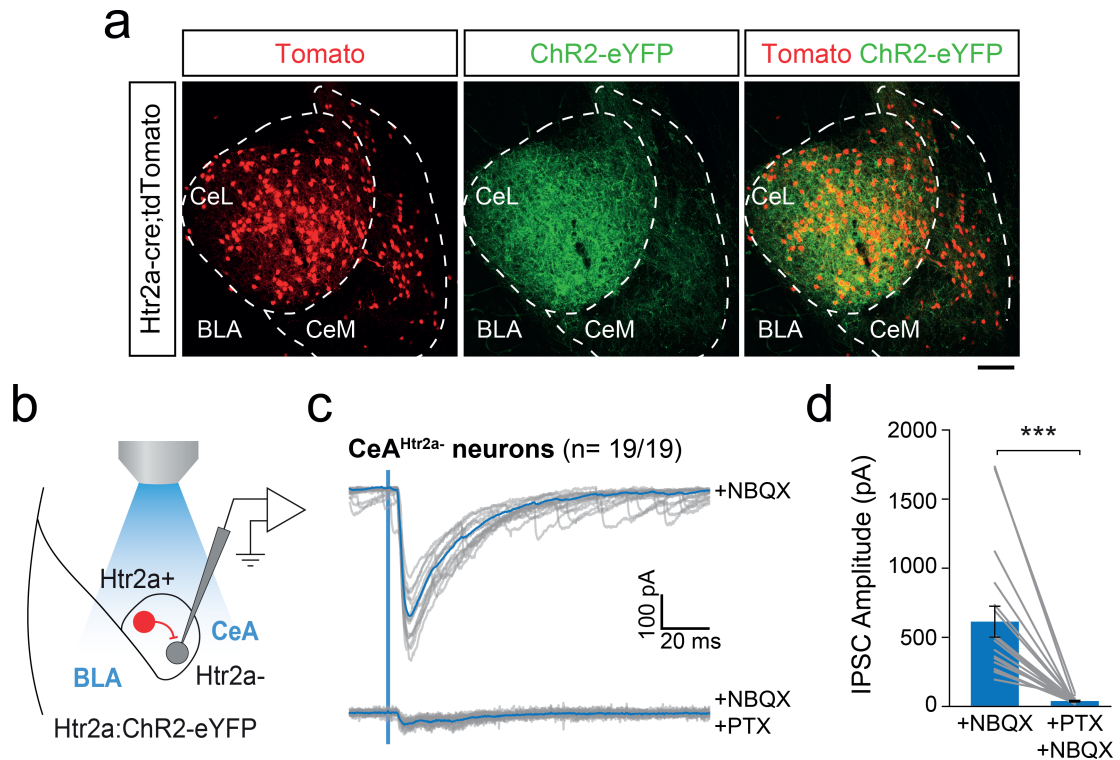


Figure 4.6: CeA^{Htr2a} neurons inhibit other neurons within the CeA local circuit. **a)** Representative image of the CeA from a coronal brain section from a *Htr2a-cre;tdTomato* mouse where cre-dependent AAV-ChR2-eYFP was delivered stereotaxically into the CeA. Left: tdTomato expression marks CeA^{Htr2a} neurons. Middle: Expression of ChR2-eYFP. Right: overlapping expression of tdTomato and ChR2-eYFP. **b)** Scheme of experimental setup where *Htr2a-cre;tdTomato* neurons were transduced with ChR2-eYFP and whole-cell recordings were performed from neighboring CeA^{Htr2a-cre;tdtomato-negative} neurons. **c)** Photoactivation of CeA^{Htr2a} neurons with ChR2 induces high amplitude PTX-sensitive IPSCs in CeA^{Htr2a-negative} neurons. Overlay of 473 nm light evoked (blue bar, 1ms pulse) individual (grey) and average (blue) IPSCs recorded from postsynaptic CeA^{Htr2a-negative} neurons (average onset latency of 2.7 0.05 ms). Top: IPSCs in the absence of PTX. Bottom: IPSCs in the presence of PTX. All recordings include NBQX to block excitatory synaptic transmission. **d)** Quantification of 473 nm light evoked responses in the absence (left) and presence (right) of PTX (mean IPSC amplitude 604.93 106.04 pA). Light evoked responses require synaptic transmission via GABA_A receptors. (n= 19 cells from 4 mice)

CeL; central lateral amygdala, CeM; central medial amygdala, BLA; basolateral amygdala. Scale bar is 100μm. Bar plots indicate mean ±SEM. Two-tailed paired t-test. ***p<0.001

CeA^{PKCδ+} neurons. Additionally, input mapping experiments using rabies tracing technique in our lab have revealed that PKCδ neurons receive inputs from CeA^{Htr2a} neurons (data not shown, experiment by Marion Ponsérre). Together with previous studies that demonstrate similar results for CeA^{PKCδ} neurons [14, 39], this suggests that within the CeA there is a high degree of reciprocal connectivity between the neurons.

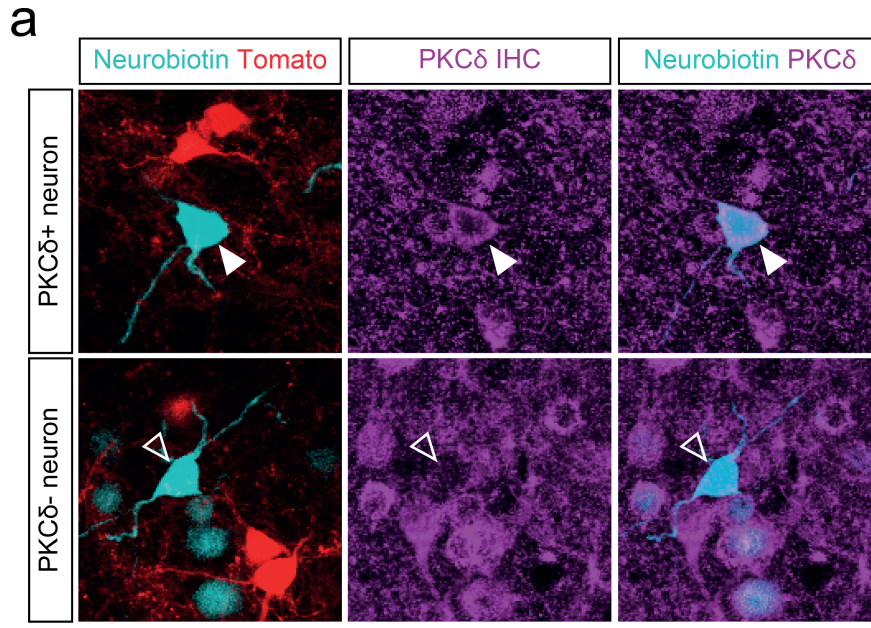


Figure 4.7: CeA^{Htr2a+} neurons locally inhibit $CeA^{PKC\delta+}$ neurons. a) Example images of neurobiotin-filled $CeA^{Htr2a-cre;tdtomato-negative}$ neurons (Left) from the experiments in Figure 4.6. Filled neurons (white arrow-head) were post-hoc identified as PKC δ + (3/6 neurons) and PKC δ -negative (Left) by immunostaining for PKC δ (Middle). Top: Example of a neurobiotin-filled, tdTomato-negative, PKC δ + neuron (white arrow-head). Bottom: Examples of a neurobiotin-filled, tdTomato-negative, PKC δ -negative neuron (open-arrowhead).

CeL; central lateral amygdala, CeM; central medial amygdala, BLA; basolateral amygdala. Scale bar is 50 μ m.

4.4 *in vivo* activity dynamics of CeA^{Htr2a} during appetitive behaviors

A recent study has demonstrated that $CeA^{PKC\delta}$ neurons mediate the action of multiple anorexigenic signals, as activation of these neurons leads to the cessation of food consumption [14]. Additionally, this study proposed that $CeA^{PKC\delta}$ neurons function by locally inhibiting PKC δ -negative neurons within the CeA, which suggests that these cells promote food intake. My experiments described in the previous sections suggest that CeA^{Htr2a} neurons may functionally oppose $CeA^{PKC\delta}$ neurons within the CeA. As CeA^{Htr2a} neurons are a non-overlapping subpopulation of PKC δ -negative neurons and locally inhibit $CeA^{PKC\delta}$ neurons, this suggests that CeA^{Htr2a} neurons may promote food intake. Indeed, a series of behavioral experiments involving manipulation of the CeA^{Htr2a} neurons *in vivo*

revealed that activation of these neurons promotes food consumption (data not shown, experiments by Amelia Douglass). These experiments demonstrated that CeA^{Htr2a} neurons are involved in food intake. However, they did not allow an appreciation of the endogenous activity of CeA^{Htr2a} neurons during food consumption, which is necessary to fully investigate how these neurons modulate eating behavior. To investigate this we performed *in vivo* Ca²⁺ imaging of CeA^{Htr2a} neurons in freely behaving animals.

To-date, monitoring of the activity dynamics of several populations of neurons involved in appetite regulation by *in vivo* Ca²⁺ imaging has provided considerable insight into how these neurons function. Previously, it was shown that non-overlapping ensembles of GABAergic neurons in the lateral hypothalamus (LH) differentially respond to appetitive or consummatory aspects of food consumption [48]. Conversely, AgRP-expressing 'hunger' neurons in the arcuate nucleus of the hypothalamus showed high levels of activity while mice were hungry and rapidly reduced their activity upon consumption of food [9]. These different results suggest, on the one hand, that GABAergic LH neurons appear to regulate food-seeking and the consumption phases of eating while AgRP neurons code for the hunger state of the animal to drive foraging behavior. Thus, an appreciation of the activity dynamics of CeA^{Htr2a} was a necessary part of this study.

In doing so, we performed *in vivo* Ca²⁺ imaging at single cell resolution. Here, a Cre-dependent GCaMP6s viral construct was delivered into the CeA in *Htr2a-Cre* mice. GCaMP expression specific to Htr2a-Cre+ neurons were confirmed by delivering Cre-dependent AAV-GCaMP into the CeA of *Htr2a-cre;tdTomato* mice. After 4 weeks of viral expression, only tdTomato+ neurons expressed GCaMP6s (Figure 4.8a). To visualize GCaMP-expressing CeA^{Htr2a} neurons in freely behaving mice, a GRIN lens was implanted above the CeA and the activity dynamics of CeA^{Htr2a} neurons were recorded with a lightweight head-mounted miniaturized microscope [73, 90] (Figure 4.8b).

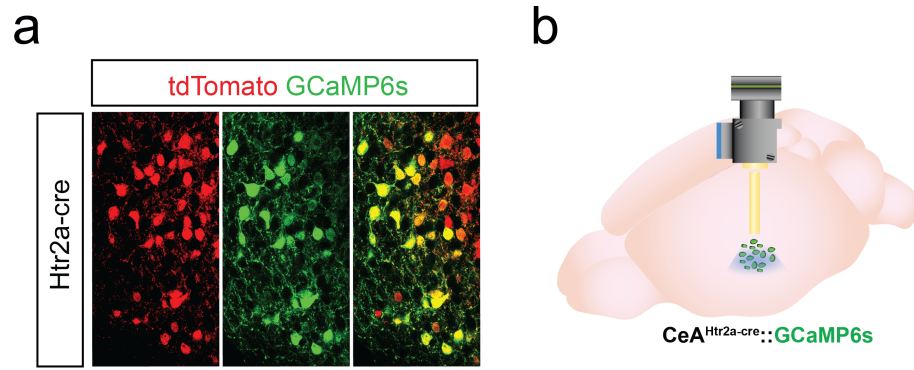


Figure 4.8: *in vivo* Ca^{2+} imaging of CeA^{Htr2a} neurons. **a)** Scheme of *in vivo* Ca^{2+} imaging approach. Cre- dependent GCaMP6s was expressed in CeA^{Htr2a} neurons. GCaMP fluorescence changes were monitored through a GRIN lens implanted above the CeA and captured using a head-mounted miniature microscope. **b)** Image of CeA neurons from a $Htr2a$ -cre;tdTomato mouse expressing GCaMP6s in $Htr2a$ -cre;tdTomato+ neurons.

Scale bar is 100 μm .

The Ca^{2+} activity of CeA^{Htr2a} neurons was observed through the GRIN lens and recorded at 20 Hz (Figure 4.9a). After data acquisition, activity traces of individual neurons were identified using PCA/ICA (Figure 4.9b, details of this procedure are explained in Methods).

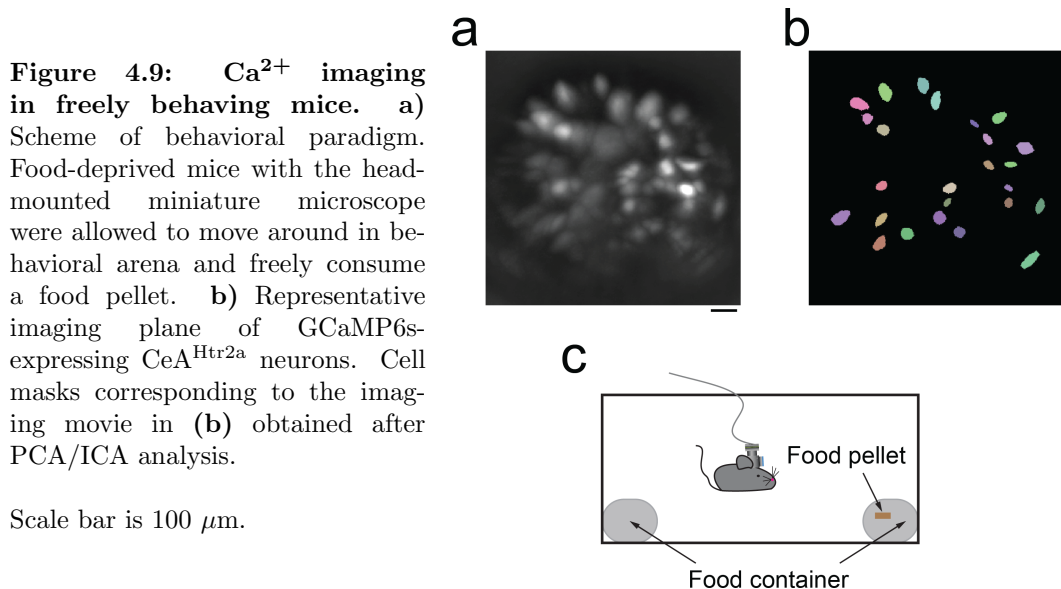


Figure 4.9: Ca^{2+} imaging in freely behaving mice. **a)** Scheme of behavioral paradigm. Food-deprived mice with the head-mounted miniature microscope were allowed to move around in behavioral arena and freely consume a food pellet. **b)** Representative imaging plane of GCaMP6s-expressing CeA^{Htr2a} neurons. Cell masks corresponding to the imaging movie in **(b)** obtained after PCA/ICA analysis.

Scale bar is 100 μm .

First, we examined the activity of CeA^{Htr2a} neurons during hunger and eating. CeA^{Htr2a} :GCaMP6s mice, which had been food deprived overnight, were given free access to a food pellet placed in one corner of the behavioral arena (Figure 4.10a). We reasoned that fol-

lowing overnight fasting the food had the highest saliency during the first eating bout. For this reason, we investigated the activity of CeA^{Htr2a} neurons during the first eating bout of each mouse. In all four mice imaged, when the first bout was considered, the average activity of all recorded neurons increased upon eating onset in the case of every mouse (Figure 4.10b). When all recorded neurons were considered together, the average activity of all neurons (69 neurons from 4 mice) increased their activity significantly upon eating onset during the first bout (Figure 4.10b, c). Furthermore, the mean Ca^{2+} activity of all neurons also increased when the mouse contacted the food for the first time (Figure 4.10d). However, by investigating responses of individual neurons to the start of food consumption during the first eating bout we observed heterogeneity in their responses. While some neurons increased their activity upon the start of eating, some did not respond or reduced their activity (Figure 4.10e).

We, therefore, classified the neurons based on their response profiles. Here, we analyzed the activity traces of each neuron over the course of all eating bouts that the animal engaged in. We calculated a preference index (P.I.) by comparing the activity of neurons during all eating bouts to the activity during the preceding inter-bout interval (Figure 4.11a). Then, we identified the neurons that changed their activity significantly upon the start of eating and classified each neuron based on the calculated P.I. values. This classification revealed that a sizable subset of CeA^{Htr2a} neurons (22%) consistently increased their activity upon eating across all the eating bouts (Figure 4.11b-d). On the other hand, a smaller subset of CeA^{Htr2a} neurons (10%) reduced their activity during eating, while the rest of the neurons did not show any significant response to eating (Figure 4.11b-e). Furthermore, individual neurons that were classified as increasing or decreasing their activity during eating displayed consistent activity patterns throughout the eating bouts (Figure 4.11f). Therefore, our results revealed that CeA^{Htr2a} neurons increase their activity upon food consumption, supporting our behavior data which shows

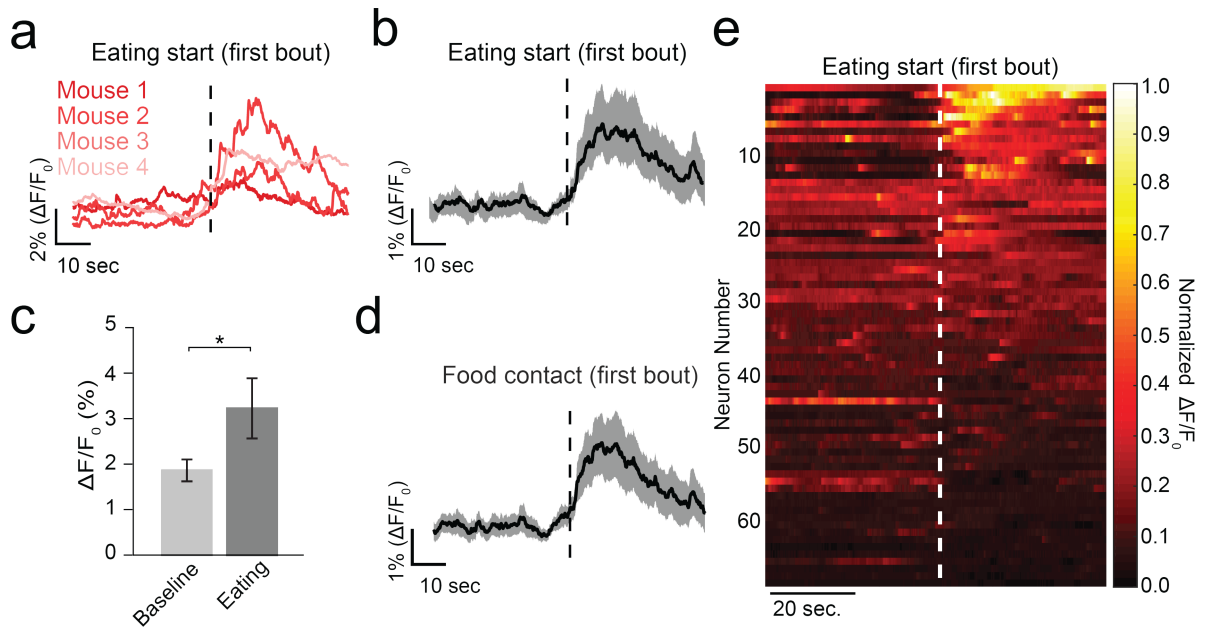


Figure 4.10: CeA^{Htr2a} neurons increase activity during eating. **a)** Average GCaMP6s fluorescence responses of $CeA^{Htr2a}::GCaMP6s$ neurons from four mice. Traces are aligned to the eating onset of the first bout after the overnight fast. **b)** Population average of GCaMP6s fluorescence response of all $CeA^{Htr2a}::GCaMP6s$ neurons from four mice. Traces are aligned to the eating onset of the first bout after the overnight fast ($n = 69$ cells). Shading represents \pm SEM. **c)** Average GCaMP6s fluorescence response of all $CeA^{Htr2a}::GCaMP6s$ neurons during baseline and eating ($n = 69$ cells). **d)** Average GCaMP6s fluorescence response of individual $CeA^{Htr2a}::GCaMP6s$ neurons during baseline and eating. Each joined point is one cell. **e)** Population average of GCaMP6s fluorescence response of all $CeA^{Htr2a}::GCaMP6s$ neurons from four mice. Traces are aligned to the moment the mice first contacted the food after the overnight fast ($n = 69$ cells). Shading represents \pm SEM. **f)** Normalized GCaMP6s fluorescence responses of individual $CeA^{Htr2a}::GCaMP6s$ neurons proximal to the first each bout after the overnight fast. Each row is one cell. White stippled line marks the eating onset.

Bar plots indicate mean \pm SEM. Scale bar is 100 μ m.

these neurons modulate food consumption.

Next, to further understand which aspect of eating CeA^{Htr2a} neurons encode we investigated their activity dynamics during appetitive or consummatory phases of eating. To do this, we recorded the GCaMP6s fluorescence changes of CeA^{Htr2a} neurons during a fixed ratio 1 (FR1) behavioral task. In this behavioral paradigm, the animals were trained to differentiate between two nose pokes, one of which (the 'active' nose poke) delivered a food pellet of 20 mg after a short auditory and visual cue (Figure 4.12a). Three mice were trained for 7-10 days until they reached a stable success rate. The imaging session was conducted for 12 active pokes per mouse which took approximately 20 minutes. During

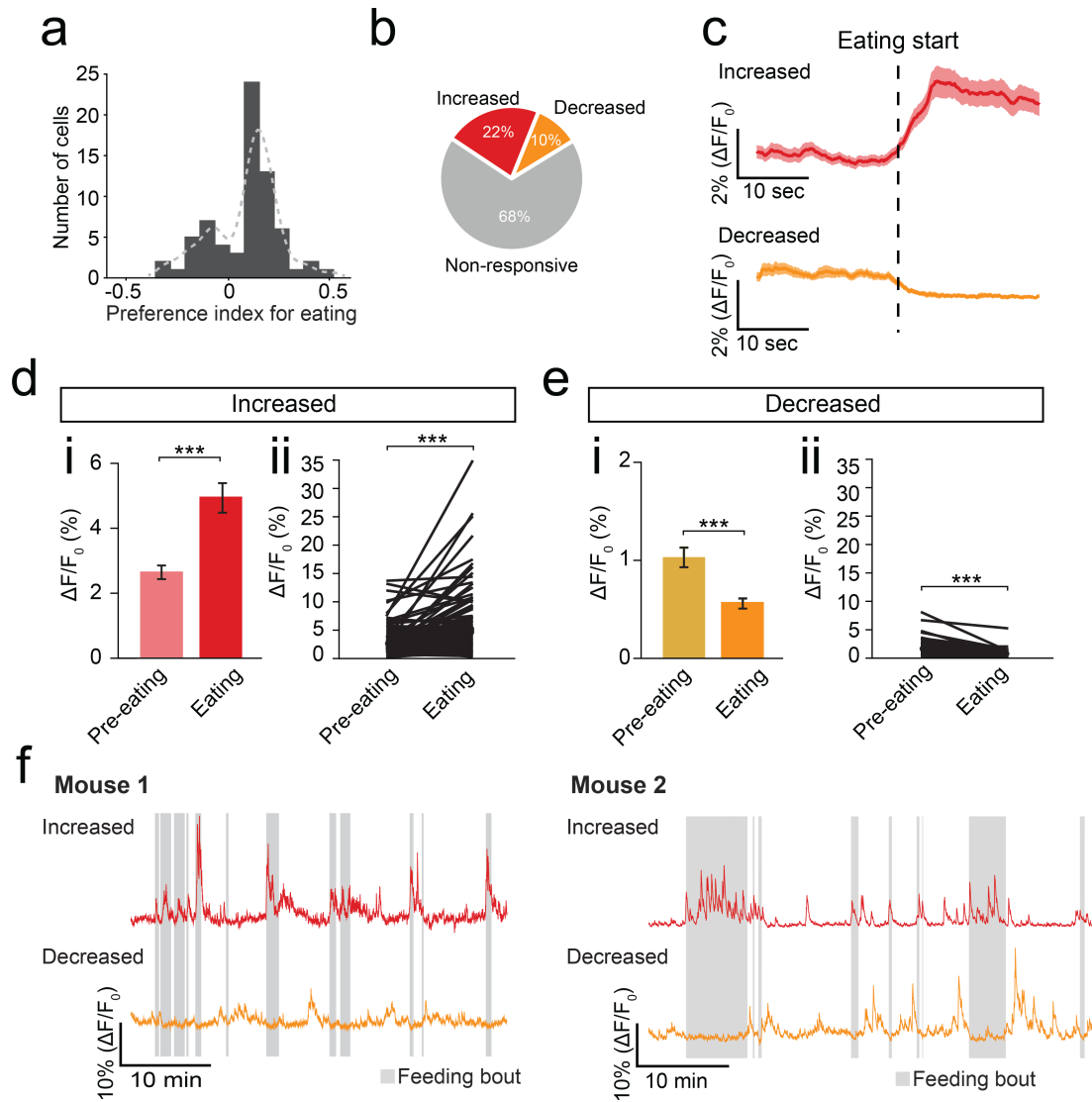


Figure 4.11: A subpopulation of CeA^{Htr2a} neurons increase activity during eating. **a)** Distribution of preference indexes of all imaged $CeA^{Htr2a}::GCaMP6s$ neurons, classified according to whether activity was increased during eating bouts compared to non-eating periods (see Methods). **b)** Classification of all 69 $CeA^{Htr2a}::GCaMP6s$ neurons. Neurons were classified according to whether activity was significantly changed during eating and preference index sign (see Methods). The classification was based on activity during all eating bouts in the imaging session. **c)** Population average of GCaMP6s fluorescence response of all $CeA^{Htr2a}::GCaMP6s$ neurons classified as significantly increasing (15/69 cells; upper) or decreasing (7/69; lower) during eating. All eating bouts during the imaging session were used to obtain an average for each cell. **d) i.** Average GCaMP6s fluorescence response of all $CeA^{Htr2a}::GCaMP6s$ neurons classified as having increased activity during eating compared to baseline. **ii.** Same as (D) i.) with each joined point depicting one cell. **e) i.** Average GCaMP6s fluorescence response of all $CeA^{Htr2a}::GCaMP6s$ neurons classified as having decreased activity during eating compared to baseline. **ii.** Same as (E) i.) with each joined point depicting one cell. **f)** Example GCaMP6s fluorescence responses of four cells from two mice classified as 'Increased' (upper) and 'Decreased' (lower). Grey shading marks the feeding bouts.

Bar plots indicate mean \pm SEM.

the test day, all mice tested performed with a success rate of 95-100% (Figure 4.12b). The average duration of the eating bouts was 8.32.5s (Figure 4.12c).

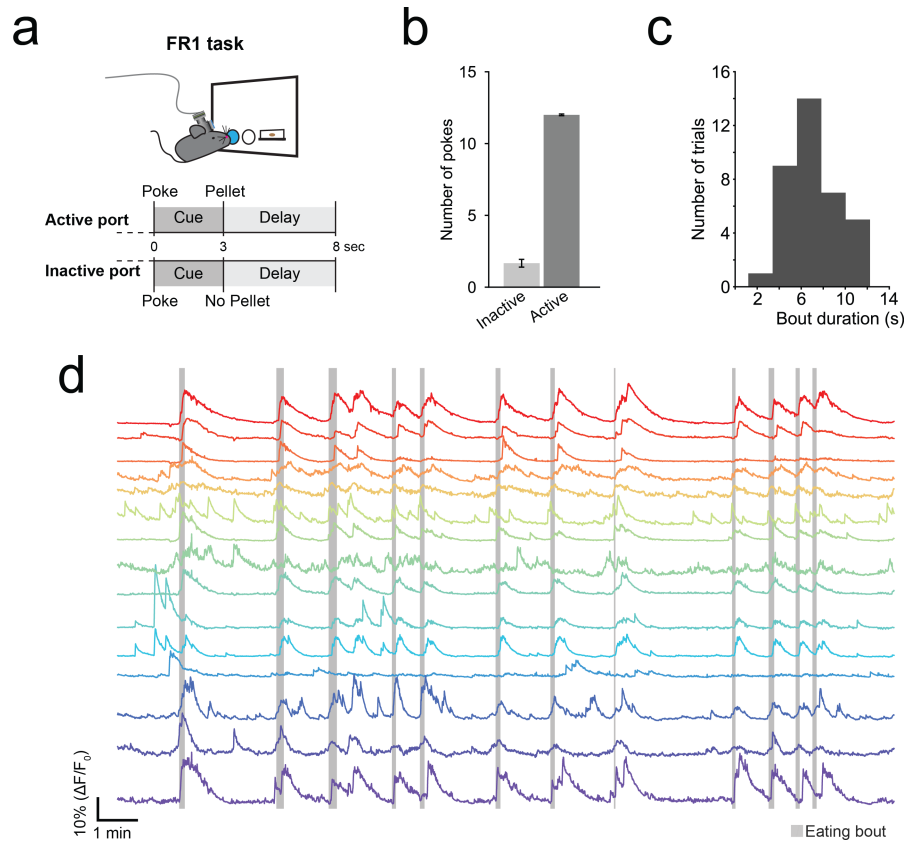


Figure 4.12: *in vivo* Ca^{2+} imaging of CeA^{Htr2a} neurons during a food-seeking task. **a)** Scheme of behavior fixed-ratio 1 (FR1) paradigm. Mice were allowed to freely nose-poke in two different ports. Active port = compound tone/light cue and delivery of 20mg food pellet. Inactive port = different compound tone/light cue and no food pellet (see Methods). **b)** Average number of nose-pokes made by three mice used for the experiments in Fig. 12-14. Imaging was performed for the equivalent duration of 12 FR1 active nose-poke trials. **c)** Distribution of the durations of the length of individual feeding bouts during the FR1 imaging sessions in Fig. 12-14. **d)** GCaMP6s fluorescence responses from individual $CeA^{Htr2a}::GCaMP6s$ cells obtained from one mouse during 12 FR1 active nose-poke trials. Each row is one cell. Grey shading marks the feeding bouts.

Bar plots indicate mean \pm SEM.

A total of 36 cells were imaged from three mice. The activity dynamics of individual cells was mostly consistent across the 12 active pokes (Figure 4.12d). To distinguish CeA^{Htr2a} neuron activity during the appetitive (active nose poke) and consummatory (eating) phases of food intake, each $CeA^{Htr2a}::GCaMP6s$ cell was classified according to whether the activity significantly during the active nose poke or eating onset (see Meth-

ods). During the active poke, very few $CeA^{Htr2a::GCaMP6s}$ neurons significantly changed their activity (5.6% Increased, 94.4% Non-responsive) (Figure 4.13a). In contrast, on average $CeA^{Htr2a::GCaMP6s}$ neurons increase activity upon eating onset (44.4% Increased, 16.7% Decreased, 38.9% Non-responsive) (Figure 4.13b). Interesting, the Ca^{2+} activity of the population remained elevated even after eating had ceased (Figure 4.13c).

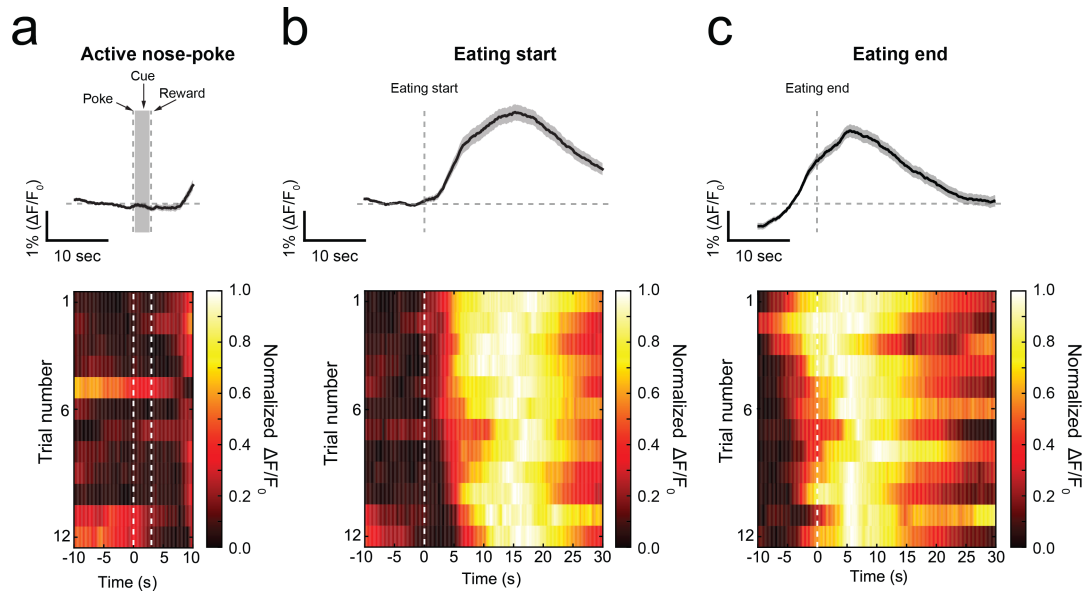


Figure 4.13: CeA^{Htr2a} neurons increase activity during eating but not during food-seeking. **a)** Left: Population average of GCaMP6s fluorescence response of all $CeA^{Htr2a::GCaMP6s}$ neurons (36 from 3 mice) aligned to the active nose poke of 12 FR1 active nose poke trials. Shading represents \pm SEM. Right: Normalized GCaMP6s fluorescence responses of all $CeA^{Htr2a::GCaMP6s}$ neurons averaged for each trial. Each row is one FR1 active nose poke trial. White stippled lines marks the duration of the nose poke. **b)** Left: Population average of GCaMP6s fluorescence response of all $CeA^{Htr2a::GCaMP6s}$ neurons (36 from 3 mice) aligned to the eating start of 12 FR1 active nose poke trials. Shading represents \pm SEM. Right: Normalized GCaMP6s fluorescence responses of all $CeA^{Htr2a::GCaMP6s}$ neurons averaged for each trial. Each row is one FR1 active nose poke trial. White stippled line marks the eating onset. **c)** Left: Population average of GCaMP6s fluorescence response of all $CeA^{Htr2a::GCaMP6s}$ neurons (36 from 3 mice) aligned to the eating end of 12 FR1 active nose poke trials. Shading represents \pm SEM. Right: Normalized GCaMP6s fluorescence responses of all $CeA^{Htr2a::GCaMP6s}$ neurons averaged for each trial. Each row is one FR1 active nose poke trial. White stippled line marks the eating stop.

Upon closer examination, individual cells showed variation in the latency with which the Ca^{2+} signal increased (Figure 4.14a, upper), with some cells (Example cells 1 and 2) increasing upon eating onset while others (Example cells 3 and 4) increased activity with a delay. These response profiles of individual cells were generally consistent across the 12

active poke trials (Figure 4.14a, lower).

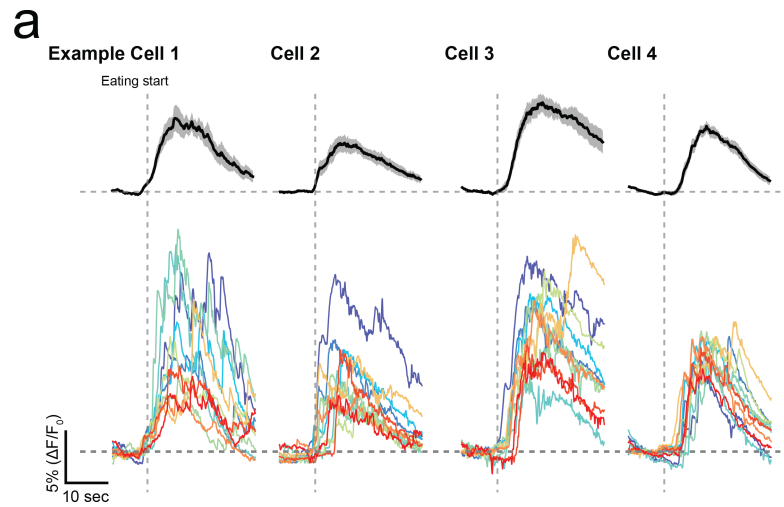


Figure 4.14: CeA^{Htr2a} neurons increase activity during eating but not during food-seeking. a) Average GCaMP6s fluorescence responses of four example $CeA^{Htr2a}::GCaMP6s$ cells aligned eating start. Upper: average response from 12 FR1 active nose poke trials. Lower: responses of each FR1 active nose poke trial.

These data show that CeA^{Htr2a} neurons are active during consumption and not during the appetitive/food-seeking phases. The average increase in Ca^{2+} activity was constant across the 12 trials (Figure 4.15a). Additionally, these data reveal that CeA^{Htr2a} neurons become recruited to the active ensemble during eating as the increase in Ca^{2+} activity differs in latency at the level of individual cells. Thus, the specificity of CeA^{Htr2a} neural activity to periods of eating strongly supports a role for these neurons in food consumption.

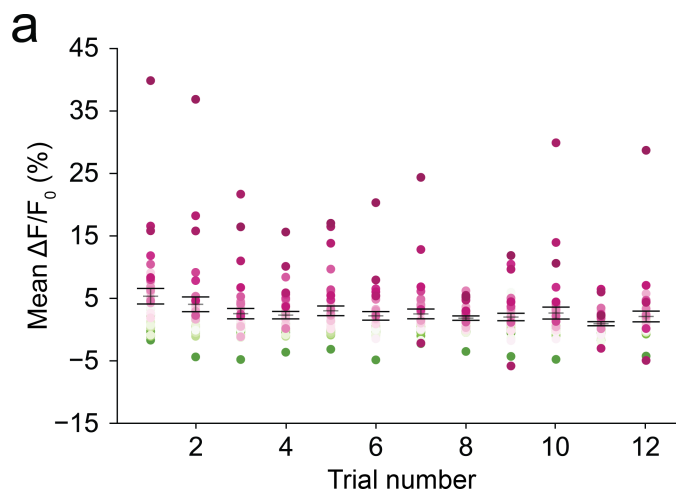


Figure 4.15: Activity of CeA^{Htr2a} neurons remains constant over FR1 trials. a) Average \pm SEM GCaMP6s fluorescence responses of all $CeA^{Htr2a}::GCaMP6s$ neurons over 12 FR1 active-poke trials. Each dot of one color corresponds to one cell.

Line plots indicate mean \pm SEM.

4.5 CeA^{Htr2a} neuron efferent projections

4.5.1 Anatomical mapping of CeA^{Htr2a} neuron innervation fields

Next, I investigated the long-range circuits in which CeA^{Htr2a} neurons function by first anatomically mapping their efferent projection fields. Using Cre-dependent ChR2 tagged with eYFP I could visualize the axonal fibers and terminals originating from CeA^{Htr2a} neurons. CeA^{Htr2a} neuron innervation was observed in many regions including the forebrain, midbrain, hypothalamus and brainstem. The most prominent regions were the lateral and medial parts of the parabrachial nucleus (PBN), the bed nucleus of the stria terminalis (BNST), and ventral lateral periaqueductal gray (PAG). Less dense projections were observed in the nucleus of the solitary tract (NTS) and the lateral hypothalamic area (LH), adjacent to the substantia nigra (SN) and ventral tegmental area (VTA) (Figure 4.16a, b).

Since the presence of ChR2-eYFP terminals in a specific brain region does not allow synapses to be distinguished from fibers of passage, I investigated the projection targets by additional anatomical methods. I was also interested in understanding whether these projection targets were specific to CeA^{Htr2a} neurons or whether other CeA populations also projected to these regions. Since the PBN was a major target of CeA^{Htr2a} neurons, I first focused on characterizing the projection to this region. To do so, fluorescent beads (retrobeads), that are taken up by axon terminals and retrogradely transported along the axon to the cell body, were stereotaxically injected into the PBN of *Htr2a-cre;tdTomato* mice (Figure 4.17 and Appendix I). After 10 days the animals were sacrificed and brain slices stained for PKC δ . Injection of retrobeads into the PBN (both lateral or medial) revealed that the inputs from the CeA arise predominantly from CeA^{PKC δ -} neurons, with 67% of retrobead-positive neurons colocalizing with CeA^{Htr2a;tdTomato}, while less than 1%

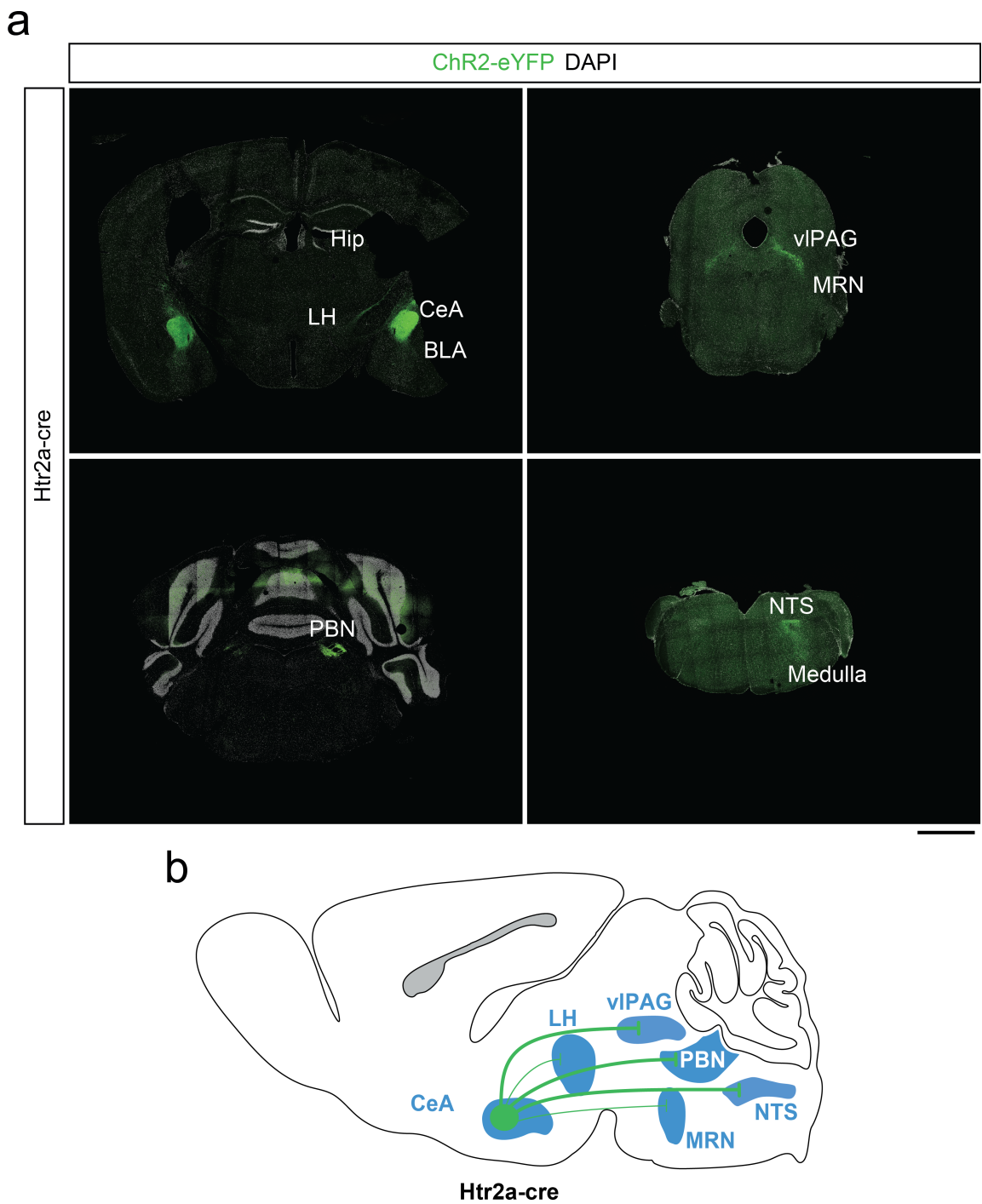


Figure 4.16: Innervation fields of axon terminals from CeA^{Htr2a} neurons. a) Representative images of coronal brain slices from mouse where Cre-dependent Chr2-EYFP was targeted into CeA^{Htr2a} neurons. CeA^{Htr2a} axons strongly innervate vIPAG, PBN and NTS. LH, MRN and medulla receives minor collaterals. b) Scheme depicting all the major and minor projection target regions of CeA^{Htr2a} neurons.

Scale bar is 1 mm. CeA; central amygdala, BLA; basolateral amygdala, Hip; hippocampus, LH; lateral hypothalamus, vIPAG; ventrolateral periaqueductal gray, PBN; parabrachial nucleus, MRN; Median raphe nucleus, NTS; nucleus of the solitary tract.

of the CeA→PBN projecting neurons were PKC δ + (Figure 4.17b, c). Taken together, these results demonstrate that CeA^{Htr2a} neurons differentially project to PBN compared to CeA^{PKC δ} neurons suggesting a potential circuit that could mediate PBN activity via GABAergic inhibition.

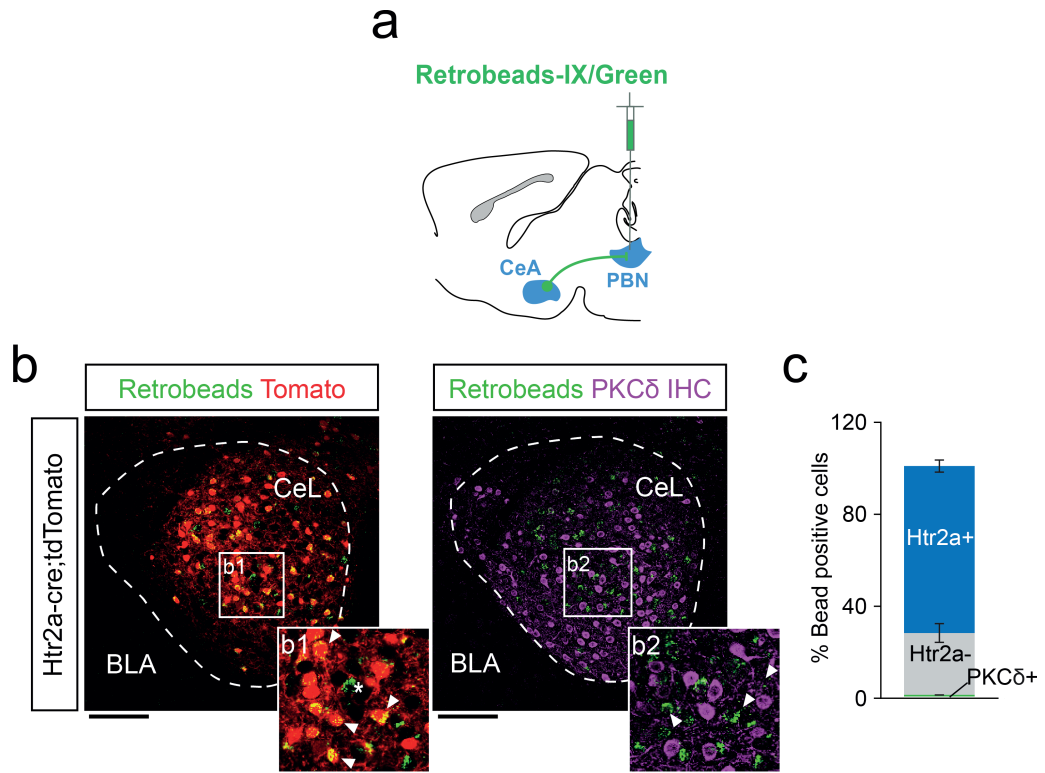


Figure 4.17: PBN-projecting CeA neurons are predominantly Htr2a+. **a)** Scheme of retrograde tracing approach to identify CeA neurons that project to the PBN. Green retrobeads were injected stereotaxically into the PBN of *Htr2a-cre;tdTomato*, taken up by the axon terminals of PBN-projecting neurons and retrogradely transported to the cell bodies in the CeA. **b)** Representative images of the CeA from a coronal brain section from a *Htr2a-cre;tdTomato* mouse where green retrobeads were injected into the PBN. Left: Colocalization of retrobead+ neurons with Htr2a-cre;tdTomato+ neurons. Right: Colocalization of retrobead+ neurons with PKC δ immunostaining. White boxes correspond to higher power images in b1 and b2. White arrowheads in b1 and b2 denote retrobead+ neurons. White asterisk in (b1) and (b2) denotes a retrobead+/Htr2a-cre;tdTomato- neuron. Retrobead+ neurons predominantly colocalize with CeA^{Htr2a} neurons. **c)** Quantification of the percentage of CeA^{retrobead+} neurons that express either Htr2a or PKC δ . The majority of CeA→PBN projecting neurons are Htr2a+. (n= 3 sections from 3 mice)

CeA; central amygdala; CeL; central lateral amygdala, BLA; basolateral amygdala, PBN; parabrachial nucleus. Scale bars are 100 μ m in (b), 50 μ m in (b1, b2). Bar graphs indicates mean \pm SEM.

I also investigated the projection from CeA^{Htr2a} neurons to the LH and VTA, as both regions are strongly implicated in feeding and reward-related behaviors [61, 80, 101]. For

the LH projectors, interestingly, most of the retrobead-positive nuclei were situated within the CeM, with 20% of the neurons in the whole CeA expressing *Htr2a* (Figure 4.18a, b). A similar picture emerged for CeA-VTA projectors, which predominantly originated in the CeM and were largely negative for *Htr2a* (Figure 4.18a, c). Furthermore, double targeting of LH and VTA revealed that non-overlapping neurons project to these two regions and that the neurons projecting to either of the two regions were PKC δ - (Figure 4.18d). These results suggest that the LH and VTA do not constitute a large projection target for *CeA^{Htr2a}* neurons.

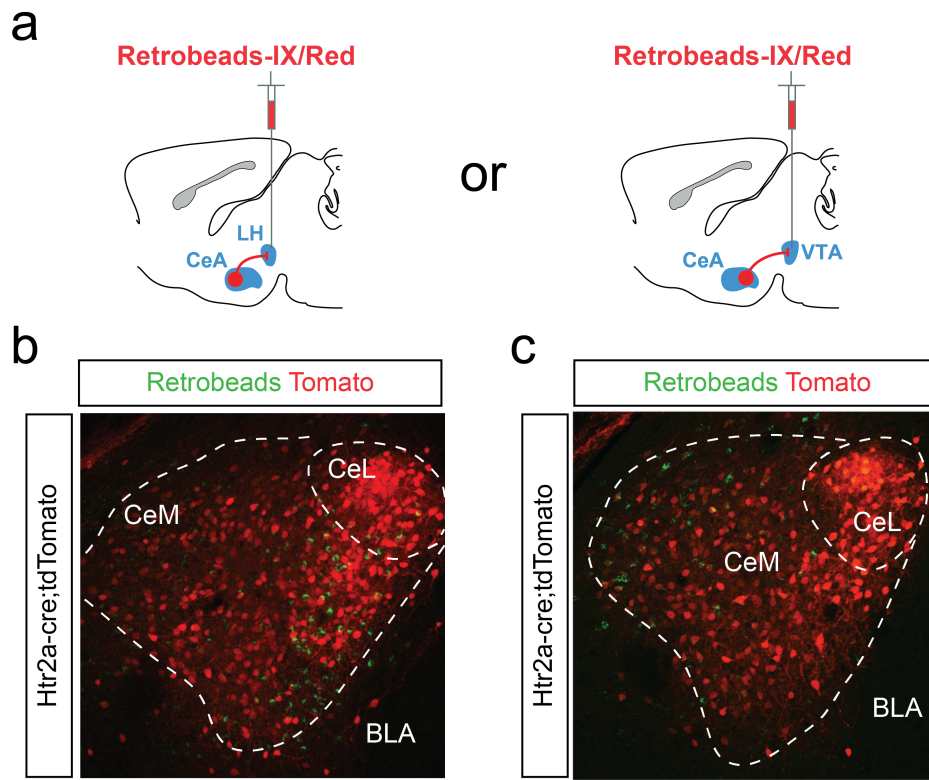


Figure 4.18: *CeA^{Htr2a}* neurons do not directly project to LH and VTA. a) Scheme of retrograde tracing approach to identify CeA neurons that project to the LH (Left) or VTA (Right). Green retrobeads were injected stereotaxically into the LH (Left) or VTA (Right) of *Htr2a-cre;tdTomato*, taken up by the axon terminals and retrogradely transported to the LH-projecting (Left) or VTA-projecting (Right) cell bodies in the CeA. b) Representative images of the CeA from a coronal brain section from a *Htr2a-cre;tdTomato* mouse where green retrobeads were injected into the LH. Retrobead+ neurons do not colocalize with *Htr2a-cre;tdTomato*+ neurons in CeA. (n = 9 sections from 3 mice) c) Representative images of the CeA from a coronal brain section from a *Htr2a-cre;tdTomato* mouse where green retrobeads were injected into the VTA. Retrobead+ neurons do not colocalize with *Htr2a-cre;tdTomato*+ neurons in CeA. (n = 6 sections from 2 mice)

CeA; central amygdala; CeL; central lateral amygdala, BLA; basolateral amygdala, LH; parabrachial nucleus, VTA; Ventral Tegmental Area. Scale bars are 100 μ m in (b, d and f).

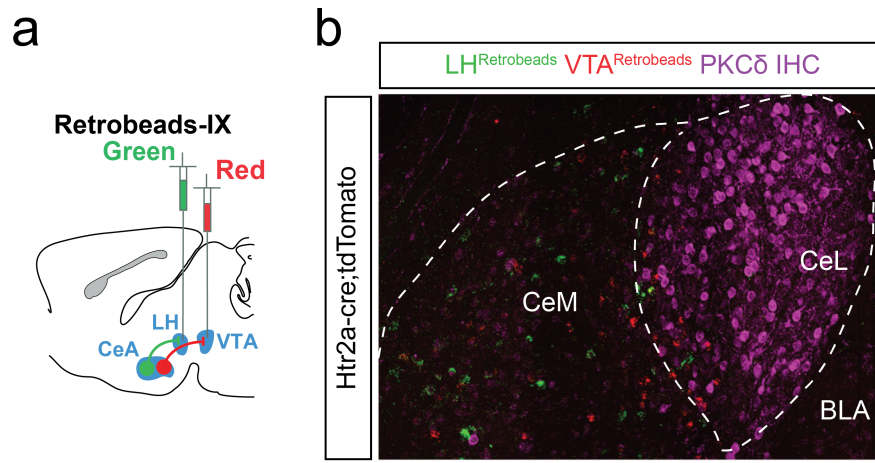


Figure 4.19: *CeA^{Htr2a}* neurons do not directly project to LH and VTA. a) Scheme of retrograde tracing approach to identify CeA neurons that project to both LH and VTA. Green retrobeads were injected stereotaxically into the LH and red retrobeads in the VTA of wild type taken up by the axon terminals and retrogradely transported to the cell bodies in the CeA. b) Representative images of the CeA from a coronal brain section from a mouse where LH and VTA projecting CeA neurons are labeled with green and red retrobeads, respectively. LH and VTA backlabeling is present mostly in CeM and do not colocalize with each other. PKC δ + neurons do not colocalize with green or red retrobeads+ positive neurons. (n = 6 sections from 2 mice)

CeA; central amygdala; CeL; central lateral amygdala, BLA; basolateral amygdala, LH; parabrachial nucleus, VTA; Ventral Tegmental Area. Scale bars are 100 μ m in (b, d and f).

4.5.2 Optogenetic investigation of *CeA^{Htr2a}* efferent projections to the PBN

In order to investigate the functionality of the major CeA efferent projections, I expressed Cre-dependent ChR2-eYFP in the CeA of *Htr2a-cre* or *PKC δ -cre* mice (Figure 4.20a), performed whole cell recordings from blindly selected neurons inside the area of ChR2 innervation in acute slices (Figure 4.20b). I first focused on projections to the lateral PBN. In *Htr2a-cre* animals, I detected light-evoked, picrotoxin-sensitive IPSCs of short latency in the majority of all recorded PBN neurons (14 of 15 cells) (Figure 4.20c, e). Light stimulation at 10 Hz was also able to suppress firing of PBN neurons evoked by current injection in all recorded neurons (Figure 4.21f, g). Recordings in slices derived from PKC δ mice supported my anatomical tracing data as very few PBN cells responded (6 of 24 cells) and the amplitudes were significantly smaller than for *Htr2a* neurons (Figure 4.20d,

e).

4.5.3 Identification of PBN CeA^{Htr2a} target neurons

The CeA and PBN are reciprocally connected brain regions. However, the anatomy and function of the PBN to CeA input has been more thoroughly described. Neurons within the lateral PBN that express CGRP innervate the CeA and drive suppression of feeding predominantly through activation of PKC δ neurons [14, 17]. We and others have shown that the CeA projects back to both the lateral and medial PBN largely via CeA^{PKC δ -negative} neurons (Figure 4.16a and Figure 4.20b); [67]). It is possible that PBN input to the CeA onto CeA^{PKC δ} neurons and output to the PBN from CeA^{PKC δ -negative} neurons is indicative of an integration of sensory input within the CeA and modulation of PBN activity via a feedback loop. To test this, I first determined whether the same PBN population sends and receives input from the CeA. At the completion of the Chr2-assisted mapping experiments, the recorded PBN neurons were filled with neurobiotin and immunostained for CGRP. This revealed that only a small number of recorded neurons were CGRP+ (2 of 14 cells) (Figure 4.21). Further examination of the anatomical location of the CeA^{Htr2a::Chr2-eYFP} fibers and CGRP expression revealed that they occupy mostly separate anatomical compartments within the PBN, with CGRP+ neurons located in a more lateral position (Figure 4.21). These experiments revealed that CeA^{Htr2a} neurons inhibited largely CGRP-negative neurons of the lateral PBN.

4.5.4 CeA^{PKC δ} neurons inhibit PBN-projecting neurons of the CeA

Given that PBN input to the CeA is predominantly onto PKC δ + neurons [14], I next examined whether CeA^{PKC δ} neurons inhibited local CeA neurons that project back to the PBN. This could suggest the existence of a feedback loop between the CeA and PBN.

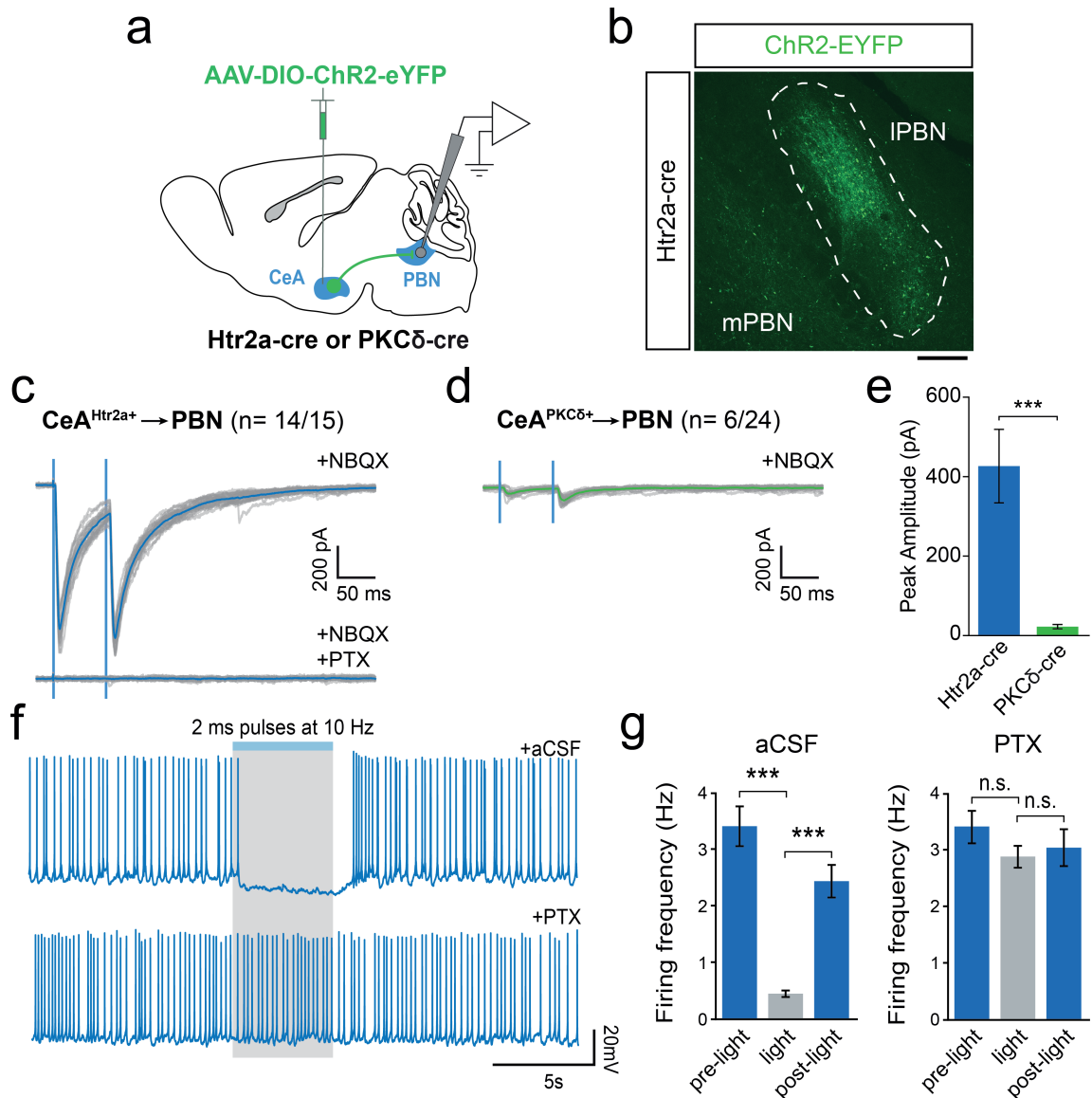


Figure 4.20: CeA^{Htr2a} neurons by not CeA^{PKC δ} neurons strongly inhibit the PBN. **a)** Scheme of approach to investigate the CeA-PBN projection *ex vivo*. Cre-dependent ChR2-eYFP was stereotactically injected into the CeA of *Htr2a-cre* or *PKC δ -cre* mice. Whole-cell recordings were performed in acute slices in area of innervation marked by ChR2+ fiber expression within the PBN. **b)** Representative image from a coronal brain section of a *Htr2a-cre* mouse where CeA^{Htr2a}::ChR2 axons that terminate in the PBN. **c)** Activation of CeA^{Htr2a} terminals in the PBN evoked high amplitude PTX-sensitive IPSCs in 14/15 PBN neurons. Overlay of 470 nm light evoked (blue bars, 1 ms pulse) individual (grey) and average (blue) IPSCs recorded from postsynaptic PBN neurons. Top: IPSCs in the absence of PTX. Bottom: IPSCs in the presence of PTX. All recordings include NBQX to block excitatory synaptic transmission. **d)** Activation of CeA^{PKC δ} terminals in the PBN evoked low amplitude PTX-sensitive IPSCs in 6/24 PBN neurons. Overlay of 470 nm light evoked (blue bars, 1 ms pulse) individual (grey) and average (green) IPSCs recorded from postsynaptic PBN neurons. **e)** 470 nm light evoked responses in the absence of PTX in *Htr2a-cre* mice (Left) were significantly higher than in *PKC δ -cre* (Right) mice (mean IPSC amplitude 426.6 pA and 30.7 pA respectively). **f)** Photoactivation of CeA^{Htr2a} terminals in the PBN by 2 ms 470 nm light pulses at 10 Hz suppressed firing of PBN neurons induced by current injection in a PTX-dependent manner. **g)** Photoactivation of CeA^{Htr2a} terminals in the PBN reduced the firing frequency of recorded PBN neurons. Quantification of the firing frequency of PBN neurons in (f) before (Left), during 470 nm light stimulation (Middle) and after light stimulation (Right). **h)** Reduction of firing frequency of PBN neurons upon photoactivation of CeA^{Htr2a} terminals in the PBN in (f, and g) was abolished by PTX.

CeA; central amygdala; PBN; parabrachial nucleus; mPBN; medial parabrachial nucleus, IPBN; lateral parabrachial nucleus. Scale bar = 100 μ m. Bar plots indicate mean \pm SEM. Two-tailed unpaired t-test. *** $p < 0.001$

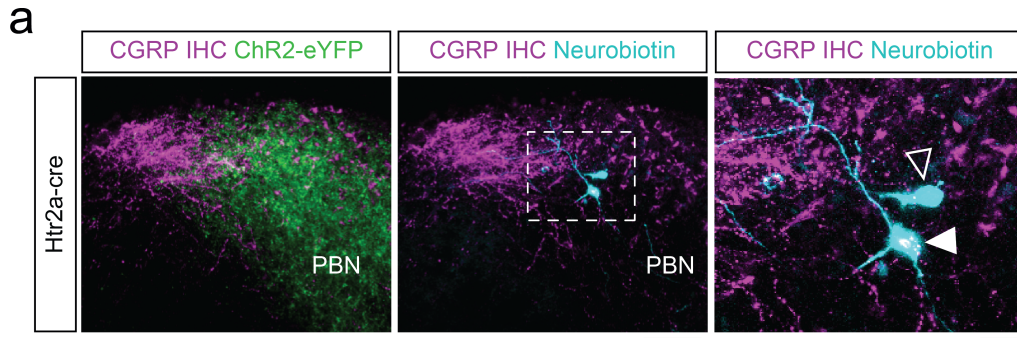


Figure 4.21: *CeA^{Htr2a}* neurons predominantly inhibit PBN^{CGRP-negative} neurons. a) Representative image from a coronal brain section showing *CeA^{Htr2a}::ChR2* fibers within the PBN relative to expression of CGRP detected by immunostaining (Left). Example image of neurobiotin-filled PBN neurons (Middle) from the experiments in Fig. 10 with adjacent CGRP immunostaining. White box corresponds to higher power image (Right). Filled neurons were *post-hoc* identified by colocalization with CGRP immunostaining (Right). CGRP+ neurons (filled arrowhead) ($n = 2/14$ neurons) and CGRP-negative neurons (empty arrowhead) were identified.

Therefore, I expressed ChR2-eYFP in *PKC δ -cre* mice and injected red retrobeads into the PBN so as to identify CeA to PBN projectors (Figure 4.22a, b). Whole-cell recordings of retrobead-filled CeA neurons demonstrated that short latency IPSCs were evoked by ChR2-mediated activation of *CeA^{PKC δ}* neurons (Figure 4.22c). These results suggest that long-range inhibition of the PBN by *CeA^{PKC δ -negative}* neurons might be subject to modulation by *CeA^{PKC δ}* neurons.

4.6 *CeA^{Htr2a}* innervation of the PBN modulates feeding and reward behaviors

Given the robust inhibition of the PBN by *CeA^{Htr2a}* neurons, we sought to determine the function of this projection in behavior. Since visceral malaise and satiety signals are relayed from the PBN to the forebrain and overall suppress food intake [16, 17], we reasoned that activation of *CeA^{Htr2a}* \rightarrow PBN projectors may inhibit these signals, leading to increased food consumption. To test this, I stereotaxically introduced ChR2-eYFP into the CeA of *Htr2a-cre* mice and placed optic fibers bilaterally above the ChR2-eYFP terminals in the PBN (Figure 4.23a, b and Appendix II). Then, we tested if stimulation

of this projection could evoke food intake in mice at the start of the light circadian period when mice typically consume little food. Indeed, we found that photostimulation of the *CeA^{Htr2a}* terminals with 20 Hz 473 nm light in the PBN resulted in a moderate increase in food consumption that was reversed upon cessation of the stimulation (Figure 4.23c). This effect was not seen with 5 Hz 473 nm light stimulation (Figure 4.23d).

As much of the signals processed by the PBN are of negative valence, including malaise and pain [44, 97], we reasoned that the *CeA^{Htr2a}*→PBN pathway may be rewarding when activated. We tested this by first performing real-time place preference (RTPP) experiments. Here, *Htr2a-cre* mice expressing ChR2 in the CeA with optic fibers implanted above the PBN were allowed to explore a two-compartment arena with entry to one randomly allocated side of the arena paired with 20 Hz stimulation of the *CeA^{Htr2a}*→PBN projection (Figure 4.24a). This experiment revealed that mice preferred to spend time

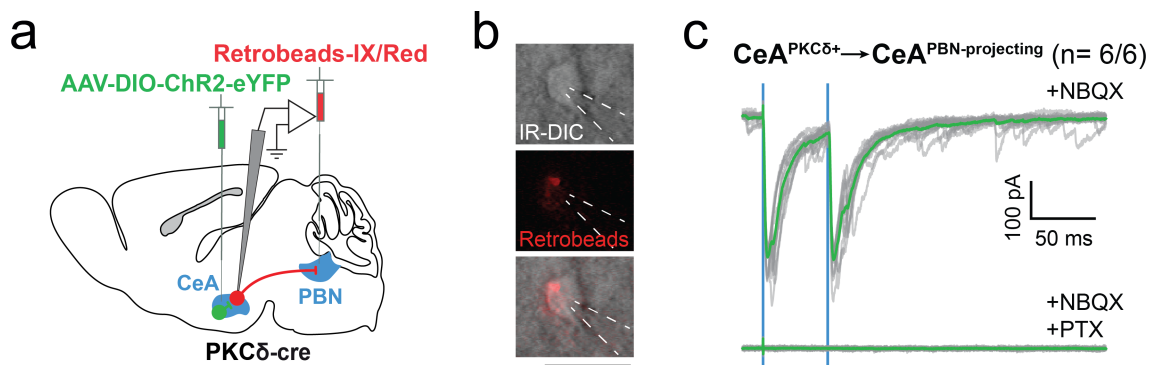


Figure 4.22: *CeA^{PKCδ}* inhibit local *CeA*→PBN projecting neurons. **a)** Scheme of approach to investigate local inhibition of PBN-projecting *CeA^{PKCδ-negative}* neurons by *CeA^{PKCδ+}* neurons. Red retrobeads were injected stereotactically into the PBN of *PKCδ-cre* mice, taken up by the axon terminals of PBN-projecting neurons and retrogradely transported to the cell bodies in the CeA. Cre-dependent ChR2-eYFP was injected into the CeA in the same animal. Whole-cell recordings were performed in acute slices from *CeA^{retrobead+}* neurons while *CeA^{PKCδ::ChR2}* were photostimulated. **b)** Images of a representative *CeA^{retrobead+}* neuron. Top: IR-DIC channel shows the cell morphology. Middle: Epifluorescent channel shows retrobeads. Bottom: overlap of IR-DIC channel and epifluorescent channel shows location of retrobeads inside the cell. Stippled lines indicate location of the recording pipette. **c)** Photoactivation of *CeA^{PKCδ}* neurons with ChR2 induces high amplitude PTX-sensitive IPSCs in 6/6 *CeA^{retrobead+}* neurons. Overlay of 470 nm light evoked (blue bars, 1 ms pulse) individual (grey) and average (green) IPSCs recorded from postsynaptic *CeA^{retrobead+}* neurons. Top: IPSCs in the absence of PTX. Bottom: IPSCs in the presence of PTX. All recordings include NBQX to block excitatory synaptic transmission.

CeA; central amygdala; PBN; parabrachial nucleus. Scale bar is 20 μ m.

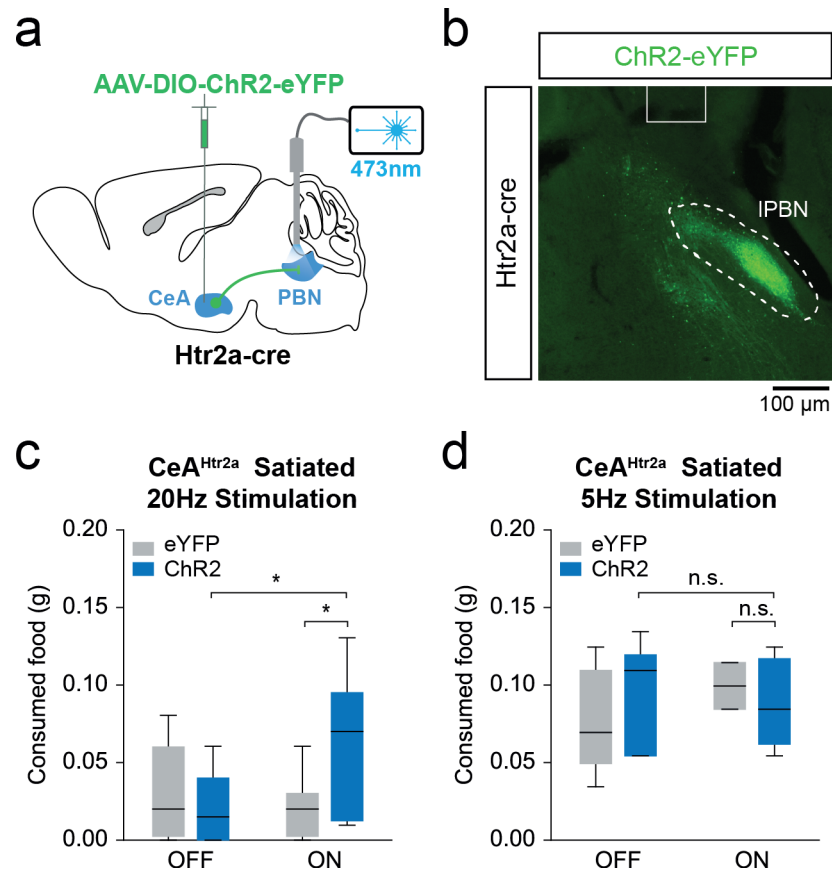


Figure 4.23: Activation of $CeA^{Htr2a} \rightarrow PBN$ projection modestly evokes food consumption. **a)** Scheme for *in vivo* activation of CeA^{Htr2a} terminals in the PBN. Cre-dependent ChR2-eYFP was bilaterally injected into the CeA of *Htr2a-cre* mice and optic fibres were bilaterally implanted over the PBN (only one side is shown). **b)** Representative image from a coronal brain section showing approximate placement of the optic fiber (boxed area) relative to expression of $CeA^{Htr2a}::ChR2$ fibers within the PBN (only one side is shown). **c)** *in vivo* stimulation of CeA^{Htr2a} terminals in the PBN at 20 Hz modestly increases food consumption in the photostimulated epoch relative to the non-photostimulated epoch in $CeA^{Htr2a} \rightarrow PBN::ChR2$ mice under satiated conditions. There was no significant difference in the amount of food consumed by *CeA^{Htr2a} \rightarrow PBN::ChR2* and *CeA^{Htr2a} \rightarrow PBN::eYFP* mice during the photostimulated epoch. Left: Non-photostimulated epoch. Right: Photostimulated epoch. (n = 10 mice per group) **d)** *in vivo* stimulation of CeA^{Htr2a} terminals in the PBN at 5 Hz does not evoke food consumption in $CeA^{Htr2a} \rightarrow PBN::ChR2$ in satiated mice. Left: Non-photostimulated epoch. Right: Photostimulated epoch. (n = 7-8 mice per group)

CeA; central amygdala; PBN; parabrachial nucleus. Scale bar: 100 μ m. Boxwhisker plots display median, interquartile range and 5th-95th percentiles of the distribution. Two-tailed unpaired t-test or two-tailed paired t-test. * $p < 0.05$

on the side of the area where they received 20 Hz but not 5 Hz photostimulation (Figure 4.24b-d). This suggests that activation of the $CeA^{Htr2a} \rightarrow PBN$ pathway is rewarding since mice prefer to spend time in an area where this projection is activated.

To determine whether this is a motivated behavior we investigated whether mice would nose-poke for optical activation of this projection using an intracranial self-stimulation

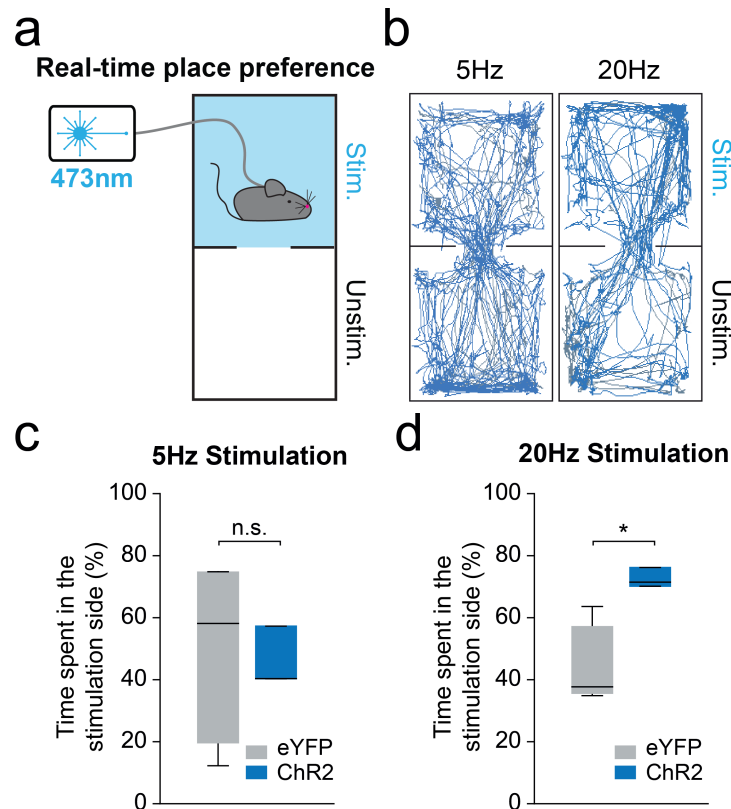


Figure 4.24: Activation of $CeA^{Htr2a} \rightarrow PBN$ projection induces place preference. **a)** Scheme of real-time place preference (RTPP) assay where one side of a two-chamber arena marked 'Stim.' was randomly paired with 5 Hz or 20 Hz 473 nm intracranial photostimulation of CeA^{Htr2a} terminals in the PBN in $CeA^{Htr2a} \rightarrow PBN::ChR2$ mice. **b)** Representative locomotor traces of $CeA^{Htr2a} \rightarrow PBN::ChR2$ mice during the RTTP assay where 5 Hz (left) or 20 Hz (right) photostimulation was received in the side of the chamber marked 'Stim.' **c)** The percentage of time spent on the photostimulated side of the arena by $CeA^{Htr2a} \rightarrow PBN::ChR2$ and $CeA^{Htr2a} \rightarrow PBN::eYFP$ mice was not significantly different when 5 Hz photostimulation was received. ($n = 5-6$ mice per group) **d)** $CeA^{Htr2a} \rightarrow PBN::ChR2$ mice spent significantly more time on the photostimulated side of the arena than $CeA^{Htr2a} \rightarrow PBN::eYFP$ mice when 20 Hz photostimulation was received. ($n = 5-6$ mice per group)

Boxwhisker plots display median, interquartile range and 5th-95th percentiles of the distribution. Two-tailed unpaired t-test. * $p < 0.05$

(ICSS) paradigm. To do this I built a behavioral set up where mice can nose poke in two side-by-side ports one of which would deliver a short pulse of light stimulus. In this behavioral paradigm, mice were trained to nose-poke at a two port apparatus where pokes in the active port delivered a 20 Hz pulse train of 473 nm light into $CeA^{Htr2a}::ChR2-eYFP$ expressing neurons while pokes in the inactive port had no consequence (Figure 4.25a). Mice strongly nose-poked for activation of the $CeA^{Htr2a} \rightarrow PBN$ projection more than eYFP control animals and they interacted very little with the inactive port (Figure 4.25b, c).

This revealed that activation of the $CeA^{Htr2a} \rightarrow PBN$ projection is rewarding as mice are motivated to engage in ICSS behaviour. Taken together, these data demonstrate that the $CeA^{Htr2a} \rightarrow PBN$ projectors function in food intake and also mediate reward-seeking behaviour.

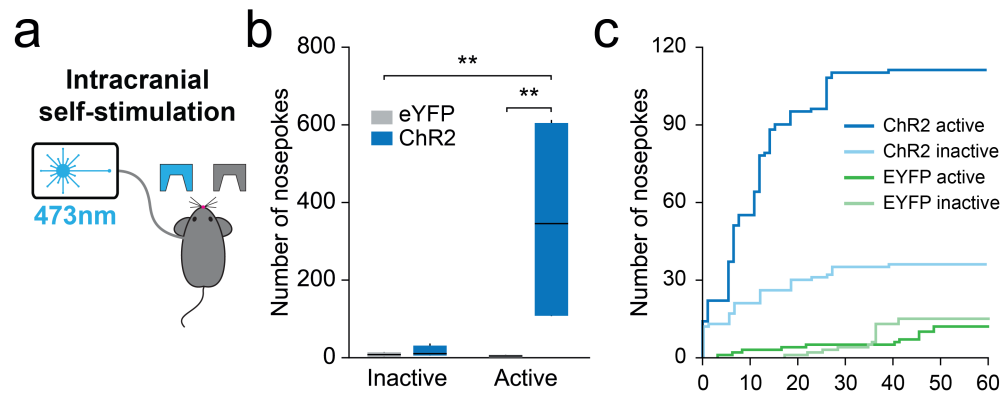


Figure 4.25: The $CeA^{Htr2a} \rightarrow PBN$ projection supports self-stimulation behaviour. **a)** Scheme of the intracranial self-stimulation (ICSS) assay where $CeA^{Htr2a} \rightarrow PBN::ChR2$ and $CeA^{Htr2a} \rightarrow PBN::eYFP$ mice were trained to nosepoke at two ports. The 'Active' port (blue) triggered 473 nm 20 Hz intracranial photostimulation while the 'Inactive' port (grey) did not. **b)** $CeA^{Htr2a} \rightarrow PBN::ChR2$ made significantly more 'Active' nosepokes compared to $CeA^{Htr2a} \rightarrow PBN::eYFP$ controls and compared to nosepokes made at the 'Inactive' port. (n = 6 mice per group) **c)** Cumulative nosepokes responses by representative $CeA^{Htr2a} \rightarrow PBN::ChR2$ and $CeA^{Htr2a} \rightarrow PBN::eYFP$ mice during the 60 minute session.

Boxwhisker plots display median, interquartile range and 5th-95th percentiles of the distribution. Two-way ANOVA with Bonferroni *post-hoc* test. **p<0.01

Chapter 5

Thesis Summary

In the work presented in this thesis, I characterized, through molecular, electrophysiological, imaging and behavioral analysis, a genetically defined population of CeA neurons that express the serotonin receptor Htr2a. Characterization of these neurons revealed this population to be mutually exclusive of the well-characterized CeA^{PKC δ} population that has a described role in food consumption [14] and to display a homogeneous electrophysiological phenotype. ChR2-assisted circuit mapping revealed that CeA^{Htr2a} neurons inhibit other neurons within the CeA and that many of which are PKC δ +. This suggests that CeA^{Htr2a} and CeA^{PKC δ} neurons are functionally opposing cell types. Using cellular-resolution Ca²⁺ imaging, CeA^{Htr2a} neurons are found to be excited during eating behavior but not during food seeking, suggesting that these neurons may have a role in feeding behavior.

I also investigated the long-range neural circuits in which these neurons function. Using various methods including anterograde efferent projection tracing and retrograde tracing approaches, I identified the projection targets of CeA^{Htr2a} neurons. The PBN as a prominent target, specific to CeA^{Htr2a} neurons as compared to CeA^{PKC δ} neurons.

CeA^{Htr2a} neuron-mediated inhibition of the PBN promotes food consumption and reward-related behaviors, demonstrating this projection as a functional output of CeA^{Htr2a} neurons. Together these findings reveal a potential role for CeA^{Htr2a} neurons in appetitive behaviors and propose possible local and long-range circuit mechanisms that underlie these effects.

Chapter 6

Discussion

6.1 Identification of central amygdala neural subpopulations

The central nucleus of the amygdala is classically known to mediate aversive behaviors including conditioned fear and anxiety. Although a number of studies have implicated this region in reward-related behaviors and positive consummatory behavior, this area of research has received relatively little attention. To identify the neural components that mediate these diverse behaviors as well as the circuits in which they function, molecular markers have been relied upon as an entry point for classifying, accessing, manipulating and observing specific subpopulations of CeA neurons. Previous studies have identified neural subpopulations using immunohistochemistry and pharmacology [43], in situ hybridization [107] and microarray analysis [69].

Two recent studies were the first to describe two major neuronal subpopulations that express PKC δ and SOM, respectively, that form antagonistic components of the fear circuit [39, 59]. In my thesis work, I characterized a CeA neuronal subpopulation that expresses serotonin receptor type 2a (Htr2a) in central amygdala. Immunohistochemical analysis revealed that CeA^{Htr2a} neurons are exclusively PKC δ negative while partially

overlapping with SOM. Even though each of these markers comprises of 25-30% of CeA neurons individually, their expression coverage fails to include all CeA neurons. The results presented in this thesis suggest that there may be other uncharacterized subpopulations of central amygdala neurons.

The mutually exclusive expression of Htr2a and PKC δ in the CeA makes these neurons an ideal entry point for targeting CeA neurons that promote appetitive behaviors, in opposition to PKC δ neurons. It is important to consider, however, that expression of a molecular marker is only one feature by which a group of neurons can be categorized and that expression of a common marker does not necessarily imply that these neurons form a functionally homogeneous population. Considering the molecular heterogeneity of CeA and that most of the markers have overlapping expression patterns, intersectional genetics approaches using two or more markers [49] may be a better method to target and probe genetically defined subpopulations of CeA. Other approaches to identify neural subpopulations and to assess their role in behavior include identifying molecularly-defined neurons based on activity during behavior [9, 55] or projection target [17, 50, 78], which if applied to the CeA may yield more insight into functional neural populations and their connections with different brain regions.

In addition to a molecular characterization of the CeA^{Htr2a} neuron population, I characterized these neurons in terms of their electrophysiological properties, which have been used to ascribe CeA neurons to different classes [63, 69, 95]. This analysis revealed that most CeA^{Htr2a} neurons are late firing ($\sim 85\%$), where the firing of action potentials occurs with a delay after current injection. Of the previously characterized CeA molecularly-identified subpopulations, the electrophysiological properties of CeA^{SOM} and CeA^{PKC δ} have been characterized. CeA^{SOM} neurons are electrophysiologically heterogeneous (60% regular spiking, 40% late firing) [59] while CeA^{PKC δ} are homogeneous (86% late firing)

[39]. Thus, compared to another CeA^{PKC δ -negative} population (CeA^{SOM}), CeA^{Htr2a} and CeA^{PKC δ} neurons are more electrophysiologically homogenous. Despite this property, it is unclear how it is functionally important during behavior. However, since late firing neurons require larger current injections in order to fire action potentials [63], stronger inputs may be required *in vivo* to excite these neurons, than for regular spiking neurons. This may arise from one of two scenarios: 1) a large current from a single neuron source may be required to elicit action potentials in the neuron or, 2) multiple smaller inputs which together sum to a large input current may be required to excite the cell. The latter case suggests that these neurons may receive multiple different inputs and that integration of these signals within the cell is required for their excitation. However, clear evidence for this phenomenon is still lacking.

Here I have used the cellular marker Htr2a as a means to genetically access a population of CeA^{PKC δ -negative} neurons. However, an important open question is how expression of Htr2a affects the physiology of these cells and how serotonin is implicated in their function. Previously, it was shown that the selective Htr2a antagonist glemanserin reduces activity of CeA^{Htr2a} neurons, suggesting that serotonin increases the firing of these cells [45]. Further, monosynaptic rabies tracing performed in our lab revealed that these neurons receive input from the dorsal raphe in which a large population of serotonergic neurons are located (data not shown, experiments done by Marion Ponsérre). It will therefore be interesting to further assess the role of serotonin in the function of these neurons. Use of Htr2a-specific agonists and antagonists which can be delivered *in vivo* into the CeA during behavior will help unravel how serotonin influences their physiology and control of behavior.

6.2 Local connectivity of central amygdala neuronal subtypes

Previous studies have shown a great deal of interconnectivity between molecularly identified neuronal subpopulations in central amygdala. Two independent studies have shown, using ChR2-assisted circuit mapping, that CeA^{PKC δ} neurons can inhibit other cells in the CeL [14, 39]. In addition, CeA^{PKC δ} neurons were shown to inhibit PAG projecting CeM neurons [39]. Connections between other CeA molecularly-defined subpopulations have also been shown. Recently, Li *et al.* showed that optogenetic activation of SOM+ neurons in CeL induced IPSCs in SOM-negative cells of CeL [59]. Another study from Fadok and colleagues proposed a local circuit mechanism where CRH+ neurons form a reciprocal connection between SOM+ and PKC δ + neurons of CeL, albeit to different extents [29]. In this thesis, I have shown, using ChR2-assisted ex vivo circuit mapping, that CeA^{Htr2a} neurons were able to inhibit both PKC δ positive and negative neurons within the CeA local circuitry. Considering, the extensive interconnectivity between neurons within the CeA, my results suggest that Htr2a+ and PKC δ + neurons of CeA form reciprocal connections at the microcircuit level.

Given that activation of CeA^{PKC δ} neurons decreases food consumption, behavior experiments were performed in the lab to assess the function of CeA^{Htr2a} neurons in feeding behavior (experiments done by Amelia Douglass). This revealed that activation of these neurons promotes food consumption (data not shown). Thus, CeA^{Htr2a} and CeA^{PKC δ} are functionally antagonistic cell types that reciprocally inhibit one another. The high degree of connectivity within the CeA local circuit, suggests that inhibitory connections between defined cell types may constitute a circuit mechanism through which the CeA can bidirectionally influence behavior through the activity of functionally opposing cell

types. However, to better understand how such a mechanism may function, further studies are necessary to address important questions. First, the differences in synaptic strength between the two populations should be addressed to determine whether the connection between them is equally weighted. Second, the *in vivo* firing rates of genetically targeted neuronal populations should be defined during the behavior of interest in order to understand how antagonistic behaviors are encoded at the circuit level. Third, the nature of the input signals to functionally opposing CeA subpopulations and their *in vivo* dynamics should be determined. This will reveal the reciprocity of their endogenous activity patterns and allow insight into how the balance in the activity of two populations overall influences behavior. To achieve this goal, advanced intersectional genetic tools to target more than one subpopulation in the same mouse could be beneficial. This will permit the monitoring of reciprocally connected CeA populations using Ca^{2+} indicators whose expression is dependent on different recombinases (eg. Cre or Flp recombinases).

6.3 **CeA^{Htr2a} neurons increase their activity during food consumption**

A recent study showed that activation of CeA^{PKC δ} neurons rapidly inhibits food consumption. This study also suggested a circuit mechanism where inhibition of food intake by CeA^{PKC δ} neurons was via GABA-mediated inhibition of local CeA neurons [14]. However, the existence of a CeA subpopulation that can positively modulate food intake or the identity of such a group of cells was not identified. My initial findings presented in this thesis showed that PKC δ -negative CeA^{Htr2a} neurons form reciprocal inhibitory connections with CeA^{PKC δ} neurons. Thus, I hypothesized that they could be functionally reciprocal to CeA^{PKC δ} neurons and may promote food intake. Behavior experiments performed in our lab have shown that activation of CeA^{Htr2a} neurons indeed promotes

food consumption (data not shown, experiments done by Amelia Douglass). Functional reciprocity between CeA^{PKC δ} and CeA^{Htr2a} neurons supported by the reciprocal inhibitory connectivity strongly suggests an important role for CeA in antagonistic control of food consumption.

Eating behavior is composed of multiple phases that include food-seeking (known as appetitive behavior) and consumption (known as the consummatory phase). Our *in vivo* Ca²⁺ imaging experiments of CeA^{Htr2a} neural activity in freely behaving mice demonstrated that CeA^{Htr2a} neurons increased their activity during food consumption and consistently do so across different experiments and multiple trials. In the FR1 experiment, where mice had to perform a nose poke in order to receive a food pellet, CeA^{Htr2a} neurons responded only during food consumption and not during the nose poke that triggered food delivery (appetitive phase) or upon presentation of cues that signaled food delivery. Additionally, chemogenetic activation of CeA^{Htr2a} neurons didn't increase animal's motivation to work for food reward in a progressive ratio task (data not shown, experiments by Amelia Douglass). Taken together these results suggest that CeA^{Htr2a} neurons are unlikely to be involved in food seeking but specifically in food consumption.

The timing of CeA^{Htr2a} neuron activity changes with respect to eating onset also reveals additional information about their function. During the FR1 imaging experiment, the neurons increase activity proximal to eating start. Since behavior experiments demonstrate that the activity of these neurons promotes food intake, the activity of these neurons during eating suggests their activity does not contribute to the drive to eat food but instead modulates food intake once it has begun. Food intake is influenced early on during consumption through modulating the palatability, taste and sensory properties of food [24]. Thus, because CeA^{Htr2a} neurons are active during this early part of eating, the activity of these neurons may influence food intake by modulating these properties. Indeed,

additional behavior experiments have revealed that the activity of CeA^{Htr2a} neurons is positively reinforcing and can influence the rewarding properties of food including taste and palatability (data not shown, experiments done by Amelia Douglass). Together, these data suggest that the activity of CeA^{Htr2a} neurons during eating positively influences the rewarding properties of food to promote its consumption.

Our imaging experiments also revealed heterogeneity in the latency with which CeA^{Htr2a} neurons changed activity. Some neurons increased activity as soon as eating commenced while others increased with a latency. This heterogeneity in the response latencies suggests that the activity of these neurons is not necessarily driven by a single input but by the combination of multiple converging inputs onto them. It is highly likely that information about different aspects of food reward and value, sensation and palatability of the food, and internal state arrive onto the CeA as well the anorexigenic information conveyed by CeA^{PKC δ} which interact with CeA^{Htr2a} neurons. This may also explain why there is heterogeneity in the response profiles of CeA^{Htr2a} neurons during eating- with some neurons increasing, decreasing or not changing their activity. Thus, the CeA may receive multiple inputs that are integrated within the CeA^{Htr2a} population and through local interactions with other molecularly-defined CeA neuron populations. Interestingly, our *in vivo* imaging experiments also revealed that the Ca²⁺ signal in the CeA^{Htr2a} neuron population remained elevated even after eating had ceased. This could reflect an accumulation of GCaMP signal resulting from multiple inputs converging on the population. Since GCaMP6s displays a slow rise and decay as a result of multiple action potentials [20], the slow decay in signal that we observed after eating has ceased may reflect the heterogeneity in CeA^{Htr2a} activity onset. Nevertheless, together the data from our imaging experiments show that CeA^{Htr2a} neurons are an important circuit node important for modulating food consumption.

6.4 Inhibition of PBN neurons by CeA descending projections is rewarding and modulates consummatory behavior

Analysis of the efferent projections of CeA^{Htr2a} neurons revealed a dense innervation of the PBN. I independently confirmed that CeA^{Htr2a} neurons inhibit neurons within the PBN. Descending projections from the CeA to the PBN has been described and has been postulated to modulate taste processing [65, 67]. However, it is not clear how CeA-mediated PBN inhibition relates to behavior. A recent study described that a subpopulation of PBN neurons that express CGRP mediate feeding suppression as a result of sickness, ingestion of unpalatable foods and satiety through activation of CeA^{PKC δ} neurons [14, 16, 17]. My retrograde tracing and electrophysiology experiments that compared innervation of the PBN by CeA^{Htr2a} and PKC δ -expressing neurons showed that very little innervation of the PBN from the CeA originates from PKC δ neurons. This suggested that a loop between the CeA and PBN, where via one arm, malaise and satiety information arises from the PBN and is relayed onto the CeA, leading to feeding suppression, while the other arm comprises an inhibitory feedback projection from the CeA to the PBN that gaits the output of the PBN. Therefore, the CeA-PBN projection may function to promote food consumption by controlling the anorexigenic PBN output and compliment the local inhibition of PKC δ neurons in CeA.

We found that photostimulation of CeA^{Htr2a} axons in the PBN was modestly promoted increased food consumption but intriguingly was rewarding as mice were motivated to self-stimulate this projection and preferred to spend time in an area where photostimulation was received. The modest effects on food intake suggest that modulating food consumption is unlikely to be a major function of this projection. This was corroborated

by my attempts to uncover the identity of the PBN neurons targeted by CeA^{Htr2a} neurons. This revealed a dissociation between the projection field of CeA^{Htr2a} neurons and expression of CGRP in the PBN and only a small percentage of post-hoc identified PBN neurons after electrophysiological recordings were CGRP+. This suggests that CeA^{Htr2a} neurons likely do not inhibit the same neurons that convey anorexigenic signals to the CeA.

Overwhelmingly, the PBN is known to process signals of negative valence which in addition to visceral and gustatory signals include pain [38, 92]. The possibility, therefore, remains that CeA^{Htr2a} neurons target another subpopulation of neurons that carry negative valence signals which may underlie the rewarding effects of activating this projection. However, despite our finding that CeA^{Htr2a}→PBN activity is rewarding, the conditions under which CeA^{Htr2a} neurons function to gate the output of the PBN remains to be fully elucidated.

My tracing experiments also revealed other sites of CeA^{Htr2a} neuron innervation. These include the LH, VTA, BNST, PAG and NTS. Among the sites targeted by CeA neurons, the PAG has received the most attention. CeA projections PAG-projecting neurons have a role in driving conditioned freezing responses [84, 104, 106]. Since we have identified a role for CeA^{Htr2a} neurons in food consumption, I focused on further characterizing the projections from CeA^{Htr2a} neurons to the LH and VTA, as these regions are known to be involved in food consumption and appetitive motivated behaviors [48, 61, 80, 100, 101]. Use of retrograde tracing revealed that most CeA neurons projecting to the LH and VTA were CeA^{Htr2a}-negative and originated predominantly from the CeM. Thus, the LH and VTA are not major projection targets of CeA^{Htr2a} neurons. However, given the high degree of connectivity within the CeA, CeA^{Htr2a} neurons may function through the VTA and LH through a polysynaptic circuit. For example, CeA^{Htr2a} neurons may locally inhibit VTA or

LH-projecting CeA neurons which tonically inhibit their VTA or LH targets. Activation of CeA^{Htr2a} neurons would relieve this inhibition, leading to activation of the VTA or LH cell. A disinhibitory circuit mechanism was shown to underlie the food consumption and reward-related effects of activating LH neurons that project to the VTA. Here, GABAergic LH neurons inhibit GABAergic VTA neurons which in turn inhibit their inhibition of dopaminergic VTA neurons, leading to dopamine release in the NAc [80]. Since the behaviors elicited by CeA^{Htr2a} neurons are strikingly similar to those controlled by LH GABAergic neurons, a similar interaction with the mesolimbic dopamine system may exist here. However, further work is needed to understand the nature of circuit interactions between the CeA and brain regions classically implicated in reward processing.

Chapter 7

Conclusions & Outlook

The work presented in this thesis has shed light onto the incredible complexity of the CeA and associated circuits. Here, I have characterized a relatively undescribed population of CeA neurons that express Htr2a. Through *in vivo* imaging, electrophysiological and circuit mapping approaches, this work has provided insight into how this population of CeA neurons promotes appetitive behaviors. Further, by showing local circuit interactions between CeA^{Htr2a} neurons and CeA^{PKC δ} neurons that suppress appetite this work has also revealed a mechanism by which the same brain region can function in both food intake and suppression.

Following on from this work, there are several interesting avenues of research that can be taken to further understand the function of the CeA. It is clear that neurons within the CeA are highly interconnected and that local inhibitory microcircuits underlie the function of the CeA in behavior. However, it will be important to gain a complete picture of local CeA connectivity between defined cell types and the strength of these connections during specific behaviors. The idea that reciprocal antagonistic interactions between CeA^{Htr2a} and CeA^{PKC δ} neurons determined whether feeding is suppressed or promoted is an attractive

model. However, the respective synaptic strength of these connections, whether both connections are in competition or whether there is tonic inhibition in one direction and how the activity of one population comes to dominate behavioral output remains unknown. Answering these questions will provide a much greater understanding of the function of local CeA microcircuits.

Although we found that CeA^{Htr2a} neurons are active during eating behavior and promote food consumption, the activity dynamics of CeA^{PKC δ} neurons are less clear. CeA^{PKC δ} neurons were shown to be activated by anorexigenic compounds and during satiety [14]. However, these conclusions were based on staining of the neural activity marker c-fos, which only provides a snapshot of neural activity at a given time point with relatively little temporal specificity. Given they are active during satiety, it may be the case the CeA^{PKC δ} neurons are tonically active during non-eating periods to inhibit CeA^{Htr2a} neurons or they may be active only during meal termination to promote satiety. These neurons may also become active upon administration of compounds that suppress appetite. It will be important to perform *in vivo* Ca²⁺ imaging experiments to determine how the activity of CeA^{PKC δ} neurons is reconcilable with that of CeA^{Htr2a} neurons given their opposing control of food consumption.

To determine how CeA^{Htr2a} neurons function in food consumption it will be critical to determine the inputs that excite these neurons. Monosynaptic pseudo-rabies viral tracing methods have revealed that CeA^{Htr2a} neurons receive inputs from many brain regions with previously described roles in feeding, reward and motivated behaviors (data not shown, experiments done by Marion Ponserre). However, this approach is purely anatomical and does not implicate any of these inputs in transmitting feeding relevant information. Additionally, it does not allow an appreciation of the nature of the inputs (excitatory or inhibitory), the identity of the cells that provide input nor the type of information that

is being transmitted. Therefore, it will be important to identify the inputs that excite CeA^{Htr2a} neurons.

Although I have shown that CeA^{Htr2a} neurons strongly inhibit the PBN and that activation of this projection promotes both food intake and positive reinforcement, several questions remain outstanding regarding the CeA^{Htr2a}→PBN projection. The identity of PBN neurons that receive CeA^{Htr2a} input and their behavioral relevance remains unknown. I showed through posthoc immunostaining of recorded PBN neurons, that most do not express CGRP. This suggests that the neurons are largely mutually exclusive of those that mediate feeding suppression [16, 17]. However, whether these cells are synaptically connected with CGRP neurons, meaning that CeA^{Htr2a} neurons may indirectly gate the anorexigenic output of the PBN remains an important question.

The modest effects of activating the CeA^{Htr2a}→PBN projection compared to activation of the CeA^{Htr2a} population as a whole (data not shown, experiments done by Amelia Douglass), suggests that inhibition of the PBN may not be the major projection that modulates food intake. It will be important to electrophysiologically and behaviorally probe the other outputs of CeA^{Htr2a} neurons including the NTS and BNST, however, it is also possible that CeA^{Htr2a} neurons also function through polysynaptic pathways. My retrograde tracing experiments from the VTA and LH, regions strongly implicated in reward and feeding, revealed that most neurons projecting to these regions were in the CeM and were Htr2a negative. Since disinhibitory circuits involving CeL→CeM interactions are a key component underlying the expression of learnt fear [22, 39], a similar mechanism may underline the modulating of feeding by CeA^{Htr2a} neurons. To explore this idea, the functional connectivity between CeA^{Htr2a} neurons and CeM^{Htr2a-negative} neurons identified by their projection target should be determined. Additionally, experiments that allow *in vivo* monitoring of Ca²⁺ activity of CeA^{Htr2a} neuron subpopulations classified according

to their projection target or inputs will allow a further understanding of the functional circuits in which these neurons are incorporated.

Classically, the CeA has been considered as a major mediator of fear and anxiety behaviors. Despite this notion, it has recently become clear that the CeA functions in a broad range of behaviors and that CeA circuits are flexibly engaged depending on the behavioral context. Indeed CeA neurons that express CRH and SOM have been shown to modulate both appetitive and aversive behaviors [71, 104, 53]. This demonstrates that the CeA functions in multiple behavioral contexts and that genetically-defined CeA neural circuits participate in a variety of behaviors. In the case of Htr2a-expressing CeA neurons, these cells were recently shown to be inhibited by innately-fearful stimuli [45], suggesting that these neurons function in both appetitive and aversive behaviors, albeit in an opposite manner. Further, since activity of CeA^{Htr2a} neurons is rewarding, these cells may modulate other appetitive behaviors in addition to feeding. Such an effect has been shown for GABAergic LH neurons, which promote consumption of food and water as well as social exploration and while activity of these neurons is intrinsically rewarding [80, 79]. Together these data, highlight that engagement of CeA neurons may depend on the internal state of the animal and the behavioral environment and suggests that appetitive and aversive behavioral states may interact at the level of the CeA. Therefore, the study of this region is important for understanding how emotional states influence behavior.

Bibliography

- [1] R. Adolphs, D. Tranel, H. Damasio, and A. Damasio. Impaired recognition of emotion in facial expressions following bilateral damage to the human amygdala. *Nature*, 372(6507):669–72, 1994. (Cited on 1)
- [2] B. D. Allen, A. C. Singer, and E. S. Boyden. Principles of designing interpretable optogenetic behavior experiments. *Learn Mem*, 22(4):232–8, 2015. (Cited on 20)
- [3] R. Andero, B. G. Dias, and K. J. Ressler. A role for *tac2*, *nkb*, and *nk3* receptor in normal and dysregulated fear memory consolidation. *Neuron*, 83(2):444–54, 2014. (Cited on 2, 3)
- [4] A. K. Anderson and E. A. Phelps. Lesions of the human amygdala impair enhanced perception of emotionally salient events. *Nature*, 411(6835):305–9, 2001. (Cited on 1)
- [5] D. Atasoy, J. N. Betley, H. H. Su, and S. M. Sternson. Deconstruction of a neural circuit for hunger. *Nature*, 488(7410):172–7, 2012. (Cited on 16, 18)
- [6] P. F. Baker, A. L. Hodgkin, and E. B. Ridgway. Depolarization and calcium entry in squid giant axons. *J Physiol*, 218(3):709–55, 1971. (Cited on 20)
- [7] R. P. Barretto, B. Messerschmidt, and M. J. Schnitzer. In vivo fluorescence imaging with high-resolution microlenses. *Nat Methods*, 6(7):511–2, 2009. (Cited on 22)
- [8] J. N. Betley, Z. F. Cao, K. D. Ritola, and S. M. Sternson. Parallel, redundant circuit organization for homeostatic control of feeding behavior. *Cell*, 155(6):1337–50, 2013. (Cited on 8)
- [9] J. N. Betley, S. Xu, Z. F. Cao, R. Gong, C. J. Magnus, Y. Yu, and S. M. Sternson. Neurons for hunger and thirst transmit a negative-valence teaching signal. *Nature*, 521(7551):180–5, 2015. (Cited on 34, 48, 71)
- [10] P. Botta, L. Demmou, Y. Kasugai, M. Markovic, C. Xu, J. P. Fadok, T. Lu, M. M. Poe, L. Xu, J. M. Cook, U. Rudolph, P. Sah, F. Ferraguti, and A. Luthi. Regulating anxiety with extrasynaptic inhibition. *Nat Neurosci*, 18(10):1493–500, 2015. (Cited on 23)
- [11] S. Boverto and D. Richard. Lesion of central nucleus of amygdala promotes fat gain without preventing effect of exercise on energy balance. *Am J Physiol*, 269(4 Pt 2):R781–6, 1995. (Cited on 23)
- [12] E. S. Boyden, F. Zhang, E. Bamberg, G. Nagel, and K. Deisseroth. Millisecond-timescale, genetically targeted optical control of neural activity. *Nat Neurosci*, 8(9):1263–8, 2005. (Cited on 16)

- [13] Sanger Brown and E. A. Schafer. An investigation into the functions of the occipital and temporal lobes of the monkey's brain. *Philosophical Transactions of the Royal Society of London. (B.)*, 179:303–327, 1888. (Cited on 1)
- [14] H. Cai, W. Haubensak, T. E. Anthony, and D. J. Anderson. Central amygdala pkc-delta(+) neurons mediate the influence of multiple anorexigenic signals. *Nat Neurosci*, 17(9):1240–8, 2014. (Cited on 3, 11, 12, 23, 24, 44, 46, 47, 61, 68, 73, 74, 77, 81)
- [15] E. M. Callaway and L. Luo. Monosynaptic circuit tracing with glycoprotein-deleted rabies viruses. *J Neurosci*, 35(24):8979–85, 2015. (Cited on 17)
- [16] C. A. Campos, A. J. Bowen, M. W. Schwartz, and R. D. Palmiter. Parabrachial cgrp neurons control meal termination. *Cell Metab*, 23(5):811–20, 2016. (Cited on 63, 77, 82)
- [17] M. E. Carter, M. E. Soden, L. S. Zweifel, and R. D. Palmiter. Genetic identification of a neural circuit that suppresses appetite. *Nature*, 503(7474):111–4, 2013. (Cited on 11, 12, 61, 63, 71, 77, 82)
- [18] M. D. Cassell, T. S. Gray, and J. Z. Kiss. Neuronal architecture in the rat central nucleus of the amygdala: a cytological, hodological, and immunocytochemical study. *J Comp Neurol*, 246(4):478–99, 1986. (Cited on 4)
- [19] N. L. Chamberlin, B. Du, S. de Lacalle, and C. B. Saper. Recombinant adeno-associated virus vector: use for transgene expression and anterograde tract tracing in the cns. *Brain Res*, 793(1-2):169–75, 1998. (Cited on 17, 22, 34)
- [20] T. W. Chen, T. J. Wardill, Y. Sun, S. R. Pulver, S. L. Renninger, A. Baohan, E. R. Schreiter, R. A. Kerr, M. B. Orger, V. Jayaraman, L. L. Looger, K. Svoboda, and D. S. Kim. Ultrasensitive fluorescent proteins for imaging neuronal activity. *Nature*, 499(7458):295–300, 2013. (Cited on 20, 21, 76)
- [21] B. Y. Chow, X. Han, A. S. Dobry, X. Qian, A. S. Chuong, M. Li, M. A. Henninger, G. M. Belfort, Y. Lin, P. E. Monahan, and E. S. Boyden. High-performance genetically targetable optical neural silencing by light-driven proton pumps. *Nature*, 463(7277):98–102, 2010. (Cited on 16)
- [22] S. Ciocchi, C. Herry, F. Grenier, S. B. Wolff, J. J. Letzkus, I. Vlachos, I. Ehrlich, R. Sprengel, K. Deisseroth, M. B. Stadler, C. Muller, and A. Luthi. Encoding of conditioned fear in central amygdala inhibitory circuits. *Nature*, 468(7321):277–82, 2010. (Cited on 7, 82)
- [23] W. L. Conte, H. Kamishina, and R. L. Reep. Multiple neuroanatomical tract-tracing using fluorescent alexa fluor conjugates of cholera toxin subunit b in rats. *Nat Protoc*, 4(8):1157–66, 2009. (Cited on 17)
- [24] I. E. de Araujo. *Frontiers in Neuroscience Multiple Reward Layers in Food Reinforcement*. CRC Press/Taylor Francis Llc., Boca Raton (FL), 2011. (Cited on 75)
- [25] W. Denk, J. H. Strickler, and W. W. Webb. Two-photon laser scanning fluorescence microscopy. *Science*, 248(4951):73–6, 1990. (Cited on 21)
- [26] F. H. Do-Monte, K. Quinones-Laracuate, and G. J. Quirk. A temporal shift in the circuits mediating retrieval of fear memory. *Nature*, 519(7544):460–3, 2015. (Cited on 8)
- [27] S. Duvarci and D. Pare. Amygdala microcircuits controlling learned fear. *Neuron*, 82(5):966–80, 2014. (Cited on 2)

- [28] Teresa Esch. Floyd bloom discusses the messengers of the mind. *eNeuro*, 1(1), 2014. (Cited on 7)
- [29] J. P. Fadok, S. Krabbe, M. Markovic, J. Courtin, C. Xu, L. Massi, P. Botta, K. Bylund, C. Muller, A. Kovacevic, P. Tovote, and A. Luthi. A competitive inhibitory circuit for selection of active and passive fear responses. *Nature*, 542(7639):96–100, 2017. (Cited on 2, 7, 73)
- [30] J. H. Fallon and R. Y. Moore. Catecholamine innervation of the basal forebrain. iv. topography of the dopamine projection to the basal forebrain and neostriatum. *J Comp Neurol*, 180(3):545–80, 1978. (Cited on 8)
- [31] L. E. Fenno, J. Mattis, C. Ramakrishnan, M. Hyun, S. Y. Lee, M. He, J. Tucciaroni, A. Selimbeyoglu, A. Berndt, L. Grosenick, K. A. Zalocusky, H. Bernstein, H. Swanson, C. Perry, I. Diester, F. M. Boyce, C. E. Bass, R. Neve, Z. J. Huang, and K. Deisseroth. Targeting cells with single vectors using multiple-feature boolean logic. *Nat Methods*, 11(7):763–72, 2014. (Cited on 8, 17)
- [32] K. K. Ghosh, L. D. Burns, E. D. Cocker, A. Nimmerjahn, Y. Ziv, A. E. Gamal, and M. J. Schnitzer. Miniaturized integration of a fluorescence microscope. *Nat Methods*, 8(10):871–8, 2011. (Cited on 22)
- [33] C. Gonzales and M. F. Chesselet. Amygdalonigral pathway: an anterograde study in the rat with phaseolus vulgaris leucoagglutinin (pha-l). *J Comp Neurol*, 297(2):182–200, 1990. (Cited on 9)
- [34] B. F. Grewe, J. Grundemann, L. J. Kitch, J. A. Lecoq, J. G. Parker, J. D. Marshall, M. C. Larkin, P. E. Jercog, F. Grenier, J. Z. Li, A. Luthi, and M. J. Schnitzer. Neural ensemble dynamics underlying a long-term associative memory. *Nature*, 543(7647):670–675, 2017. (Cited on 2, 7, 17, 22, 34)
- [35] C. Grienberger and A. Konnerth. Imaging calcium in neurons. *Neuron*, 73(5):862–85, 2012. (Cited on 21)
- [36] L. A. Gunaydin, L. Grosenick, J. C. Finkelstein, I. V. Kauvar, L. E. Fenno, A. Adhikari, S. Lammel, J. J. Mirzabekov, R. D. Airan, K. A. Zalocusky, K. M. Tye, P. Anikeeva, R. C. Malenka, and K. Deisseroth. Natural neural projection dynamics underlying social behavior. *Cell*, 157(7):1535–51, 2014. (Cited on 22)
- [37] E. J. Hamel, B. F. Grewe, J. G. Parker, and M. J. Schnitzer. Cellular level brain imaging in behaving mammals: an engineering approach. *Neuron*, 86(1):140–59, 2015. (Cited on 21)
- [38] S. Han, M. T. Soleiman, M. E. Soden, L. S. Zweifel, and R. D. Palmiter. Elucidating an affective pain circuit that creates a threat memory. *Cell*, 162(2):363–74, 2015. (Cited on 8, 13, 25, 78)
- [39] W. Haubensak, P. S. Kunwar, H. Cai, S. Cioocchi, N. R. Wall, R. Ponnusamy, J. Biag, H. W. Dong, K. Deisseroth, E. M. Callaway, M. S. Fanselow, A. Luthi, and D. J. Anderson. Genetic dissection of an amygdala microcircuit that gates conditioned fear. *Nature*, 468(7321):270–6, 2010. (Cited on 2, 3, 4, 5, 7, 18, 23, 41, 42, 44, 46, 70, 72, 73, 82)
- [40] F. Helmchen and W. Denk. Deep tissue two-photon microscopy. *Nat Methods*, 2(12):932–40, 2005. (Cited on 21, 22)
- [41] D. A. Hopkins and G. Holstege. Amygdaloid projections to the mesencephalon, pons and medulla oblongata in the cat. *Exp Brain Res*, 32(4):529–47, 1978. (Cited on 9)

- [42] Z. J. Huang and H. Zeng. Genetic approaches to neural circuits in the mouse. *Annu Rev Neurosci*, 36:183–215, 2013. (Cited on 13, 15)
- [43] D. Huber, P. Veinante, and R. Stoop. Vasopressin and oxytocin excite distinct neuronal populations in the central amygdala. *Science*, 308(5719):245–8, 2005. (Cited on 70)
- [44] S. P. Hunt and P. W. Mantyh. The molecular dynamics of pain control. *Nat Rev Neurosci*, 2(2):83–91, 2001. (Cited on 12, 25, 64)
- [45] Tomoko Isosaka, Tomohiko Matsuo, Takashi Yamaguchi, Kazuo Funabiki, Shigetada Nakanishi, Reiko Kobayakawa, and Ko Kobayakawa. Htr2a-expressing cells in the central amygdala control the hierarchy between innate and learned fear. *Cell*, 163(5):1153–1164, nov 2015. (Cited on 72, 83)
- [46] P. H. Janak and K. M. Tye. From circuits to behaviour in the amygdala. *Nature*, 517(7534):284–92, 2015. (Cited on 1, 2, 8)
- [47] J. H. Jennings, G. Rizzi, A. M. Stamatakis, R. L. Ung, and G. D. Stuber. The inhibitory circuit architecture of the lateral hypothalamus orchestrates feeding. *Science*, 341(6153):1517–21, 2013. (Cited on 19)
- [48] J. H. Jennings, R. L. Ung, S. L. Resendez, A. M. Stamatakis, J. G. Taylor, J. Huang, K. Veleta, P. A. Katak, M. Aita, K. Shilling-Scrivero, C. Ramakrishnan, K. Deisseroth, S. Otte, and G. D. Stuber. Visualizing hypothalamic network dynamics for appetitive and consummatory behaviors. *Cell*, 160(3):516–27, 2015. (Cited on 48, 78)
- [49] P. Jensen and S. M. Dymecki. Essentials of recombinase-based genetic fate mapping in mice. *Methods Mol Biol*, 1092:437–54, 2014. (Cited on 8, 71)
- [50] F. Junyent and E. J. Kremer. Cav-2—why a canine virus is a neurobiologist’s best friend. *Curr Opin Pharmacol*, 24:86–93, 2015. (Cited on 6, 71)
- [51] L. C. Katz, A. Burkhalter, and W. J. Dreyer. Fluorescent latex microspheres as a retrograde neuronal marker for in vivo and in vitro studies of visual cortex. *Nature*, 310(5977):498–500, 1984. (Cited on 17)
- [52] L. C. Katz and D. M. Iarovici. Green fluorescent latex microspheres: a new retrograde tracer. *Neuroscience*, 34(2):511–20, 1990. (Cited on 17)
- [53] J. Kim, X. Zhang, S. Muralidhar, S. A. LeBlanc, and S. Tonegawa. Basolateral to central amygdala neural circuits for appetitive behaviors. *Neuron*, 93(6):1464–1479.e5, 2017. (Cited on 4, 83)
- [54] H. Klver and P. C. Bucy. ”psychic blindness” and other symptoms following bilateral temporal lobectomy in rhesus monkeys. *American Journal of Physiology*, 119:352–353, 1937. (Cited on 1)
- [55] Z. A. Knight, K. Tan, K. Birsoy, S. Schmidt, J. L. Garrison, R. W. Wysocki, A. Emiliano, M. I. Ekstrand, and J. M. Friedman. Molecular profiling of activated neurons by phosphorylated ribosome capture. *Cell*, 151(5):1126–37, 2012. (Cited on 71)
- [56] J. W. Koo, J. S. Han, and J. J. Kim. Selective neurotoxic lesions of basolateral and central nuclei of the amygdala produce differential effects on fear conditioning. *J Neurosci*, 24(35):7654–62, 2004. (Cited on 23)

- [57] M. J. Krashes, B. P. Shah, J. C. Madara, D. P. Olson, D. E. Strohlic, A. S. Garfield, L. Vong, H. Pei, M. Watabe-Uchida, N. Uchida, S. D. Liberles, and B. B. Lowell. An excitatory paraventricular nucleus to agrp neuron circuit that drives hunger. *Nature*, 507(7491):238–42, 2014. (Cited on 19)
- [58] J. E. LeDoux, J. Iwata, P. Cicchetti, and D. J. Reis. Different projections of the central amygdaloid nucleus mediate autonomic and behavioral correlates of conditioned fear. *J Neurosci*, 8(7):2517–29, 1988. (Cited on 6, 9)
- [59] H. Li, M. A. Penzo, H. Taniguchi, C. D. Kopec, Z. J. Huang, and B. Li. Experience-dependent modification of a central amygdala fear circuit. *Nat Neurosci*, 16(3):332–9, 2013. (Cited on 2, 3, 6, 7, 23, 24, 70, 71, 73)
- [60] S. Q. Lima and G. Miesenbock. Remote control of behavior through genetically targeted photostimulation of neurons. *Cell*, 121(1):141–52, 2005. (Cited on 15)
- [61] S. Liu, A. K. Globa, F. Mills, L. Naef, M. Qiao, S. X. Bamji, and S. L. Borgland. Consumption of palatable food primes food approach behavior by rapidly increasing synaptic density in the vta. *Proc Natl Acad Sci U S A*, 113(9):2520–5, 2016. (Cited on 58, 78)
- [62] G. Lopes, N. Bonacchi, J. Frazao, J. P. Neto, B. V. Atallah, S. Soares, L. Moreira, S. Matias, P. M. Itskov, P. A. Correia, R. E. Medina, L. Calcaterra, E. Dreosti, J. J. Paton, and A. R. Kampff. Bonsai: an event-based framework for processing and controlling data streams. *Front Neuroinform*, 9:7, 2015. (Cited on 31, 33)
- [63] M. Lopez de Armentia and P. Sah. Firing properties and connectivity of neurons in the rat lateral central nucleus of the amygdala. *J Neurophysiol*, 92(3):1285–94, 2004. (Cited on 5, 6, 41, 71, 72)
- [64] M. Lopez de Armentia and P. Sah. Bidirectional synaptic plasticity at nociceptive afferents in the rat central amygdala. *J Physiol*, 581(Pt 3):961–70, 2007. (Cited on 6)
- [65] Jr. Lundy, R. F. and R. Norgren. Pontine gustatory activity is altered by electrical stimulation in the central nucleus of the amygdala. *J Neurophysiol*, 85(2):770–83, 2001. (Cited on 12, 77)
- [66] L. Madisen, T. Mao, H. Koch, J. M. Zhuo, A. Berenyi, S. Fujisawa, Y. W. Hsu, 3rd Garcia, A. J., X. Gu, S. Zanella, J. Kidney, H. Gu, Y. Mao, B. M. Hooks, E. S. Boyden, G. Buzsaki, J. M. Ramirez, A. R. Jones, K. Svoboda, X. Han, E. E. Turner, and H. Zeng. A toolbox of cre-dependent optogenetic transgenic mice for light-induced activation and silencing. *Nat Neurosci*, 15(5):793–802, 2012. (Cited on 27)
- [67] A. Magableh and R. Lundy. Somatostatin and corticotrophin releasing hormone cell types are a major source of descending input from the forebrain to the parabrachial nucleus in mice. *Chem Senses*, 39(8):673–82, 2014. (Cited on 11, 61, 77)
- [68] M. Mahn, M. Prigge, S. Ron, R. Levy, and O. Yizhar. Biophysical constraints of optogenetic inhibition at presynaptic terminals. *Nat Neurosci*, 19(4):554–6, 2016. (Cited on 16)
- [69] M. Martina, S. Royer, and D. Pare. Physiological properties of central medial and central lateral amygdala neurons. *J Neurophysiol*, 82(4):1843–54, 1999. (Cited on 5, 41, 70, 71)

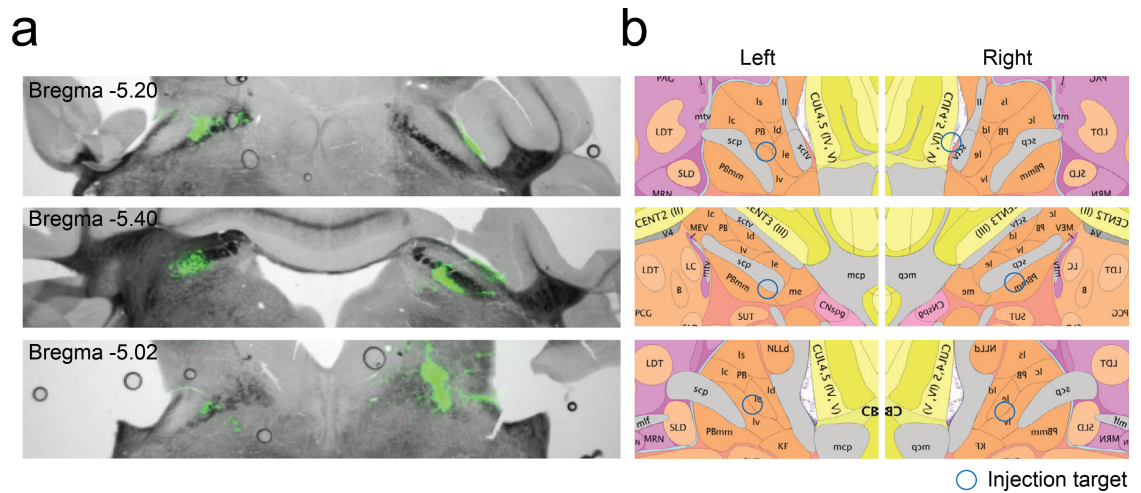
- [70] J. Mattis, K. M. Tye, E. A. Ferenczi, C. Ramakrishnan, D. J. O’Shea, R. Prakash, L. A. Gunaydin, M. Hyun, L. E. Fenno, V. Gradinaru, O. Yizhar, and K. Deisseroth. Principles for applying optogenetic tools derived from direct comparative analysis of microbial opsins. *Nat Methods*, 9(2):159–72, 2012. (Cited on 16)
- [71] J. G. McCall, R. Al-Hasani, E. R. Siuda, D. Y. Hong, A. J. Norris, C. P. Ford, and M. R. Bruchas. Crh engagement of the locus coeruleus noradrenergic system mediates stress-induced anxiety. *Neuron*, 87(3):605–20, 2015. (Cited on 23, 83)
- [72] K. L. Montgomery, A. J. Yeh, J. S. Ho, V. Tsao, S. Mohan Iyer, L. Groseknick, E. A. Ferenczi, Y. Tanabe, K. Deisseroth, S. L. Delp, and A. S. Poon. Wirelessly powered, fully internal optogenetics for brain, spinal and peripheral circuits in mice. *Nat Methods*, 12(10):969–74, 2015. (Cited on 19)
- [73] E. A. Mukamel, A. Nimmerjahn, and M. J. Schnitzer. Automated analysis of cellular signals from large-scale calcium imaging data. *Neuron*, 63(6):747–60, 2009. (Cited on 27, 34, 48)
- [74] G. Nagel, M. Brauner, J. F. Liewald, N. Adeishvili, E. Bamberg, and A. Gottschalk. Light activation of channelrhodopsin-2 in excitable cells of *Caenorhabditis elegans* triggers rapid behavioral responses. *Curr Biol*, 15(24):2279–84, 2005. (Cited on 16)
- [75] G. Nagel, D. Ollig, M. Fuhrmann, S. Kateriya, A. M. Musti, E. Bamberg, and P. Hegemann. Channelrhodopsin-1: a light-gated proton channel in green algae. *Science*, 296(5577):2395–8, 2002. (Cited on 16)
- [76] G. Nagel, T. Szellas, W. Huhn, S. Kateriya, N. Adeishvili, P. Berthold, D. Ollig, P. Hegemann, and E. Bamberg. Channelrhodopsin-2, a directly light-gated cation-selective membrane channel. *Proc Natl Acad Sci U S A*, 100(24):13940–5, 2003. (Cited on 16)
- [77] J. Nakai, M. Ohkura, and K. Imoto. A high signal-to-noise Ca^{2+} probe composed of a single green fluorescent protein. *Nat Biotechnol*, 19(2):137–41, 2001. (Cited on 20)
- [78] P. Namburi, A. Beyeler, S. Yorozu, G. G. Calhoon, S. A. Halbert, R. Wichmann, S. S. Holden, K. L. Mertens, M. Anahtar, A. C. Felix-Ortiz, I. R. Wickersham, J. M. Gray, and K. M. Tye. A circuit mechanism for differentiating positive and negative associations. *Nature*, 520(7549):675–8, 2015. (Cited on 71)
- [79] Montserrat Navarro, Jeffrey J Olney, Nathan W Burnham, Christopher M Mazzone, Emily G Lowery-Gionta, Kristen E Pleil, Thomas L Kash, and Todd E Thiele. Lateral hypothalamus GABAergic neurons modulate consummatory behaviors regardless of the caloric content or biological relevance of the consumed stimuli. *Neuropsychopharmacology*, 41(6):1505–1512, oct 2015. (Cited on 83)
- [80] E. H. Nieh, C. M. Vander Weele, G. A. Matthews, K. N. Presbrey, R. Wichmann, C. A. Leppla, E. M. Izadmehr, and K. M. Tye. Inhibitory input from the lateral hypothalamus to the ventral tegmental area disinhibits dopamine neurons and promotes behavioral activation. *Neuron*, 2016. (Cited on 19, 58, 78, 79, 83)
- [81] T. M. Otchy, S. B. Wolff, J. Y. Rhee, C. Pehlevan, R. Kawai, A. Kempf, S. M. Gobes, and B. P. Olveczky. Acute off-target effects of neural circuit manipulations. *Nature*, 528(7582):358–63, 2015. (Cited on 19)
- [82] H. C. Pape and D. Pare. Plastic synaptic networks of the amygdala for the acquisition, expression, and extinction of conditioned fear. *Physiol Rev*, 90(2):419–63, 2010. (Cited on 6)

- [83] J. A. Parkinson, T. W. Robbins, and B. J. Everitt. Dissociable roles of the central and basolateral amygdala in appetitive emotional learning. *Eur J Neurosci*, 12(1):405–13, 2000. (Cited on 23)
- [84] M. A. Penzo, V. Robert, and B. Li. Fear conditioning potentiates synaptic transmission onto long-range projection neurons in the lateral subdivision of central amygdala. *J Neurosci*, 34(7):2432–7, 2014. (Cited on 78)
- [85] L. Petreanu, D. Huber, A. Sobczyk, and K. Svoboda. Channelrhodopsin-2-assisted circuit mapping of long-range callosal projections. *Nat Neurosci*, 10(5):663–8, 2007. (Cited on 16, 18)
- [86] T. Petrov, T. L. Krukoff, and J. H. Jhamandas. Chemically defined collateral projections from the pons to the central nucleus of the amygdala and hypothalamic paraventricular nucleus in the rat. *Cell Tissue Res*, 277(2):289–95, 1994. (Cited on 8)
- [87] C. K. Pfeffer, M. Xue, M. He, Z. J. Huang, and M. Scanziani. Inhibition of inhibition in visual cortex: the logic of connections between molecularly distinct interneurons. *Nat Neurosci*, 16(8):1068–76, 2013. (Cited on 17)
- [88] Ferruccio Pisanello, Gil Mandelbaum, Marco Pisanello, Ian Oldenburg, Leo Sileo, Jeffrey Markowitz, Ralph Peterson, Andrea Della Patria, Trevor Haynes, Mohamed Emara, Barbara Spagnolo, Sandeep R Datta, Bernardo Sabatini, and Massimo De Vittorio. Dynamically controlled light delivery over large brain volumes through tapered optical fibers. *bioRxiv*, 2016. (Cited on 20)
- [89] J. V. Raimondo, L. Kay, T. J. Ellender, and C. J. Akerman. Optogenetic silencing strategies differ in their effects on inhibitory synaptic transmission. *Nat Neurosci*, 15(8):1102–4, 2012. (Cited on 16)
- [90] S. L. Resendez, J. H. Jennings, R. L. Ung, V. M. Namboodiri, Z. C. Zhou, J. M. Otis, H. Nomura, J. A. McHenry, O. Kosyk, and G. D. Stuber. Visualization of cortical, subcortical and deep brain neural circuit dynamics during naturalistic mammalian behavior with head-mounted microscopes and chronically implanted lenses. *Nat Protoc*, 11(3):566–97, 2016. (Cited on 22, 48)
- [91] T. A. Rizvi, M. Ennis, M. M. Behbehani, and M. T. Shipley. Connections between the central nucleus of the amygdala and the midbrain periaqueductal gray: topography and reciprocity. *J Comp Neurol*, 303(1):121–31, 1991. (Cited on 9)
- [92] A. M. Rosen, J. D. Victor, and P. M. Di Lorenzo. Temporal coding of taste in the parabrachial nucleus of the pons of the rat. *J Neurophysiol*, 105(4):1889–96, 2011. (Cited on 78)
- [93] P. Sah, E. S. Faber, M. Lopez De Armentia, and J. Power. The amygdaloid complex: anatomy and physiology. *Physiol Rev*, 83(3):803–34, 2003. (Cited on 2, 3, 4, 8, 9)
- [94] V. Scheuss and T. Bonhoeffer. Function of dendritic spines on hippocampal inhibitory neurons. *Cereb Cortex*, 24(12):3142–53, 2014. (Cited on 17)
- [95] M. C. Schiess, E. K. Asproдини, D. G. Rainnie, and P. Shinnick-Gallagher. The central nucleus of the rat amygdala: in vitro intracellular recordings. *Brain Res*, 604(1-2):283–97, 1993. (Cited on 5, 71)
- [96] M. C. Schiess, P. M. Callahan, and H. Zheng. Characterization of the electrophysiological and morphological properties of rat central amygdala neurons in vitro. *J Neurosci Res*, 58(5):663–73, 1999. (Cited on 5)

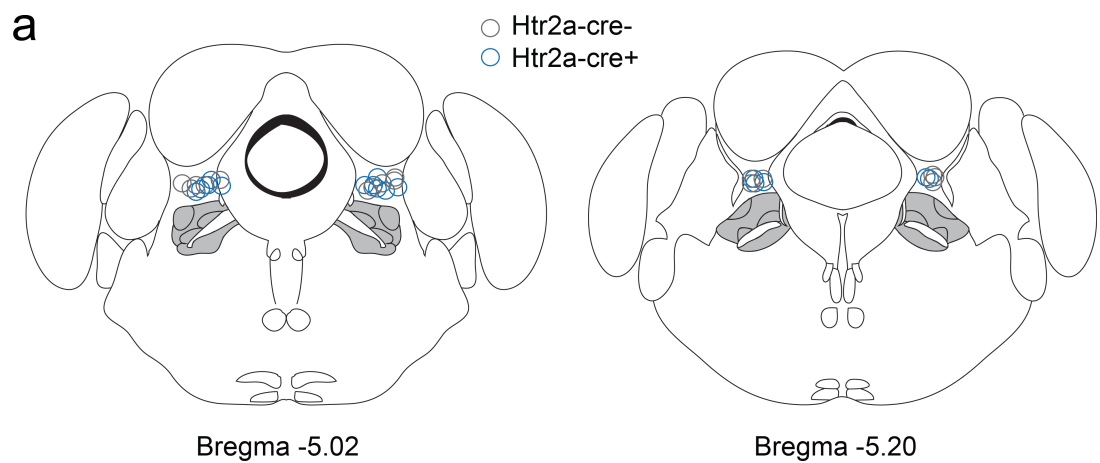
- [97] T. R. Scott and D. M. Small. The role of the parabrachial nucleus in taste processing and feeding. *Ann N Y Acad Sci*, 1170:372–7, 2009. (Cited on 25, 64)
- [98] C. Shi and M. Davis. Pain pathways involved in fear conditioning measured with fear-potentiated startle: lesion studies. *J Neurosci*, 19(1):420–30, 1999. (Cited on 12)
- [99] P. Soriano. Generalized lacz expression with the rosa26 cre reporter strain. *Nat Genet*, 21(1):70–1, 1999. (Cited on 27)
- [100] E. Stice, D. P. Figlewicz, B. A. Gosnell, A. S. Levine, and W. E. Pratt. The contribution of brain reward circuits to the obesity epidemic. *Neurosci Biobehav Rev*, 37(9 Pt A):2047–58, 2013. (Cited on 78)
- [101] G. D. Stuber and R. A. Wise. Lateral hypothalamic circuits for feeding and reward. *Nat Neurosci*, 19(2):198–205, 2016. (Cited on 58, 78)
- [102] L. W. Swanson and G. D. Petrovich. What is the amygdala? *Trends Neurosci*, 21(8):323–31, 1998. (Cited on 2)
- [103] D. W. Tank, M. Sugimori, J. A. Connor, and R. R. Llinas. Spatially resolved calcium dynamics of mammalian purkinje cells in cerebellar slice. *Science*, 242(4879):773–7, 1988. (Cited on 20)
- [104] P. Tovote, M. S. Esposito, P. Botta, F. Chaudun, J. P. Fadok, M. Markovic, S. B. Wolff, C. Ramakrishnan, L. Fenno, K. Deisseroth, C. Herry, S. Arber, and A. Luthi. Midbrain circuits for defensive behaviour. *Nature*, 534(7606):206–12, 2016. (Cited on 78, 83)
- [105] R. P. Vertes. A pha-l analysis of ascending projections of the dorsal raphe nucleus in the rat. *J Comp Neurol*, 313(4):643–68, 1991. (Cited on 8)
- [106] P. Walker and P. Carrive. Role of ventrolateral periaqueductal gray neurons in the behavioral and cardiovascular responses to contextual conditioned fear and post-stress recovery. *Neuroscience*, 116(3):897–912, 2003. (Cited on 78)
- [107] D. M. Weiner, A. I. Levey, R. K. Sunahara, H. B. Niznik, B. F. O’Dowd, P. Seeman, and M. R. Brann. D1 and d2 dopamine receptor mrna in rat brain. *Proc Natl Acad Sci U S A*, 88(5):1859–63, 1991. (Cited on 70)
- [108] I. R. Wickersham, D. C. Lyon, R. J. Barnard, T. Mori, S. Finke, K. K. Conzelmann, J. A. Young, and E. M. Callaway. Monosynaptic restriction of transsynaptic tracing from single, genetically targeted neurons. *Neuron*, 53(5):639–47, 2007. (Cited on 17)
- [109] A. E. Wilensky, G. E. Schafe, M. P. Kristensen, and J. E. LeDoux. Rethinking the fear circuit: the central nucleus of the amygdala is required for the acquisition, consolidation, and expression of pavlovian fear conditioning. *J Neurosci*, 26(48):12387–96, 2006. (Cited on 23)
- [110] F. Zhang, L. P. Wang, M. Brauner, J. F. Liwald, K. Kay, N. Watzke, P. G. Wood, E. Bamberg, G. Nagel, A. Gottschalk, and K. Deisseroth. Multimodal fast optical interrogation of neural circuitry. *Nature*, 446(7136):633–9, 2007. (Cited on 16)

Appendix I

Figures



Appendix I: Location of retrobeads injection targeting PBN. a) A) Representative images of the center of bilateral retrobeads injections in PBN (Figure 4.16) from each mice. Distance from the bregma was denoted on each image. b) Scheme depicting approximate locations of bilateral retrobeads injections in the PBN for backtracing experiments (Figure 4.16).



Appendix II: Location of optic fibers for *in vivo* optogenetics experiments. a) Scheme depicting approximate locations of implanted optic fibers over the PBN used for **in vivo** optogenetics experiments (Figure 4.20, Figure 4.21, Figure 4.22) for both CeA^{Htr2a}→PBN::ChR2 and CeA^{Htr2a}→PBN::eYFP mice.



Hakan Kucukdereli

PH.D. CANDIDATE

Am Klopferspitz 18, D-82152 Martinsried, Germany

☎ +49 (157) 5028 0178 | ✉ hakan@neuro.mpg.de | 📷 hkucukdereli | 📺 hkucukdereli | 🐦 @haganK

Education

Max Planck Institute of Neurobiology

Martinsried, Germany

PH.D. IN SYSTEMIC NEUROSCIENCES

2011 - Present

- International Max Planck Research School for Molecular and Cellular Life Sciences (IMPRS-LS) PhD Program.

Ludwig-Maximilians-Universität München (LMU)

Munich, Germany

PH.D. IN SYSTEMIC NEUROSCIENCES

2011 - Present

- Graduate School of Systemic Neurosciences Fast Track/PhD Program.

Ludwig-Maximilians-Universität München (LMU)

Munich, Germany

FAST-TRACK PREPARATORY YEAR

2010 - 2011

- Graduate School of Systemic Neurosciences Fast Track/PhD Program.

Middle East Technical University

Ankara, Turkey

B.SC. IN MOLECULAR BIOLOGY & GENETICS

2003 - 2007

Research Experience

Max Planck Institute of Neurobiology, Lab of Rüdiger Klein

Martinsried, Germany

PH.D. CANDIDATE

October 2011 - Present

- Supervisor: Rüdiger Klein
- Investigation of the role of central amygdala in food consumption and reward-related behaviors and underlying neuronal circuitry using neuronal activity manipulations, electrophysiology and calcium imaging.

Queensland Brain Institute, Lab of Pankaj Sah

Brisbane, QLD, Australia

VISITING SCIENTIST

May 2013 - September 2013

- Supervisor: Pankaj Sah, MD, PhD
- Investigation of the intra-amygdala connectivity of genetically defined neuronal subpopulations of central amygdala using ex vivo electrophysiology.

Duke University, Lab of Cagla Eroglu

Durham, NC, USA

RESEARCH TECHNICIAN

October 2008 - September 2010

- Supervisor: Cagla Eroglu, PhD
- Investigation of the role of astrocyte-secreted extracellular matrix proteins SC1/Hevin and SPARC in mouse central nervous system synapse formation.

Middle East Technical University, Lab of Mesude Iscan

Ankara, Turkey

SENIOR UNDERGRADUATE RESEARCHER

February 2007 - June 2007

- Supervisor: Mesude Iscan, PhD
- Development and optimization of a primary rat hepatocyte culture protocol for cytotoxicity measurements in a drug screen.

Stanford University, Lab of Ben A. Barres

Stanford, CA, USA

UNDERGRADUATE SUMMER RESEARCHER

June 2006 - September 2006

- Supervisors: Ben A. Barres, MD, PhD and Cagla Eroglu, PhD
- Investigation of the molecular basis of extracellular matrix protein SC1/Hevin's synaptogenic activity.

Presentations

20th IMPRS Seminar

ORAL PRESENTATION

- Central amygdala circuits modulate food consumption through a positive valence mechanism

Martinsried, Germany

December 2016

Society for Neuroscience Annual Meeting 2016

POSTER PRESENTATION

- Functional mapping of central amygdala feeding and reward circuits

San Diego, CA, USA

November 2016

GRC: Optogenetic Approaches to Understanding Neural Circuits & Behavior

POSTER PRESENTATION

- Functional mapping of central amygdala feeding and reward circuits

Newry, ME, USA

July 2016

CSHL Meeting: Neuronal Circuits

POSTER PRESENTATION

- Central amygdala Htr2a-expressing neurons control feeding and appetitive behaviors

Cold Spring Harbor, NY, USA

April 2016

17th IMPRS Seminar

ORAL PRESENTATION

- Optogenetic Dissection of Central Amygdala Circuits

Martinsried, Germany

December 2014

12th IMPRS Seminar

POSTER PRESENTATION

- Involvement of Immunoglobulin superfamily, member 9 (Igsf9) in inhibitory synapse development

Martinsried, Germany

July 2012

American Society of Neurochemistry 40th Annual Meeting

ORAL PRESENTATION

- Role of Astrocyte-Secreted Extracellular Matrix Proteins Hevin and SPARC in Central Nervous System Synapse Formation

Charleston, SC, USA

March 2009

Honors & Awards

2016

Best Poster Prize, GRC: Optogenetic Approaches to Understanding Neural Circuits & Behavior

Newry, ME, U.S.A

Academic Services

<interact> 2013 Symposium, Munich, Germany

MEMBER OF THE ORGANIZATION COMMITTEE OF <INTERACT> 2013 SYMPOSIUM

- Co-organized graduate student-run life science symposium <interact> 2013.

Munich, Germany

August 2012 - March 2013

Publications

- Douglass*, A. M., **Kucukdereli, H.***, Ponsérre*, M., Markovic, M., Gründemann, J., Strobel, C., Morales, P. L. A., Conzelmann, K.-K., Lüthi, A., and Klein, R. (2017). Central amygdala circuits modulate food consumption through a positive valence mechanism. *bioRxiv*. ***Co-authorship**.
- Hunt, S., Sun, Y., **Kucukdereli, H.**, Klein, R., and Sah, P. (2017). Intrinsic circuits in the lateral central amygdala. *eNeuro*, 4(1):ENEURO.0367–16.2017.
- **Kucukdereli, H.**, Allen, N. J., Lee, A. T., Feng, A., Ozlu, M. I., Conatser, L. M., Chakraborty, C., Workman, G., Weaver, M., Sage, E. H., Barres, B. A., and Eroglu, C. (2011). Control of excitatory CNS synaptogenesis by astrocyte-secreted proteins hevin and SPARC. *Proceedings of the National Academy of Sciences*, 108(32):E440–E449.

Declaration

Eidesstattliche Versicherung/Affidavit

Hiermit versichere ich, Hakan Kucukdereli, an Eides statt, dass ich die vorliegende Dissertation "Functional Mapping of Central Amygdala Feeding Circuits" selbstständig angefertigt habe, mich auer der angegebenen keiner weiteren Hilfsmittel bedient und alle Erkenntnisse, die aus dem Schrifttum ganz oder annhernd bernommen sind, als solche kenntlich gemacht und nach ihrer Herkunft unter Bezeichnung der Fundstelle einzeln nachgewiesen habe.

I, Hakan Kucukdereli, hereby confirm that the dissertation "Functional Mapping of Central Amygdala Feeding Circuits" is the result of my own work and that I have only used sources or materials listed and specified in the dissertation.

München, June 13, 2017

Unterschrift/Signature

Author Contributions

List of Contributors: Hakan Kucukdereli*, Amelia M. Douglass*, Milica Markovic,
Jan Gründemann

H.K. designed, performed and analyzed the histology, anatomical tracing and electrophysiology experiments presented in this thesis. H.K. and A.M.D. designed the behavior experiments and built the set-ups used in those experiments. H.K. and A.M.D. performed stereotaxic virus delivery and fiber implantation for behavioral experiments. A.M.D. performed all the behavioral experiments. H.K. and A.M.D. analyzed the data from behavioral experiments. H.K. and A.M.D. designed all the imaging experiments. H.K., A.M.D., M.M. and J.G. performed and analyzed the free-feeding imaging experiments. H.K. and A.M.D. performed the FR1 imaging experiment. H.K. and A.M.D. analyzed the FR1 imaging experiments with input from M.M. and J.G.. H.K. wrote the code for analysis of imaging experiments with input from A.M.D., M.M. and J.G..

(*) Equal contribution

München, June 13, 2017

Supervisor's Signature

Author's Signature

Co-contributor's Signature